Research of design, simulation and demonstration of solar reactor with ceria coated ceramic foam device for two-step thermochemical water-splitting cycle

２段階水熱分解サイクルのためのセリア担持セラミック発泡体デバイスによるソーラー反応器に関する設計，数値解析，及び実証試験の研究

Name: Cho Hyun Seok

Doctoral Program in Advanced Materials Science and Technology

Graduate School of Science and Technology, Niigata University

March, 2015

Chapter I

Introduction

Chapter II

Solar demonstration of thermochemical two-step water splitting cycle using CeO_2/MPSZ ceramic foam device by 45 kW_{th} KIER solar furnace

Chapter III

Improved operation of solar reactor for two-step water splitting H_2 production by ceria-coated ceramic foam device

Chapter IV

Optical modeling of flux distributions on the foam device surfaces in solar reactor

Chapter V

Solar demonstration of new solar reactor with a conical foam device without ceria coating

Chapter VI

Numerical simulation of solar reactor and case study

VI - 1. Introduction

VI - 2. CFD (Computational Fluid Dynamics) of solar reactors

VI - 3. Results and case study

VI - 3 - 1. Result of simulation pressure drop gradient, temperature, and path line

VI - 3 - 2. Case study of simulation results

VI - 4. Conclusion

Chapter VII

Conclusion

References

Abstract

A two-step thermochemical water splitting cycle using a non-stoichiometric ceria is one of the promising processes for converting concentrated solar high-temperature heat into clean hydrogen in sun-belt regions. The two-step cycle, however, requires heat above 1400˚C minimum. This provides challenges to solar "windowed" reactor concepts. Direct irradiation of the redox working material enables the reactor to respond very quickly to the intermittent heat supplied by concentrated solar radiation. Niigata University has been developing a novel solar reactor concept using a ceria-coated ceramic foam device. In this paper, this reactor concept is up-scaled for solar demonstration using a 45 kW_{th} solar furnace at Korea under the collaboration research between Niigata University and Korea Institute of Energy Research (KIER).

The first-type of the up-scaled solar reactor with the flat disk foam device coated with ceria was designed and fabricated. For the solar demonstration the solar reactor was set on to KIER solar furnace and additional operating system of the solar reactor was designed and constructed at KIER solar furnace together with KIER members. Three ceramic foam devices coated with different ceria loadings were tested in the solar reactor on hydrogen production performance at the solar furnace. 30 cycles of the two-step water splitting were demonstrated in total, and solar operation method of this foam device reactor was improved. Hydrogen could be successfully produced in the repeated cycles by input of 10-18 kW_{th} of

concentrated solar irradiation.

On the basis of the experimental data of the solar demonstration, a new design of the solar reactor with a conical or cylindrical foam device was proposed in order to improve hydrogen production performance. Comparing the previous flat foam device, the conical or cylindrical foam device can create a more uniform heat flux distribution on the foam device surface, which expands the solar-heated high-temperature region of the foam device. In addition, the conical or cylindrical foam device can improve the heat transfer between gases and foam surface.

Four different-shaped foam devices of conical or cylindrical types were designed, and numerical simulation was done for them by optical modeling. Then the second-type of the solar reactor with a conical shape foam device without ceria coating was fabricated. And the new solar reactor was tested on temperature distribution of conical foam device at the KIER solar furnace. 23 ~ 24 kW_{th} of solar concentrated radiation was irradiated to the conical foam device. More uniform temperature distribution was created on the surface of the conical device comparing with that of the flat device. The high temperature region ($T > 1400\ ^oC$) could be expanded as expected.

Additionally, the numerical simulation in terms of pressure drop, temperature distribution, and path lines of the two tested solar reactors was studied for analysis of heat transfer characteristics.

Chapter I

Introduction

I - 1. Solar energy and solar concentrating technology

Solar energy is the most abundant energy source on earth and several technologies have been suggested and developed for its utilization. Radiant energy from the sun hits the earth in wavelengths in orders ranging from 0.1 to 10 μm. The conversion of solar radiation into technically usable energy at required locations and times is an engineering challenge.

The intensity of solar light or insolation of sun is different to regions. It is not only a function of latitude, but also general geographical, meteorological, and topographical conditions. Fig. I-1 is the insolation map of the world which is determined by daily sum of DNI (Direct Normal Insolation). Deep color regions which are greatly insolated are referred to as ‘sunbelts’. In these sunbelts, maximum direct insolation reaches 1kW/m^2 [1].

For the utilization of solar energy, solar concentrating systems have been developed for about 30 years over. Systematic development of the four types of solar concentrating system (central receiver system, dish type, and beam down) has led to their increasing capability for converting concentrated solar thermal energy into electricity, process heat and chemical fuels [1]. Fig. I-2 shows four different types of solar concentrating systems schematically. Each concentrating systems have different operation systems and different concentration ratio. Generally, attainable temperature of solar concentrating systems is depending on the concentration ratio of systems. Parabolic trough systems (Fig. I-2a) use linear parabolic reflectors to focus sunlight along the focal lines of the collectors. Central concentrating system or power tower systems (Fig. I-2b) was applied to generate electricity combined with power block cycles. Solar power tower systems usually achieve concentration ratios of 300 - 1500 and can operate at temperatures up to 1600 K. Dish type systems (as shown Fig. I-2c) use a parabolic dish concentrator to focus the sunlight to the thermal receiver. Concentration ratios usually range from 1000 to 5000 and it can achieve temperatures in excess of 1800 K. The fourth type of solar thermal system which double-concentration system (Fig. I-2d) consists of a heliostat field, the ‘reflective tower’ and a ground receiver equipped with a secondary concentrator. In developed solar concentrating technologies, efficient utilization of high-temperature heat from concentrated solar radiation in the Sunbelt is a subject of

current interest [3-8]. The conversion of solar high-temperature heat to chemical fuels enables solar energy storage and transportation from the Sunbelt to remote population centers.

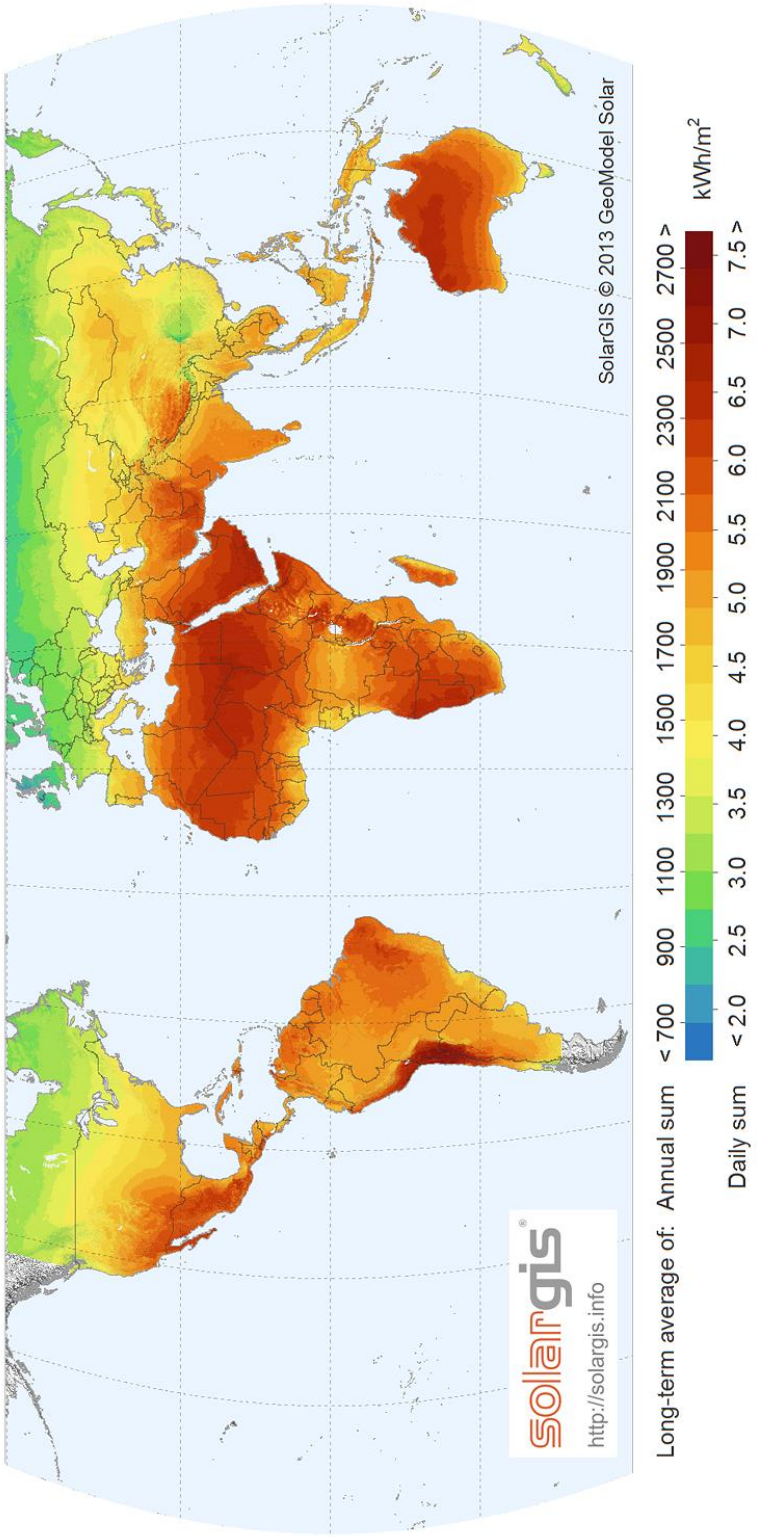

Figure I-1. Maps of Direct normal irradiation (DNI) in the world (SolarGIS © 2015 GeoModel Solar) [2]

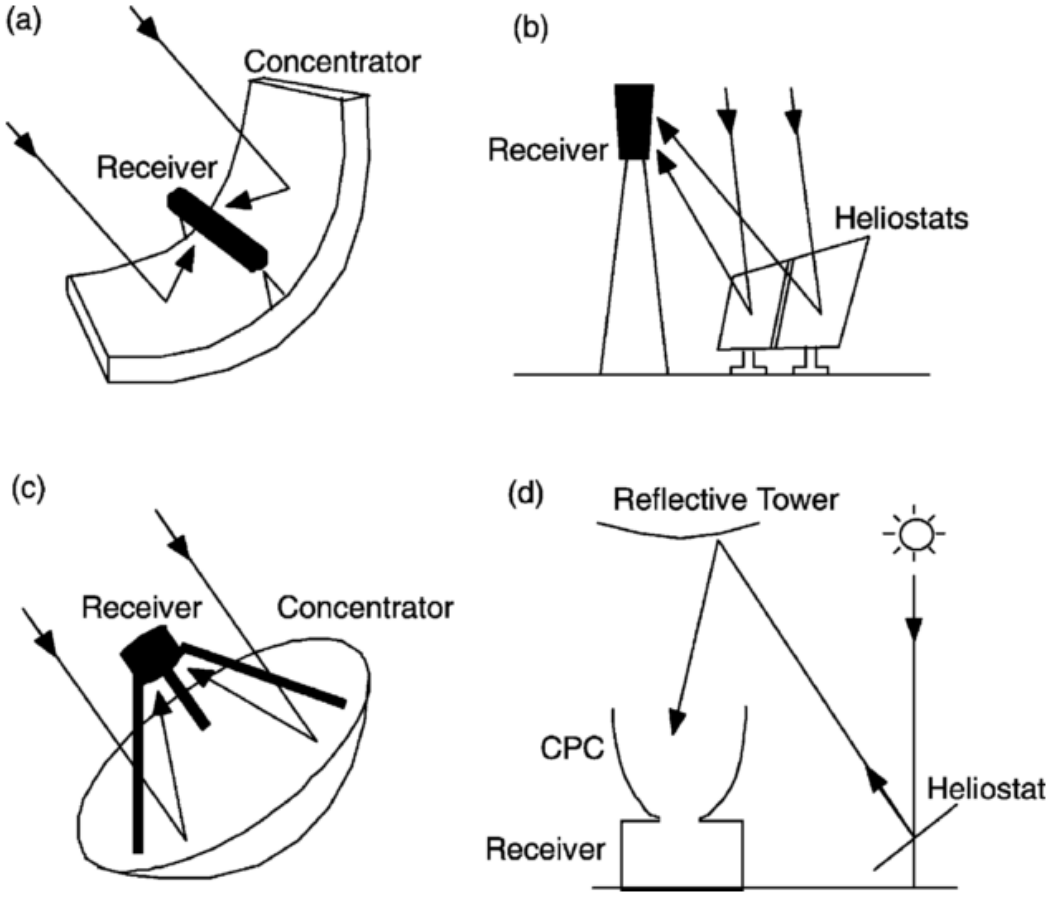

Figure I-2. Main concepts of large-scale solar concentrating systems :(a) parabolic trough, (b) central power tower, (c) dish type, and (d) double concentration [1]

I - 2. Thermochemical two-step water splitting cycle system with cerium oxide

Hydrogen production from water is one of the most important long-term goals in solar fuel production. Many investigators have studied the feasibility of hydrogen production by direct water splitting at high temperatures [9–13]. In 1977, Nakamura reported the investigation of the possibilities of direct thermochemical water splitting by utilizing solar heat at high temperatures [10]. It was shown that the thermo-dynamic requirements for the direct thermal splitter, or decomposer, are difficult to realize from the structural viewpoint and that existing separation methods are not applicable for such a decomposition process (mainly due to the extremely high operation temperatures.2500 K) if sufficiently high thermal efficiency is to be obtained.

And Kogan [13] also reported that solar thermal direct water splitting presents a formidable technological task. In the process under development at the WIS/Israel, water vapor is partially decomposed in a solar reactor at temperatures approaching 2500 K. Hydrogen is separated from the hot mixture of water splitting products by gas diffusion through a porous ceramic membrane. Kogan described the problems encountered during the development of the solar thermal water splitting process as follows:

Very high solar reactor temperatures must be achieved by secondary concentration of solar energy.

- Material problems are encountered in the manufacture of the solar reactor.

- Special porous ceramic membranes must be developed, which resist clogging by sintering at very high temperatures.

As discussed above, the challenges of direct splitting are probably too difficult to solve, so it must find to other methods to achieve the splitting of water into hydrogen. In order to reduce the reaction temperature and eliminate the need for high-temperature gas separation, various processes for the production of hydrogen by multi-step thermochemical water splitting have been proposed.

Among solar fuel production systems, the thermochemical two-step water-splitting cycle via a metal-oxide or redox pair material has been tested for feasibility [14, 15]. Two-step metal-oxide processes consisting of a regeneration step (O_2 release combined with the absorption of solar energy) and a water-splitting step (H_2 generation) are not numerous. The reaction system can be written as follows:

Step 1. Thermal reduction (endothermic) step

$$M_xO_y \rightarrow M_xO_{y-1} + 1/2O_2$$

Step 2. Water decomposition (exothermic) step

$$M_xO_{y-1} + H_2O \rightarrow M_xO_y + H_2$$

In general, two step cycles can be divided into two categories; volatile and non-volatile. Non-volatile cycles utilize metal oxides which remain in the solid state during reduction, while volatile redox cycles consist of metal oxides that undergo gas–solid phase transitions. In general, volatile reactions have a greater oxygen exchange capability than non-volatile reactions (more O_2 release/uptake, and thus fuel production, per mass of oxide) and reduction is thermodynamically more favorable due to the increased entropy generated resulting from gas phase products. Nevertheless, the volatile products must be quenched rapidly to avoid recombination, and to date this issue has not been solved in an energetically efficient fashion [12].

Non-volatile metal oxides cycles can be further categorized into two subcategories, namely stoichiometric and non-stoichiometric cycles. Stoichiometric reactions generally form solid solutions upon reduction (i.e. $Fe_3O_4(s) \rightarrow FeO–Fe_3O_4(s)$ [10]) and Fe^{3+} is partially reduced to Fe^{2+}.

Non-stoichiometric oxides remain crystallographically stable while the lattice accommodates changes in anion or cation vacancies concentrations (i.e. $CeO_2(s) \rightarrow CeO_{2-\delta}(s)$ [13]). For both stoichiometric and non-stoichiometric cycles, doping or substitution strategies are often employed to affect their thermodynamic, kinetic and physical properties. For example, doping ceria with Zr^{4+} is known to increase its oxygen storage capacity due to its ability to destabilize the fluorite lattice [14]. In general, stoichiometric reactions have a greater oxygen storage capacity than non-stoichiometric reactions, but are hindered by slower reaction kinetics (controlled by either bulk solid state diffusion or surface reactions) and poor stability (either chemical or morphological), properties which are practically related to $\eta_{solar\text{-}to\text{-}fuel}$ because they are directly tied to the specific reactor design chosen [12].

So far, various candidate redox pairs have been suggested and tested to validate hydrogen production via two-step water-splitting systems. The use of metal oxides as substrates for the thermochemical production of hydrogen was suggested by Nakamura (1977), who demonstrated cycling between Fe_3O_4 and FeO [10]. The two step water splitting cycle using Fe_3O_4/FeO could be represented as:

Step 1. Thermal reduction (endothermic) step

$$Fe_3O_4 \rightarrow 3FeO + ½\ O_2$$

Step 2. Water decomposition (exothermic) step

$$3FeO + H_2O \rightarrow Fe_3O_4 + H_2$$

Moreover, ZnO/Zn two-step cycles have been suggested and tested by Steinfeld (1998, 2002), and others [15, 16]. The reaction process was tested using H_2O/Co_2 splitting, represented as:

Step 1. Thermal reduction (endothermic) step

$$ZnO \rightarrow Zn + 1/2O_2$$

Step 2. Water decomposition (exothermic) step

$$Zn + H_2O \rightarrow ZnO + H_2$$

$$Zn + Co_2 \rightarrow ZnO + Co$$

The resulting ZnO is recycled to the first step to close the material cycle, with net reactions $H_2O \rightarrow H_2 + ½\ O_2$ and $CO_2 \rightarrow CO + ½O_2$.

However, these metal oxides require high temperatures for the thermal reduction step and additional unit operations such as gas separation processes. A major problem for ferrite cycles is the rapid deactivation of iron oxide particles during the regeneration process.

This is because of high-temperature melting and sintering of iron oxide particles [17].

Recently, ceria has received considerable attention as a redox pair for two-step water-splitting hydrogen production systems. The hydrogen production based on ceria as a redox pair was first proposed by Abanades (2006) [18].

The two step water splitting cycle based on nonstoichiometric ceria is represented by

$$CeO_2 \rightarrow CeO_{2-\delta} + 1/2\delta O_2 \qquad \text{(Thermal reduction or T-R step)}$$

$$CeO_{2-\delta} + \delta H_2O \rightarrow CeO_2 + \delta H_2 \qquad \text{(Water decomposition or W-D step)}$$

The T-R step (Thermal reduction) is highly endothermic and proceeds over 1400 ^{o}C; endothermic heat is supplied by concentrated solar radiation and oxygen is released. In this first step, ceria is thermally reduced to a nonstoichiometric state differentiated by the extent of oxygen represented by δ. The reduced ceria in the first step can react with steam in the subsequent W-D step. The W-D step (Water decomposition) is exothermic and proceeds below 1000 ^{o}C to produce hydrogen. [19–23].

Several studies have also considered the suitability of ceria for thermochemical solar fuel production. For example, thermochemical

studies have been performed for ceria pellets or powder and CO_2 splitting with reticulated pure ceria structures [24-30]. However, most implementations of a two-step water-splitting hydrogen production system with ceria have been performed at laboratory scale and tested with artificial solar simulator systems involving partially solar-driven demonstration sources at small scale.

I - 3. Objectives of this paper

In our previous works, small CeO_2/MPSZ (MgO-partially stabilized zirconia) foam devices were prepared by the spin-coating method, and tested on reactivity using 3 kW_{th} sun-simulator with Xe-arc lamps. The two-step water splitting was successfully demonstrated with the small CeO_2/MPSZ foam devices using 3 kW_{th} sun-simulator [31].

Niigata University has developed ceramic foam devices whose foam matrix is made of MgO-partially stabilized zirconia (MPSZ). The MPSZ foam matrix has superior characteristics as compared with SiSiC and SiC [31, 32], including high heat resistance and chemical inertness with ceria at high temperature. Also, the foam structure can effectively absorb light irradiation owing to its large specific surface area. These foam devices were possible for multi-cycling the two-step water splitting process [31]. Niigata University started an international project for solar two-step water splitting cycle using foam device reactor: a joint research project between Niigata University (Japan) and Inha University (Korea), started in autumn 2008. The reactive water splitting foam device was developed and prepared by Niigata University, and involves coating a zirconia foam with reactive, zirconia-supported metal oxide particles [31]. The objectives of the project are to develop reactive foam devices with metal oxide as the working material, to design and fabricate a windowed solar reactor

with the reactive foam device, and finally, to demonstrate its performance in sunlight with a 5 kW_{th} dish-type solar concentrator [33].

Recently, a new joint project on the solar demonstration of water splitting reactor using foam device of CeO_2/MPSZ was started between Niigata University (Japan) and– Korean Institute of Energy Research, KIER (Korea) from 2012. The project aims to develop a novel-type of solar water splitting reactor with reactive cerium oxides-coated foam devices to produce solar hydrogen from water, and to demonstrate its performances sunlight with a 45 kW_{th} solar furnace.

In this paper, the solar reactor with ceria-coated MPSZ foam device is up-scaled for solar demonstration using a 45kW_{th} solar furnace at KIER. The design, numerical simulation, and solar demonstration of the up-scaled solar reactors were carried out in this works.

Chapter II

Solar demonstration of thermochemical two-step water splitting cycle using CeO_2/MPSZ ceramic foam device by 45 kW_{th} KIER solar furnace

II - 1. Introduction

In this chapter, the large-sized flat type CeO_2/MPSZ (MgO partially stabilized zirconia) foam devices were first tested using the 45 kW_{th} solar furnace at KIER. The first-type of the up-scaled solar reactor with the flat disk foam device coated with ceria was designed and fabricated. Solar demonstration of the solar reactor is carried out at the KIER 45 kW_{th} solar furnace.

II - 2. Experimental setup and demonstration

II - 2 - 1. Preparation of ceria-coated foam device

Fig. II-1 shows a representative photograph of a disk type zirconia foam matrix before coat the ceria which composed of MPSZ (MgO partially stabilized zirconia). CeO_2/MPSZ foam device was prepared by using a spin coating method. The spin coating method was suggested and validated by N.Gokon [34]. In general, the preparation of the foam device required a great deal of time to be spent in the coating processes, and also required a number of calcination sat high temperatures. In the case of the spin-coating method, however, after impregnating the ceramic foam with a slurry containing high solid content, the impregnated foam is spun at a high rate that is sufficient to remove the excess slurry loaded on the foam and to prevent clogging of the pores of the foam structure. Thus, the spin-coating method makes it possible to use slurry with much higher solids content in the coating of ceramic foam than is used in a wash-coating method. Therefore, with a much-reduced coating process and preparation time, the foam device was prepared using dense slurry. In short, the advantages of the spin-coating method in the preparation of water-splitting foam devices are:

1) The preparation period can be shortened

2) The coating processes are reduced in comparison to a wash-

coating method [34].

Fig. II-2 shows the sequence of steps in the spin-coating method to achieve the desired amount of coated ceria on the foam matrix.

The yellow white-colored zirconia foam had a diameter 150 to 200 mm, thickness of 25 to 30 mm and a cell size of 7 to10 cpi (cell number per linear inch). The disk-shaped zirconia foam was impregnated with containing slurry aqueous solution consisting of 10 g of CeO_2 powder, 33 cm^3 of the distilled water, 0.10 g of dispersant (Sodium polyacrylate) and 0.10 of binder (Acrylic resin). The impregnation process was performed under reduced pressure in order to remove bubble of air contained in the foam inside and homogeneously coat the zirconia foam. The impregnated zirconia foam was set in a spin coater and then was rotated at rates of 600-1000 rpm in order to remove excess slurry on the foam. After rotation, the foam was heated up to 1100 ^oC and the foam device was calcined for 1 hour in an air stream. This process of spin coating was repeated 10 to 15 times for achieve desired weight percent value.

Consequently, the CeO_2 loaded foam device was calcined at 1350 ^oC for 1 h in an air stream. Table II-1 shows the properties of prepared foam devices which are having different size and CeO_2 weight percent. In this work, totally three ceria coated foam devices were prepared and tested. Fig. II-3 is the photograph of ceria coated CeO_2/MPSZ foam device showing whiter color than before spin-coating process.

In this work, the MPSZ foam matrix used rather than SiSiC or SiC, which have been used by other researchers as a medium for concentrated solar heat absorption or redox pair support, because MPSZ has superior heat resistance and chemical corrosion resistance [34]. The advantage of using foam matrix is that it provides a large specific surface area for effectively absorbing solar radiation. Moreover, CeO_2 react with the MPSZ foam matrix at high temperatures to form a solid–solution (ZrO_2-CeO_2). This solid-solution can react with steam to produce hydrogen. However, the reaction product SiSiC (SiC) with CeO_2 does not react with steam to produce hydrogen [34-43].

Figure II-1. The MgO partially stabilized zirconia foam matrix before the ceria coat.

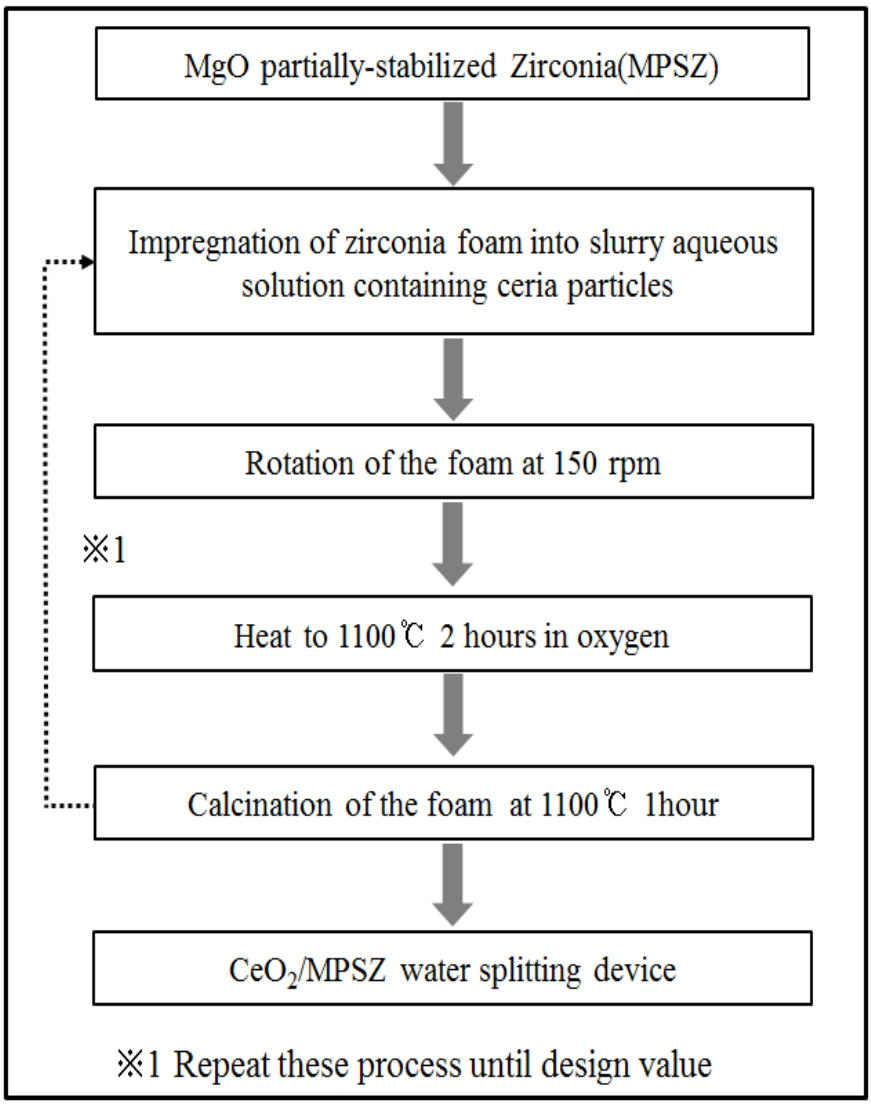

Figure II-2. Sequence of steps in the spin-coating process for preparing the CeO_2/MPSZ foam device.

Table II-1. CeO_2/MPSZ foam devices for two step water splitting cycle hydrogen production.

Device No	Diameter (mm)	Thickness (mm)	Weight of Device (g)	Weight of loaded CeO_2 (g)	Ceria loading (wt %)	Mole of loaded CeO_2 (mole)
1	150	30	473.6	82.88	17.5	0.4818
2	200	25	993.5	190.75	19.2	1.109
3	150	30	670.8	268.3	40	1.559

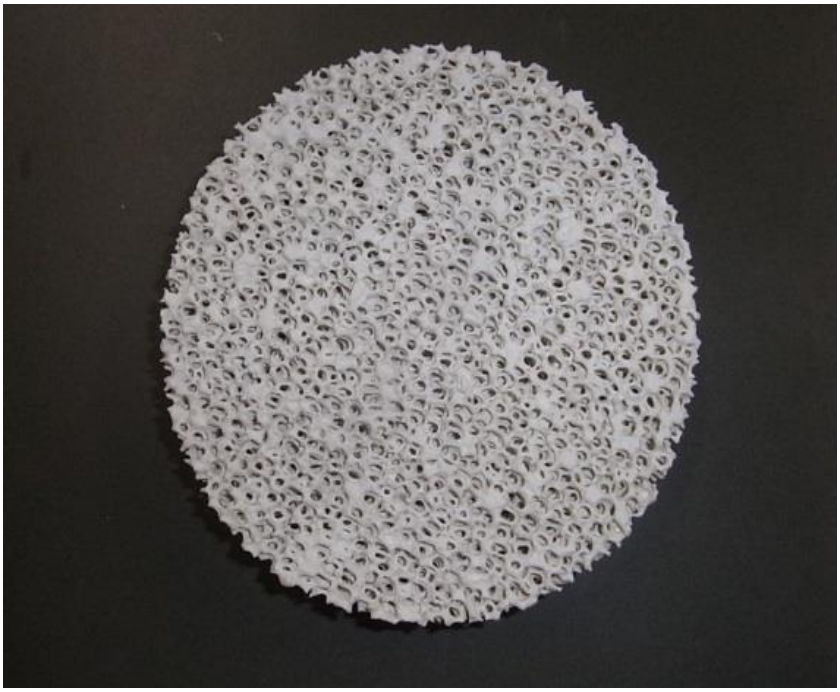

Figure II-3. The ceria coated foam device (CeO_2/MPSZ) for hydrogen production via solar demonstration.

II - 2 - 2. Solar reactor

A feature of solar chemical reactors is that the source of process heat is concentrated solar radiation. Directly irradiated reactors have the advantage of providing efficient radiation heat transfer directly to the reaction site where the energy is needed. By the appreciate condition, direct irradiation may enhance photochemical kinetics. The solar reactor equipped transparent quartz window to pass concentrated solar radiation for directly heating redox materials [10]. Fig. II-4a, and b is the design drawings and 3D drawing of reactor equipped a quartz window for direct solar irradiation. For the quench of the large quartz window (267 mm), aperture flange in which involved inert cooling channel was connected to the distilled water chiller. The major component of solar reactor is a conical cup for holding the device made by Inconel steel connected to reactor main body and a quartz window for direct introduce of concentrated solar radiation. Furthermore, to avoid the subservient reaction, the inner surface of main reactor body in which made by stainless steel 304 was covered by Inconel steel sheet. The inner diameter is 269 mm due to for next trial of several different device sizes and length of the solar reactor was 390 mm, respectively. The inlet ports were distributed to 4 lines; it is connected to the annular gap which is designed inside of the reactor by circumference direction around of device. Outlet was 1 port which is passing the gas that penetrated the foam device.

For the measurement of temperature on the foam device surface, several thermocouples were mounted in the reactor, and the front of the foam device, the R-type thermocouples in the central area of device 2, the side area 1, and the back side of the device K-type thermocouple 2 was installed. One of the R-type thermocouple which is installed into the center of the front of device is suggested to monitoring of temperature distribution, and another one is for the providing the reference temperature value to control the blind of solar furnace system. Fig. II-5 is the photographs of solar reactor aperture where equipped with foam device and thermocouples. In order to fixate the thermocouples which are front of the device, high temperature adhesive material was used as Fig. II-6.

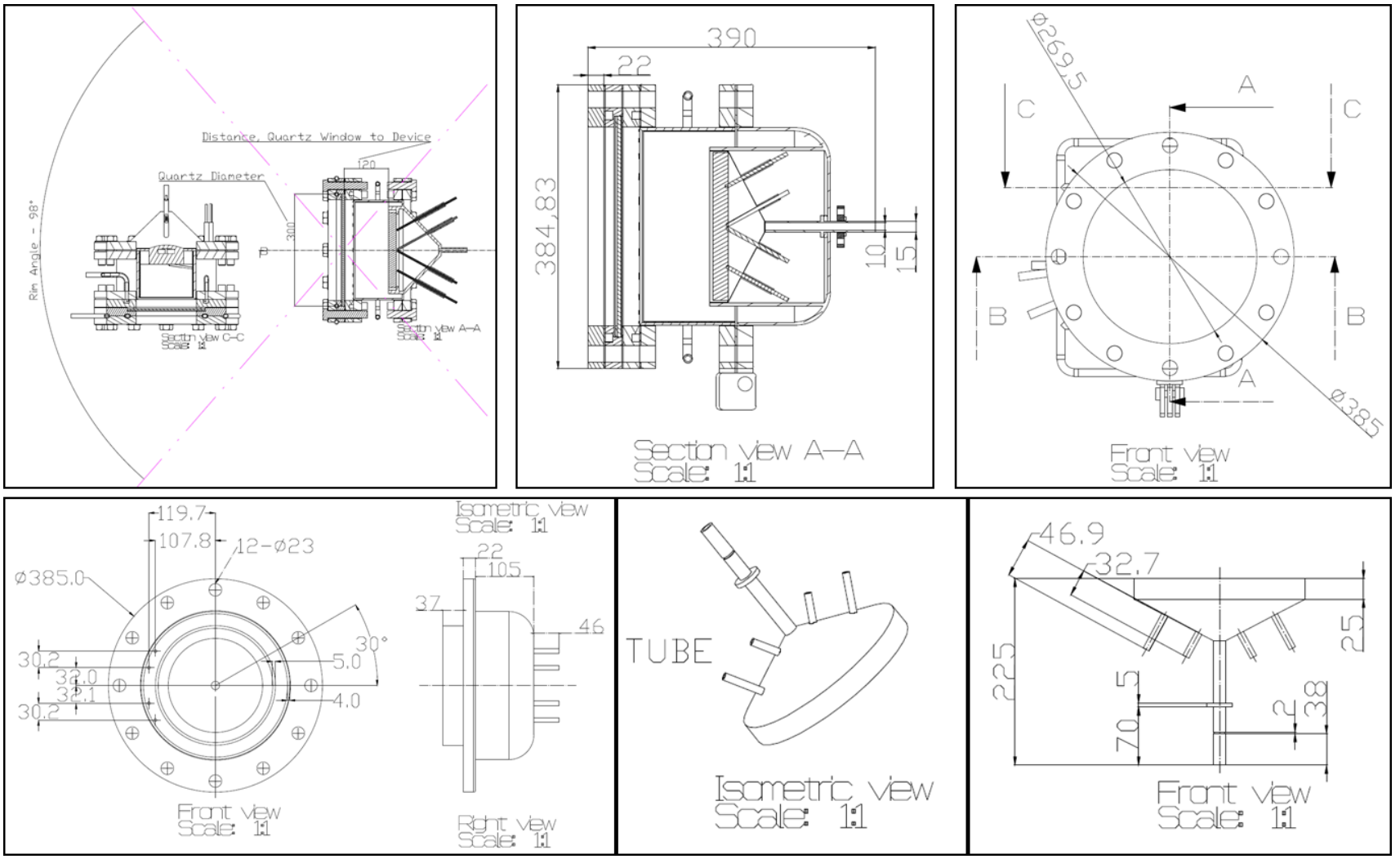

Figure II-4a. Design drawings of first type solar reactor for solar demonstration.

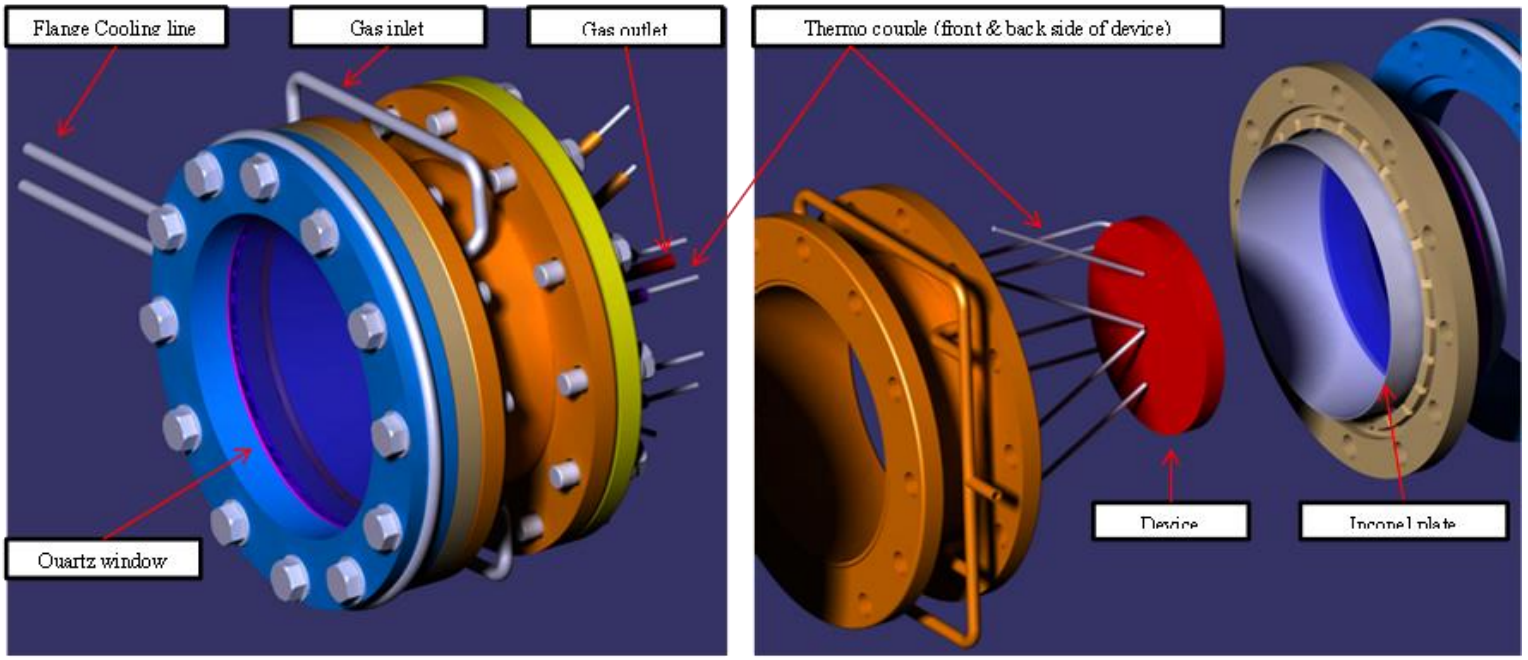

Figure II-4b. Design of windowed first type solar reactor for solar demonstration.

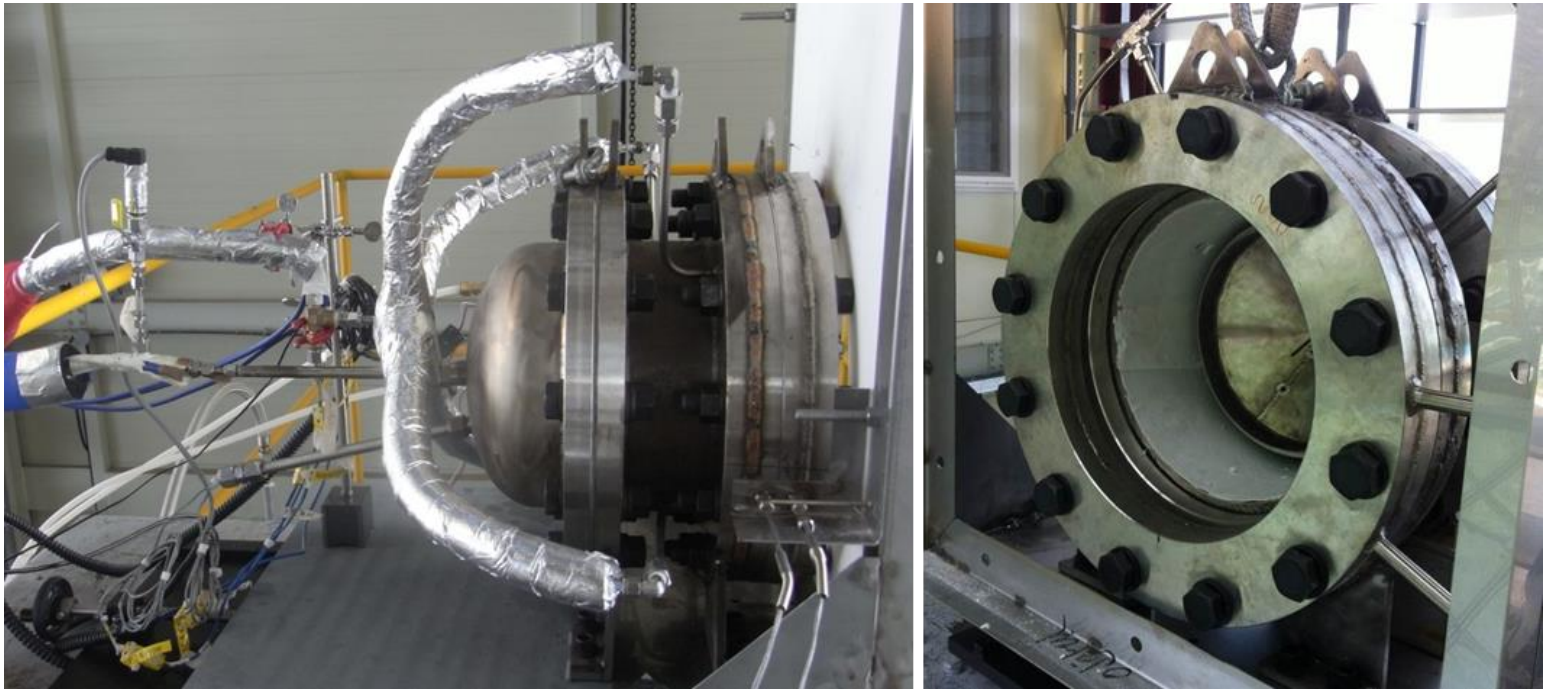

Figure II-5. Photographs of fabricated first type solar reactor for solar demonstration.

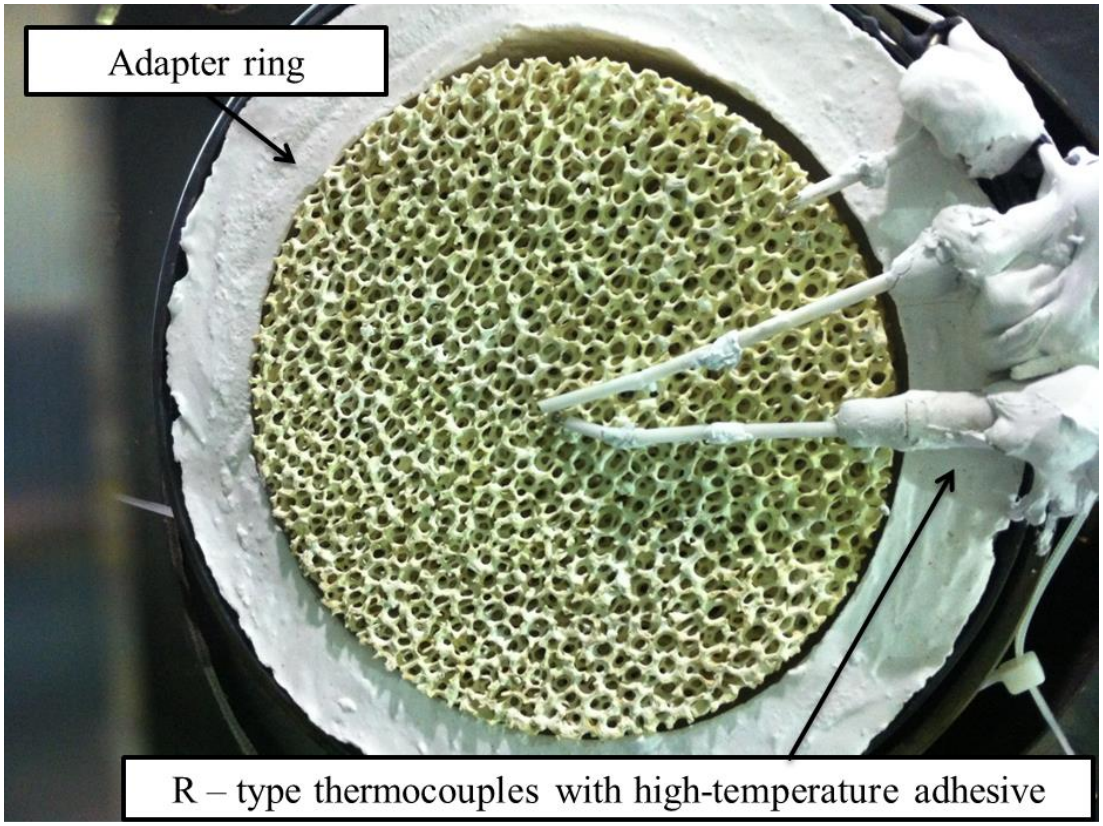

Figure II-6. Detailed photograph of device adapter part and R-type thermocouples.

II - 2 - 3. KIER solar furnace system

Fig. II-7 and Table II-2 shows a photograph and specifications of 45kW$_{th}$ KIER solar furnace system. The solar furnace system was installed in KIER (Korea Institute of Energy Research), Korea.

Since KIER researchers developed the KIER solar furnace (refer to Fig. 1a) in 2009, they have made modifications and improvements for better performance and operation. A flat reflector is comprised of aluminum-back-coated mirror facets, and its total area is 9.305 × 9.387 (～87) m^2. It tracks the sun in elevation and azimuth angle directions with two servo motors so that the reflected sunlight illuminates an indoor parabolic reflector parallel to the optic axis. Inner and outer radii of the parabolic reflector are respectively 0.75 m and 4.5 m so that its aperture area roughly becomes 62 m^2. Focal length is 4.98 m, and the corresponding rim angle becomes 48°. The parabolic reflector is also comprised of back-coated mirror facets, but coating material is silver. It is 35 m apart from the flat reflector to the south, and an array of rotating strip shutters is installed in between to adjust the amount of solar radiation. Sunlight blockage occurs due to reflector facet frames, shutter thicknesses, stage supporting structures, and so on. As a result, the effective aperture area in the parabolic reflector is reduced to approximately 85% of the designed area. A movable stage to accommodate solar receivers or chemical reactors lies around the focal

point.

The thermal capacity of the system is about 45 kW thermal powers and the maximum concentration ratio is 5050 suns. KIER solar furnace system include the blind and shutter for the control of the intensity reflected solar radiation [44].

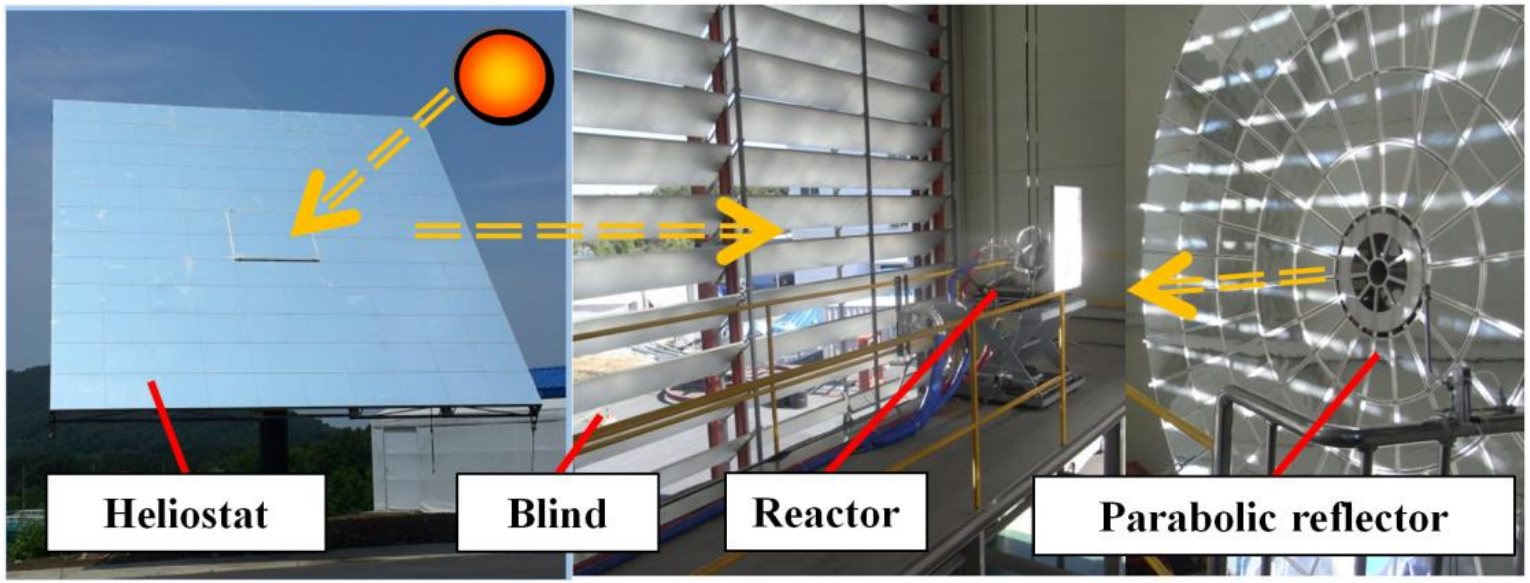

Figure II-7. A photograph of KIER 45kW$_{th}$ Solar furnace system

Table II-2. Specification of 45 kW_{th} KIER solar furnace system.

Heliostat area (m^2)	Parabolic mirror area (m^2)	Distance between heliostat and parabolic mirror (m)	Focus length (m)	Rim angle (^{o})
87.35	61.82	35	4.98	48

II - 2 - 4. Solar demonstration of two-step water splitting cycle

Fig. II-8 is represents experimental setups of the thermal reduction step (T-R) and water-decomposition steps (W-D) of thermochemical two-step water splitting cycle conducted by use of the CeO_2/MPSZ foam device. A highly purity (99.99%) N_2 gas stream in range of 2000 to 4000 mL/min was introduced from the inlet of the foam device into the solar reactor and passed through the foam device in the outlet line connected with the backside of the reactor. The solar reactor in which set up on the table in stair between heliostat and parabolic reflector was exposed to a concentrated solar radiation by solar furnace concentrating system. The surface of the ceramic foam device was set on backside in range of 7 to 10 cm position from the focal point of the concentrated solar furnace system. Because the shape of flux distribution of 45 kW_{th} KIER solar furnace is similar to Gaussian distributions, focal distance (or device position) of foam device was considered to obtain more uniform flux distribution as possible as [44].

Before the T-R step, it takes the heat up (or warm up) time of the reactor body in order to reduce a thermal shock from high concentrated irradiation abruptly. Fig. II-9 is the photographs of solar reactor under the concentration of solar radiation. One side of the CeO_2/MPSZ foam device was irradiated for 30 ~ 60 min in order to perform the T-R step. The temperature of CeO_2/MPSZ foam device for T-R step was controlled in

range of 1400 to 1600 ºC using R-type thermocouples placed at the center and side. After the T-R step, concentrated irradiation intensity was decreased using the blind shutter control for subsequent step and the gas stream introduce into the solar reactor was changed from N_2 to H_2O/N_2 mixture inside of steam generator in order to perform the W-D step.

By the DNI (Direct normal Irradiation) data acquiring real-time, the blind shutter was opened and closed automatically in order to set the aim temperature. The temperature of CeO_2/MPSZ foam device for the W-D step was controlled in range of 800 to 1100 ºC. An H_2O/N_2 gas mixture was produced by steam generator that designed coil type structure with 3 kWe heat capacity and distilled water was supplied 3-5 mL/min(liquid) to the steam generator by peristaltic pump during 20 ~ 60 min(W-D step). The T-R and W-D steps were repeated in alternately 7 cycles at a maximum with 15 cm/17.5 wt% CeO_2/MPSZ ceramic foam device, and 20 cm/19.2 wt% CeO_2/MPSZ ceramic foam device 10 cycles.

After the W-D step in each cycle, the remaining hydrogen and steam in the reactor were exhausted by passing N_2 gas through the reactor. This passing of N_2 gas was continued for several minutes before the next T-R step. During the purging of remained steam, the temperature of CeO_2/MPSZ ceramic foam device was persisted W-D step condition.

A parts of effluent gas was sampled and hydrogen concentration in the effluent gas was determined by gas chromatography (GC; Younglin Acme 6000) using TCD (thermal conductivity detector) with 3 min interval. The

amount of hydrogen evolved during the W-D step was determined to the profile of hydrogen production [45].

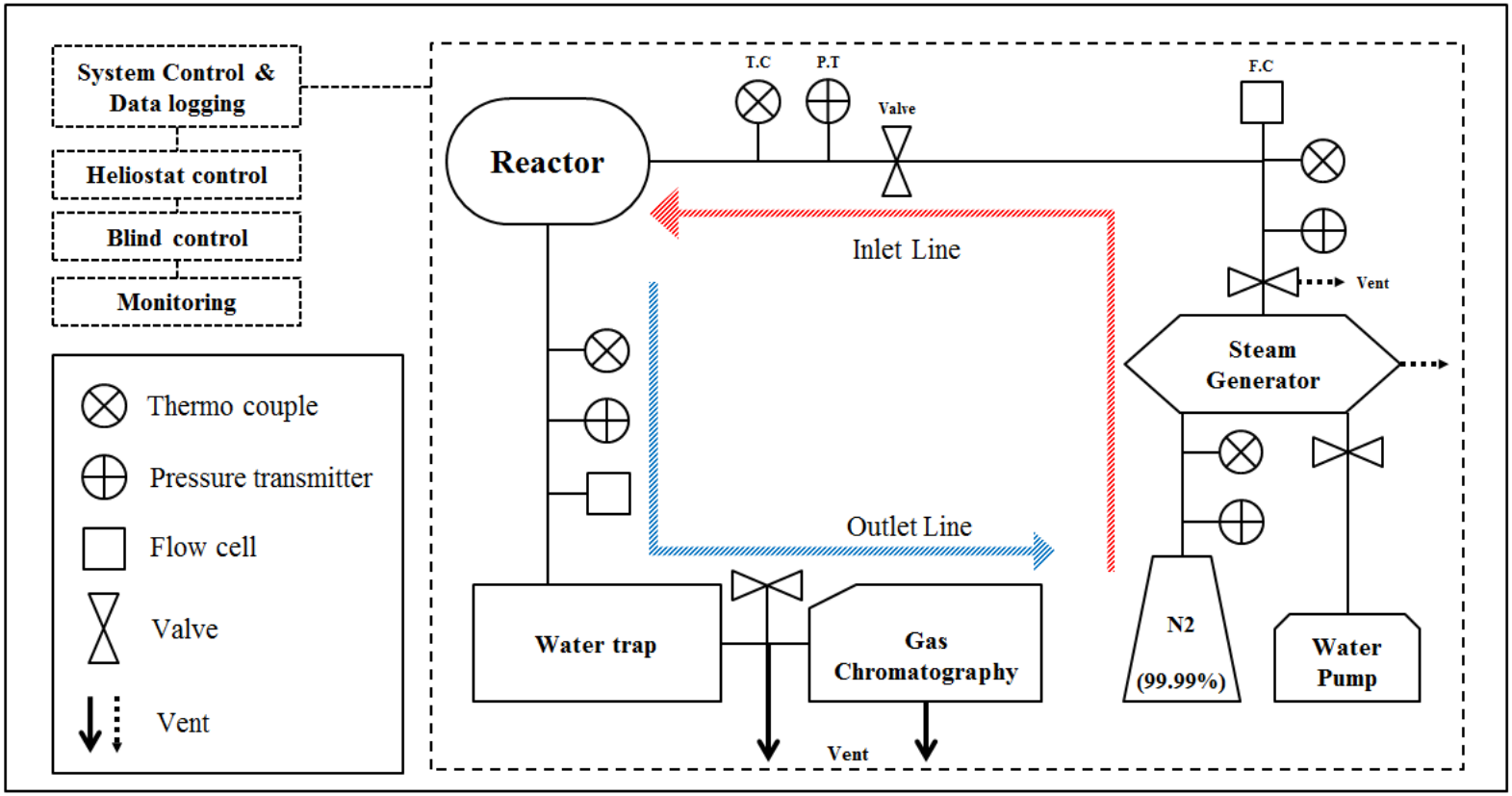

Figure II-8. Experimental setups of the T-R and W-D steps of thermochemical two-step water splitting reaction system

II - 3. Results and discussion

II - 3 - 1. Results and discussion of 15 cm/17.5wt% foam device

Fig. II-9 shows a time variation of the foam device temperature and hydrogen production rate of 1st cycle of thermochemical two-step water splitting cycle with 15 cm (17.5 wt %) CeO_2/MPSZ foam device. The experiments of solar-driven demonstration were performed from 16/10/2012 to 20/11/2012 in KIER, Daejeon, Korea. The temperatures of the device at the center position was recorded 1400 to 1600 ^oC for T-R step, and 700 to 1100 ^oC for the subsequent W-D step. Because of the sun condition, experiment time was limited to one or two cycles per day. After the one day experiment, the temperature of reactor and foam device was cooled down to ambient temperature naturally.

On other hand, when the weather conditions were possible to two cycles per day, the temperature was kept 1000℃ between the cycles. Fig. II-10a to g shows hydrogen production rate profile during the W-D step of the each cycle. As can be seen here, hydrogen was successfully produced from CeO_2/MPSZ foam device by the thermochemical two-step water-splitting cycle with the KIER 45kW_{th} solar furnace.

The rate of solar hydrogen production during the W-D step rapidly increased after steam injection, and attained to a maximum rate. After reach to the maximum rate, the hydrogen production during the W-D step gradually decreased. The amount of hydrogen production was calculated

from the integration of the profile. Table II-3 shows the total hydrogen production amount of each of cycles and experiment condition.

During the 3rd and 4th cycles with 15cm (17.5 wt %) CeO_2/MPSZ foam device, the adhesive material which used for support and fix the thermocouples were melted and then, black materials produced and attached inside of reactor and quartz window surface. Fig. II-11a to c is the photograph of black materials which attached reactor inside, inner surface of quartz window and result of EDS (Energy-dispersive X-ray spectroscopy) analysis. Energy-dispersive X-ray spectroscopy (EDS, EDX, or XEDS) is an analytical technique used for the elemental analysis or chemical characterization of a sample. It relies on an interaction of some source of X-ray excitation and a sample. Its characterization capabilities are due in large part to the fundamental principle that each element has a unique atomic structure allowing unique set of peaks on its X-ray emission spectrum [46].

EDS spectrum of the sample collected from the black materials which covered on the quartz window. It shows a peak cause by X-rays and carbon was detected 93.61 atomic percent as shown Fig. II-11c. Si also detected in the peak for 1.54 atomic percent, it seems that collected from the quartz window surface. The EDS analysis result shows that almost component was composed of carbon.

During 4th cycle, quartz window was damaged due to these carbons were clung to the surface of quartz and increased the temperature of quartz. So

the thermocouples install method and quartz window was changed in order to improvement of solar demonstration. After the thermocouple installation method change, during the preheating time of 5th cycle the remained carbon was removed by the N_2 stream almost and the two-step water splitting cycle was performed 2 cycles more.

After the 7th cycle with 15cm/17.5 wt% CeO_2/MPSZ foam device, then 20cm/19.2 wt% CeO_2/MPSZ foam device was tested. Fig. II-12 shows the hydrogen production profiles through 7 cycles with a time sequence by using 15cm/17.5 wt% foam device. At 3, 4, and 7 cycle, hydrogen production amount shows higher peak than other cycles. This result has a possibility of the additional reaction. Carbon can participate to reactions which produce the hydrogen as following equation. ($C + H_2O \rightarrow CO + H_2$) After the 4th cycle, the carbons were excreted by the N_2 purging. However it was impossible eliminate the carbon which attached on the foam surface perfectly, then it leads to results of 7th cycle which is including subservient reactions.

By the use of 15 cm/17.5wt% CeO_2/MPSZ foam device, the solar-driven demonstration of thermo-chemical two-step water splitting cycle using ceria coated zirconia foam device was performed successfully. Trough 7 cycles with 15cm/17.5 wt% CeO_2/MPSZ foam device, total hydrogen amount reached 4573 mL. These results will be discussed with subsequent foam device (20cm/19.2 wt %) results at the next section.

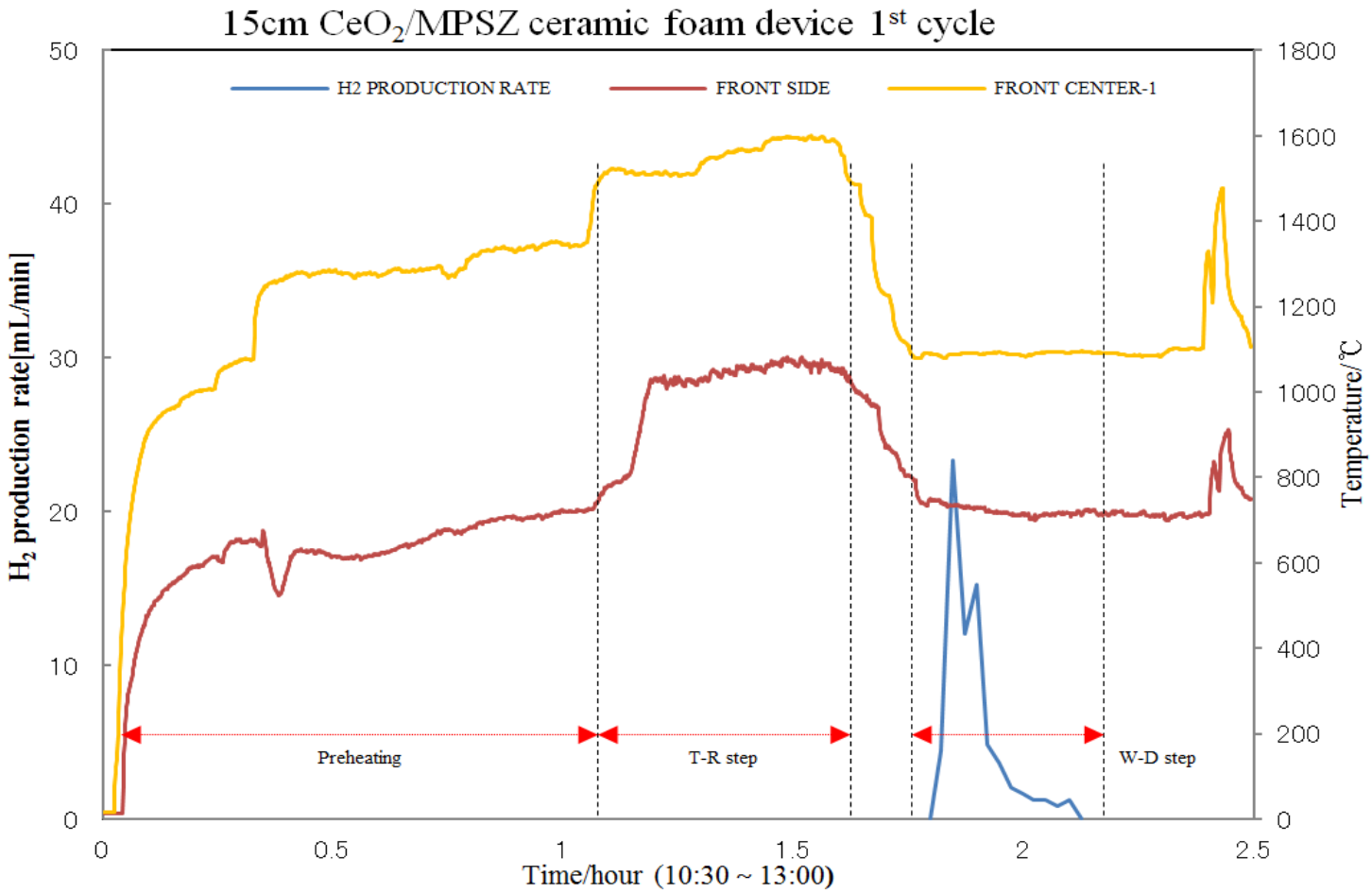

Figure II-9. The Temperature of foam device during experimental and Hydrogen production rate (15 cm/17.5 wt% foam device)

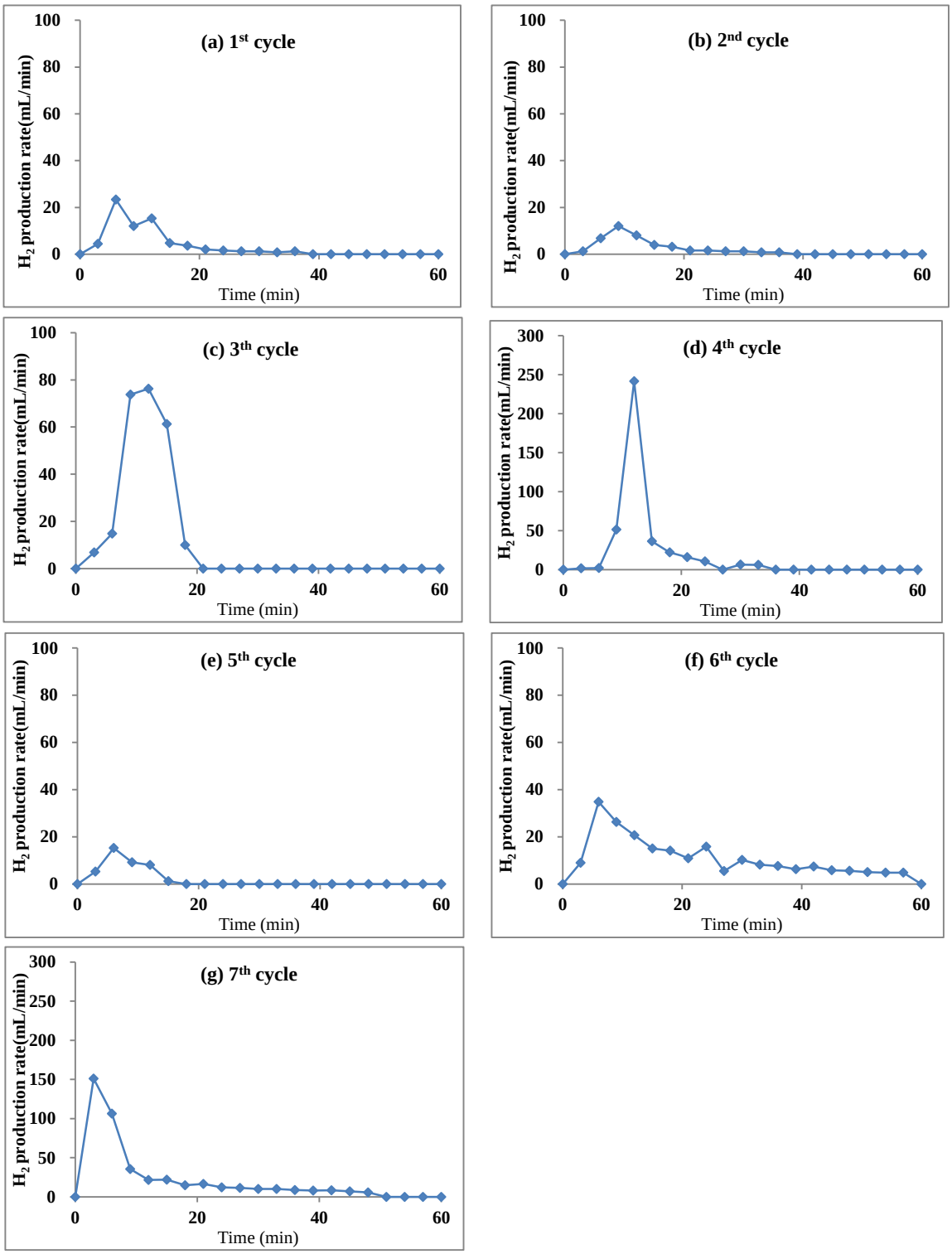

Figure II-10a to g. The Hydrogen production rate of each cycle using 15 cm (17.5 wt%) foam device (4^{th} and 7^{th} cycle has different Y-axis scale)

Table II-3. Test condition and produced hydrogen amount by 15cm/17.5wt% ceria coated foam device.

Cycle Number	1	2	3	4	5	6	7
Date	2012. 10. 16		2012. 10.18	2012. 10. 19		2012. 10. 28	
Device	15 cm/17.5 wt% ceria coated foam device						
T-R step Time (min)	45	45	55	30	15	30	35
W-D step Time (min)	30	40	30	30	30	30	30
Total amount (mL)	215.6	127.1	728.1	1183	116.3	654.5	1347.7
Conversion (%)	3.67	2.16	12.39	20.12	1.98	11.13	22.93

(a) device (b) quartz (c) SEM results

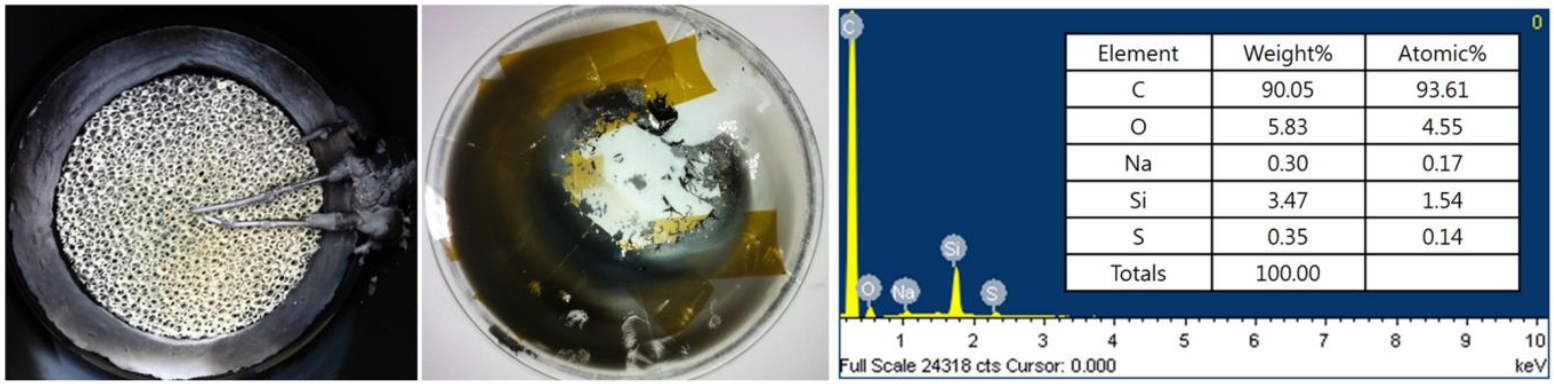

Element	Weight%	Atomic%
C	90.05	93.61
O	5.83	4.55
Na	0.30	0.17
Si	3.47	1.54
S	0.35	0.14
Totals	100.00	

Figure II-11a. The melted adhesive material (carbon based) was attached to foam device surface.

b. Quartz window was melted due to melted adhesive was attached to window surface then cracked.

c. The adhesive material was sampled and analyzed by the EDS, it was identified to carbon based material.

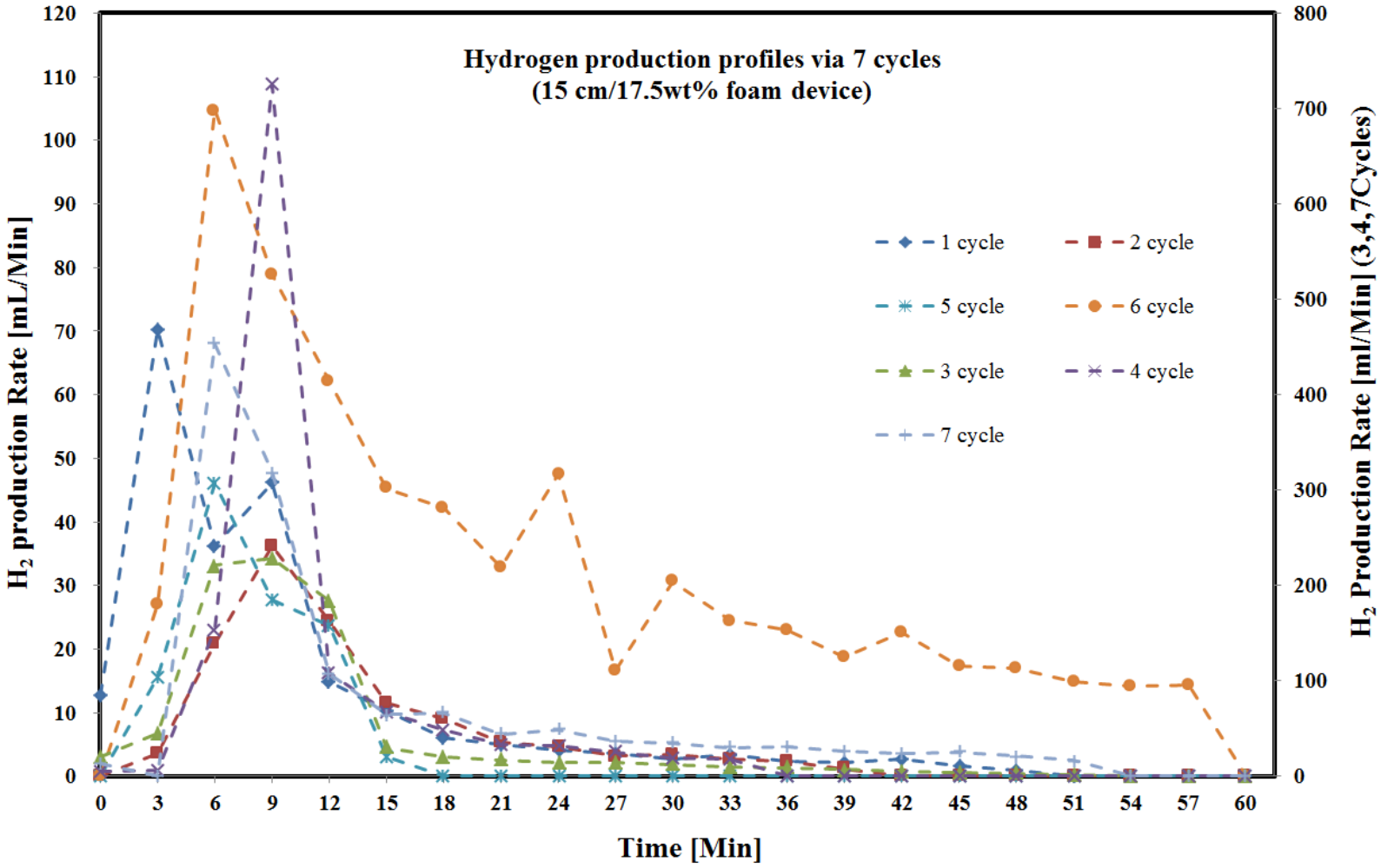

Figure II-12. Overall hydrogen production profiles through 7 cycles using 15cm/17.5wt% foam device

II - 3 - 2. Results and discussion of 20cm/19.2wt% foam device

The experiment of solar driven two-step thermochemical water splitting cycle was continued in order to develop the productivity of hydrogen and scale up of experiment. The next tested foam device is the 20cm/19.2wt% foam device as described to before section (as shown Table II-1).

The experimental condition and procedure was same as before process. However, the cycle number was expanded to 10 cycles. The experiment period was from 2012.11.20 to 2013.03.21. 1st and 2nd cycles were performed at 2012 year and then after a few enhancement of solar reactor, 3rd cycle was operated until to 10 cycle. Enhancement parts were fabrication of new thermocouples ports for exact measuring the foam device temperature and re-fabrication of steam generator for stable generation of H_2O/N_2 mixture gas.

Table II-4 shows the experimental conditions and hydrogen production at each cycle. The total hydrogen amount produce by 10 cycles reached to 2672.7 mL, and there are no subservient reaction was detected. The average hydrogen production amount per cycle is 267.2 mL. The 2nd cycle result shows the lowest hydrogen productivity for 76.7 mL and 9th cycle shows the largest hydrogen productivity for 748.5 mL.

During the solar demonstration experiment, monitoring process was improved. Before time when test the 15cm/17.5wt% foam device, CCD (Charge-coupled device) camera was applied to the operation system in order to monitoring of foam device surface condition. And it was used to just real time monitoring during the solar concentrating times. However, during the test of 20cm/19.2wt% foam device, CCD camera captured the device surface condition in sequence of step. Fig. II-13 shows the foam device surface condition captured by CCD camera. It shows the discoloration status of foam device surface.

Table II-4. Test condition and produced hydrogen amount by 20cm/19.2wt% ceria coated foam device.

Cycle Number	1	2	3	4	5	6	7	8	9	10
Date	11. 20.	11. 30.	2013. 03. 11.			2013. 03. 15.			2013. 03. 21.	
Input Power (kW)	13.19	16.29	13.91	12.69	12.88	13.28	11.50	11.40	17.17	12.93
T-R step Time (min)	25	40	40	50	50	35	30	35	50	30
Input Power (kW)	4.35	4.96	3.16	3.74	4.42	3.72	3.35	4.41	4.69	4.73
W-D step Time (min)	40	30	45	40	60	60	55	45	60	60
Total amount (mL)	443	76.7	137.3	128.9	416.9	249.9	111.7	171.3	748.5	143.5
Conversion (%)	3.27	0.57	1.01	0.95	3.08	2.18	0.83	1.27	5.53	1.06

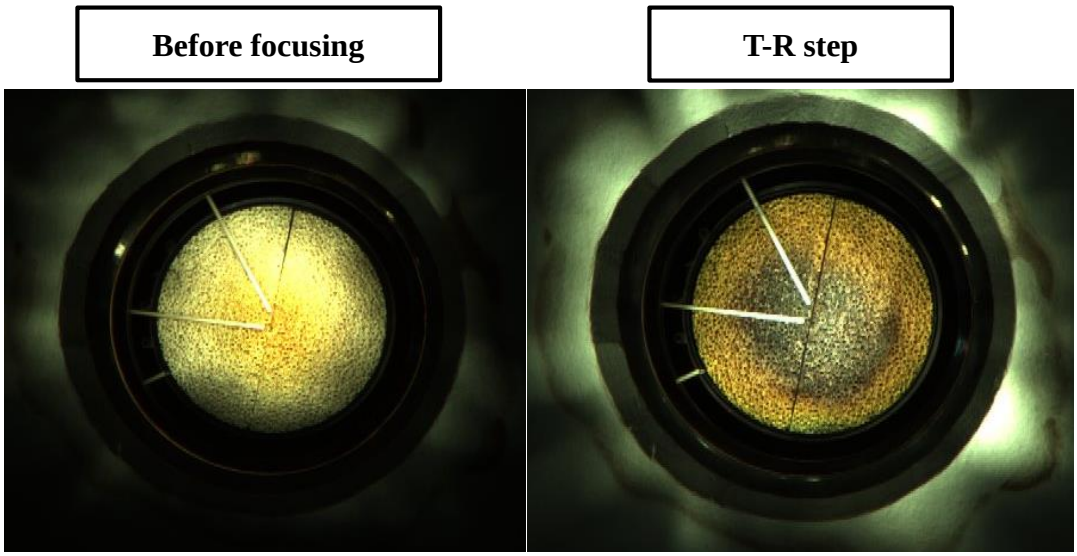

Figure II-13. CCD camera captured photograph during the solar demonstration. The change of device color due to reduction (dark color) - 20cm/19.2wt% foam device.

II - 4. Conclusion

After the solar demonstration, hydrogen was produced successfully with CeO_2/MPSZ foam device. And the results show significant information for up scaled solar reactor and clues of improvement to large scale solar fuel production system. By the 15 cm/17.5 wt% CeO_2/MPSZ foam device, the solar-driven demonstration of thermochemical two step water splitting cycle using ceria coated zirconia foam device was performed successfully. Trough 7 cycles with 15cm (17.5 wt %) foam device, total hydrogen amount reached 4573 mL. And with the 20 cm (19.2 wt %) CeO_2/MPSZ foam device, 10 cycles tested with hydrogen production amount 2672.7 mL.

The comparison of total hydrogen production amount per device shows that the 15cm/17.5wt% foam device production amount is larger than 20cm/19.2wt% foam device. However, it is because of subservient reaction which occurred during 3rd ~ 7th cycles of 15cm/17.5wt% foam device test. Especially, the amount of hydrogen production in 4th cycle is higher than other results. This result has a possibility of the additional reaction. Carbon can participate to reactions which produce the hydrogen as following equation (e.g. $C + H_2O \rightarrow CO + H_2$).

The activated area which parts of oxygen released from cerium oxide on the foam device is related with the solar irradiation intensity. The concentrated solar radiation by the dish reflectors has not homogeneous flux

distribution. It was observed by the CCD camera in which installed to center of dish reflector. The photographs which captured by CCD camera shows the different color change on the foam device surface due to the inhomogeneous flux intensity was affected to extent of reduction . To increase the reduction area of disk-shaped foam device, the flux intensity on the foam device surface has to consider carefully. In the next chapter, it was improved with the various operation methods challenge and by the device shape change or reactor redesigns.

After the every water decomposition step, the remained dark color area on the foam device where hydrogen produce reaction was not occurred was observed. It means loss of the opportunity in which hydrogen production process. On other hand, it is related with the internal flows of steam and N_2/H_2O gas mixture and partial pressure of steam. For the complete reaction from the activated surface, these factors have to optimize with consideration of solar reactors inside structure.

Chapter III

Improved operation of solar reactor for two-step water splitting H_2 production by ceria-coated ceramic foam device

III - 1. Introduction

In this chapter, the operation method of the solar reactor is improved. In order to increase the hydrogen productivity with CeO_2/MPSZ coated flat disk type foam device. Three different operation methods are tested. The gas flow direction and the focal spot position of concentrated solar radiation are changed in the three operation method.

III - 2. Experimental setup and operations

III - 2 - 1. Preparation of ceria coated foam device

Fig. III-1a and b shows a representative photograph of a ceria coated / MPSZ (MgO partially stabilized zirconia) disk type foam device and new fabricated foam device holder which including a steam nozzle for steam injection. The thermocouples for measure foam device temperature were installed to at the center and edge on the foam device surface.

CeO_2/MPSZ foam device was prepared by using a spin coating method same as before coating procedure. The white-colored zirconia foam has a diameter of 150 mm, thickness of 30 mm, and a cell size of 10 cpi (cell number per linear inch). In this chapter, a novel CeO_2/MPSZ foam device was made by supporting CeO_2 powder on MPSZ foam matrix with a target ceria loading of 40 wt% (weight percent), as explained Table III-1.

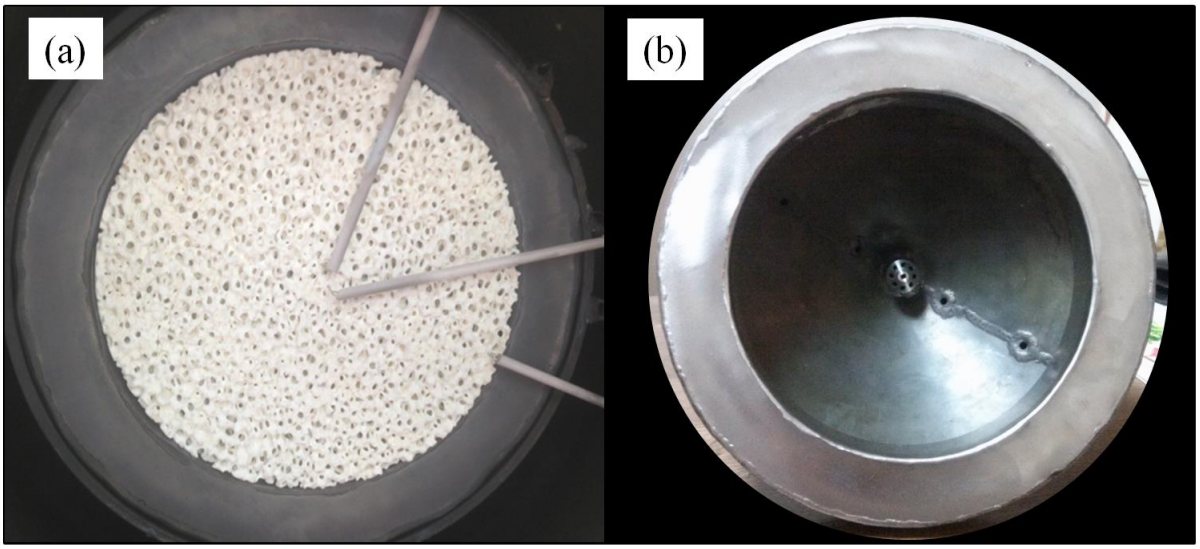

Figure III-1. (a) Ceria coated MPSZ foam device 15cm/40wt% installed in the solar reactor. (b) New fabricated foam device holder (include steam nozzle at the center).

Table III-1 CeO_2/MPSZ foam device specification.

Diameter (mm)	Thickness (mm)	Weight of device (g)	Weight of loaded CeO_2 (g)	Ceria loading (wt %)	Mole of loaded CeO_2 (mole)	cell number per linear inch(cpi)
150	30	670.8	268.3	40	1.6	10

III - 2 - 2. Operation of new device test

Fig. III-2 represents experimental setups of the thermal reduction step (T-R step) and water decomposition step (W-D step) of thermochemical two-step water splitting cycle using the CeO_2/MPSZ foam device. A highly purity (99.99%) N_2 gas stream of 3000 ~ 4000 Ncm^3/min was introduced from the inlet into the solar reactor interior, and passed through the foam device into the outlet line connected with the backside of the reactor. The solar reactor, which was set up on the table between the heliostat and parabolic reflector, was exposed to a concentrated solar radiation. The surface of the CeO_2/MPSZ foam device was set up to be 8 cm behind the focal point of KIER solar furnace system.

The CeO_2/MPSZ foam device was irradiated for 30 ~ 45 min in order to drive the T-R step. The temperature of CeO_2/MPSZ foam device for T-R step was controlled at 1500 ~ 1600 ^oC using R - type thermocouples placed at the center of the foam device surface. The thermocouples were covered by ceramic tube, and the tip points were inserted to a pore of foam matrix slightly in order to precise measuring of foam device temperature. Among the installed thermocouple, one of on the center position of foam device was connected to solar furnace control system for control blind open percent to uphold the device

temperature. After the thermal reduction step, the concentrated solar radiation intensity was reduced using the blind between the heliostat and parabolic reflector for the subsequent water decomposition (W-D) step. The gas stream introduced into the solar reactor was also changed from nitrogen to a nitrogen/steam mixture, and passed through a steam generator. The blind was opened and closed automatically based on real time DNI (Direct normal insolation) measurement in order to maintain the target temperature. The temperature of CeO_2/MPSZ foam device center for the W-D step was controlled at 800 ~ 1100 ^oC. An H_2O/N_2 gas mixture was produced by steam generator that designed coil type structure with 3 kWe heat capacity and distilled water was supplied 9 Ncm^3/min (liquid phase) to the steam generator by peristaltic pump during 30 ~ 60 min (W-D step). The thermochemical two-step water splitting cycle for hydrogen production were operated 13 cycles during 2013.06.07 to 2013.12.03 under the real solar conditions at KIER solar furnace site. After the W-D step in each cycle, the remaining hydrogen and steam in the reactor were swept out by passing N_2 gas through the reactor for a few minutes. This passing of N_2 gas was continued for several minutes before the next T-R step. During the purging of remaining steam, the temperature of foam device was maintained at the W-D condition.

Over a period of 13 solar driven cycles, three different operation methods were tested. This chapter focused on improves the hydrogen

production via change of operation methods under the given experimental system.

Operation A is the reverse flow method which introduced flows from the backside of the device over a diffuser nozzle for enhanced distribution of the stream. Operation method B was suggested the flow direction which introduced from annular inlets at the front of the foam device for comparison of operation A. Operation method C as operation method B flow direction, but including a modified moving reactor position in order to expand the high flux irradiated area on the foam device. In fact, the hot spot area which was active for O_2 release from the CeO_2/MPSZ foam device was limited by the concentrated solar radiation intensity distribution, which is smaller than device diameter. Because the CeO_2 reduction is strongly related to the temperature of device, high flux irradiation was introduced to zoned area by the use of 3-axis movable table with solar reactor. Concentrating point was moved at every 15 min by 4 section zoning through the device surface. This method has a different points compare with precedent researches. Generally, the concentrated irradiations were introduced to one aim point where the solar receiver or reactor is placed on the focus point, by the adjusting of the reflectors like as heliostat or dish. So, the moving parts are not solar receiver or reactor [16]. However, in this chapter the solar furnace offer only fixed focal points due to the secondary reflector (dish) are fixed in one position

for concentrate the reflected sun rays from the heliostat. So, the operation method C was suggested in order to improve a limited condition which is fixed focal point with highly concentrated heat flux but, want to offer the highly concentrated heat flux to foam device surface entirely. Fig. III-2a, b, and c shows the operation methods involving flow direction and zoned section concentrating methodology.

A side stream was taken from the effluent gas and the hydrogen concentration in the effluent gas was determined by gas chromatography (GC; Young-lin Acme 6000) using TCD (thermal conductivity detector) of 3.1 min intervals. The amount of hydrogen evolved during the W-D step was determined by integrating the profile of hydrogen production.

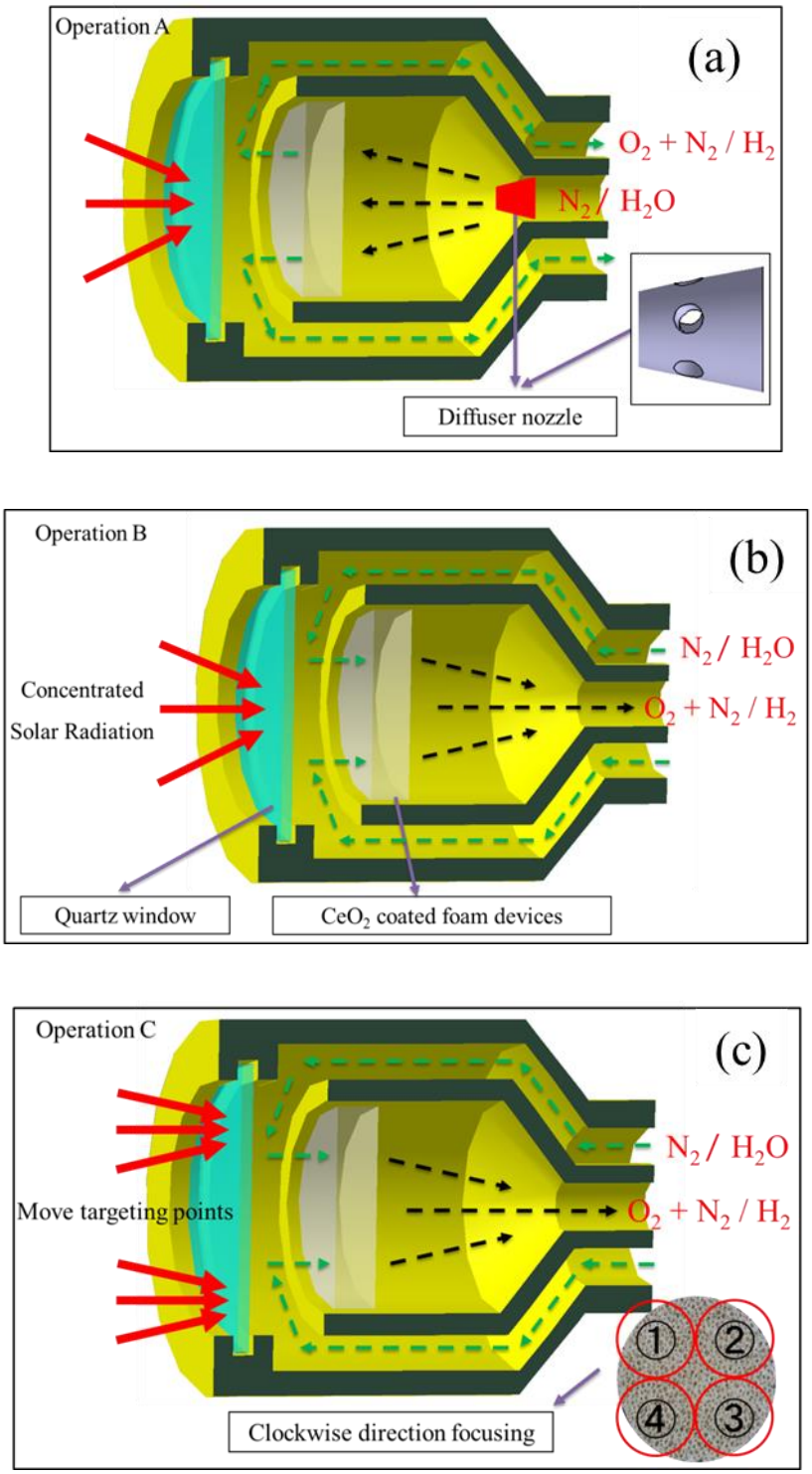

Figure III-2. Solar driven water splitting system operation method A, B, C.

III - 3. Results and discussion

III - 3 - 1.Input power of operation cycles

The desired reaction temperature for the thermal reduction step is the range of 1500 ~ 1600 ^{o}C on the CeO_2/MPSZ foam device [45]. Fig. III-3 shows the typical temperature profiles of the foam device (for the first cycle under operation method A) in the thermal reduction and the water decomposition steps. In order to avoid thermal shock to the foam device in the reactor by irradiation of high fluxes of concentrated solar radiation, the foam device was gradually heated up to 1200 ^{o}C (at the center of the front side of the foam device) in a preheating step. After the preheating step, the thermal reduction step was started. In the thermal reduction step, the temperature at the center of the front side of the foam device quickly reached above 1450 ^{o}C and was kept constant at the range of 1450-1570 ^{o}C for about 30 min. The temperature at the edge of the front side of the foam was about 1100 ~ 1200 ^{o}C. Thus, the temperature gap between the center and edge of the front side of the foam device was considerable at over 200 ~ 300 ^{o}C.

The time variation of DNI (Direct Normal Irradiation, W/m^2) during the cycle is also shown in Fig. III-3. By the DNI data and the flux mapping data which was measured before two-step water splitting cycle experiment, the input solar power into the CeO_2/MPSZ foam

device (15 cm-diameter of the foam device surface) was calculated for each step [44]. In the reduction step of the first cycle, the average input power was calculated to be 10.19 kW and the total solar energy input to the foam device was 5.44 kWh.

For the water decomposition step at the desired temperature of 1100 ^{o}C [43], the solar input power to the foam device was reduced by adjusting the blinds of the solar furnace (e.g. from 70 % opening to 30%). As shown in Fig. III-3, the temperature at the center of the foam device went down to 1100 ^{o}C within a few minutes. The steam/nitrogen mixture was taken fed to the reactor, with a hydrogen evolution peak appearing soon after injection of the steam/nitrogen mixture (black dotted line in Fig. III-3). The hydrogen evolution gradually decreased to effectively zero over 45 min. The input solar power into the CeO_2/MPSZ foam device was also calculated for the water decomposition step of each cycle. The average input power during the water decomposition step of the first cycle was about 3.24 kW and total solar energy input to the foam device was 2.43 kWh for the first water decomposition step. For the overall first cycle (the thermal reduction and water decomposition cycles), overall solar energy input was calculated to be 7.87 kWh.

Fig. III-4 shows the average solar input power and total solar energy input to the foam device during the thermal reduction and water decomposition steps for each cycle. The average input power for one

reduction step and that for one water decomposition step were estimated to be 11.85 kW and 3.53 kW respectively. The average of solar input energy for one reduction step and that for one water decomposition step in repeated cycles were 8.04 kWh and 3.34 kWh respectively. Thus, the average solar input energy for one cycle was 11.38 kWh.

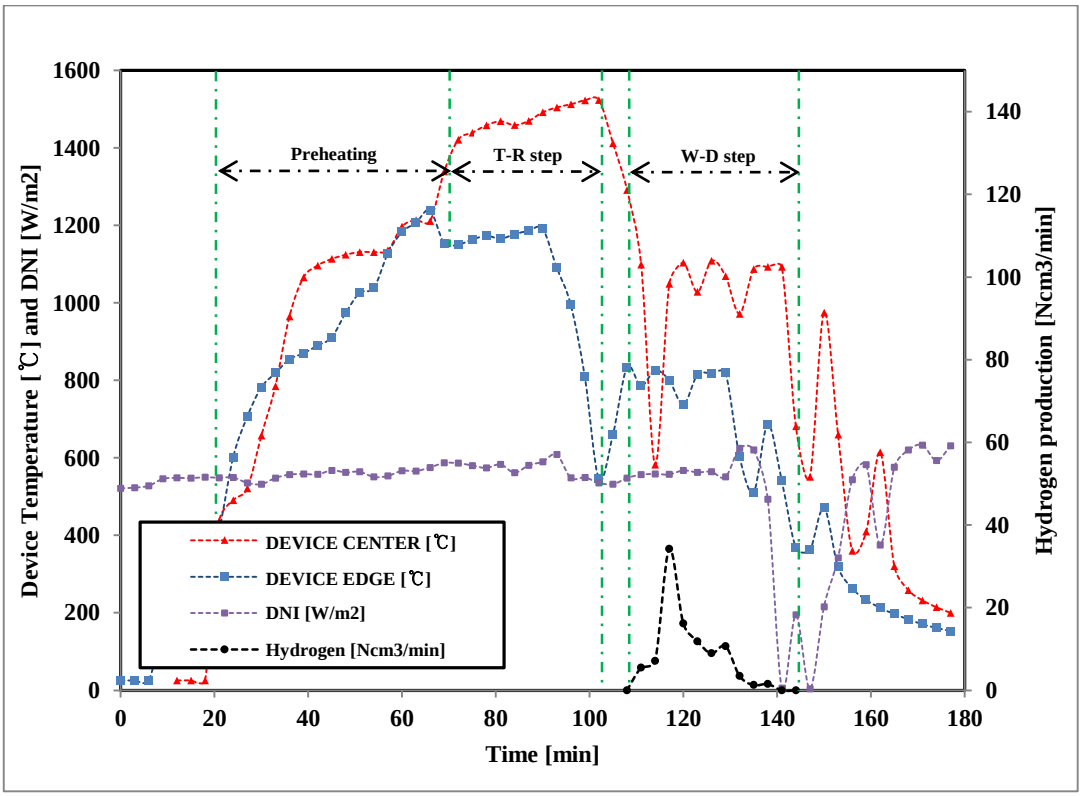

Figure III-3. Temperature variation on the device center, edge, DNI, and hydrogen evolution of 1st cycle (Operation method A).

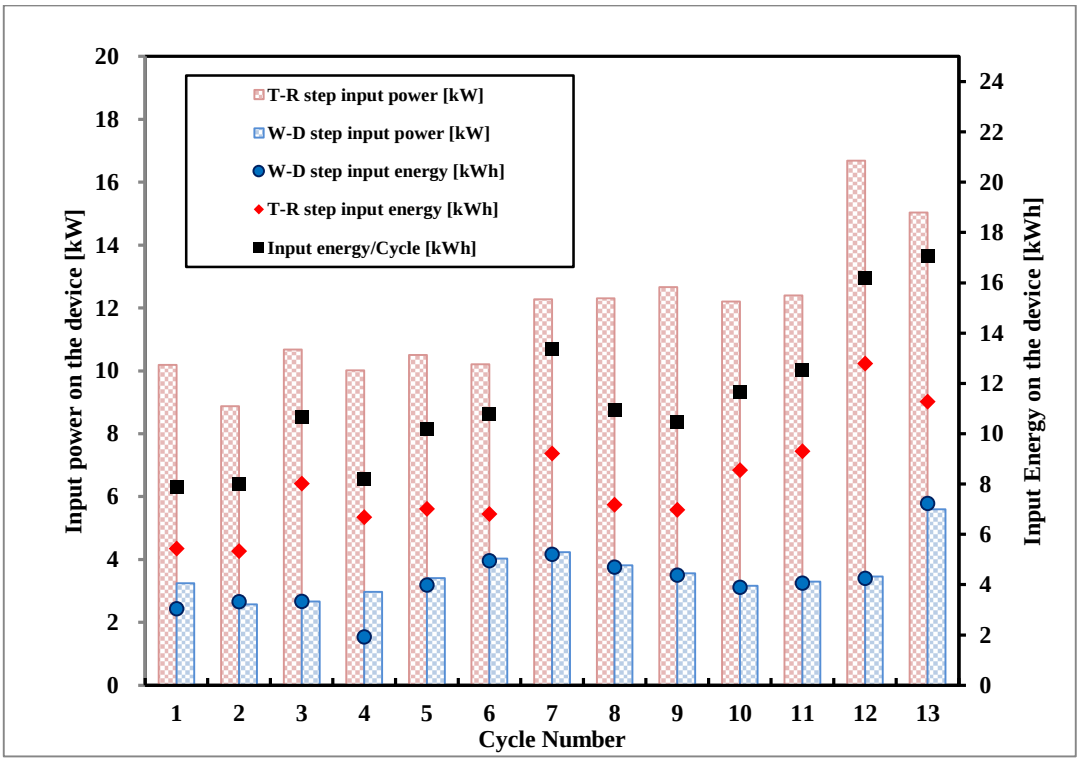

Figure III-4. Input power (kW) & Input energy (kWh) on the device on overall cycles.

III - 3 - 2. Hydrogen evolution

Fig. III-5 shows the hydrogen production amounts during the water decomposition step of the repeated cycles. 13 cycles were performed during eight days by changing the operation method in the order of A, B and C. The total amount or sum of produced hydrogen in the 13 cycles reached to 6882.2 Ncm^3. The largest amount of hydrogen evolution per cycle was 1546.6 Ncm^3 which was observed at 9th cycle (2013.09.26), in which the operation method C was started.

Depending on the operation methods of A, B and C, the different levels of hydrogen production amount were observed. The level or average of hydrogen evolution amount/cycle increased in the order of operation methods of A, B, and C, as shown by the dotted lines (Average hydrogen evolution amount per operation method) in Fig. III-5.

The average produced hydrogen amount of the operation method A was 201.9 Ncm^3/cycle whereas for the method B was 515.8 Ncm^3/cycle and for the method C was 802.2 Ncm^3/cycle. These results show good approach of improvement of operation was done for the solar thermochemical water splitting reactor with CeO_2/MPSZ foam device.

Table III-2 shows the summary of the experimental conditions for

operation methods, A, B and C, the produced hydrogen amounts for each cycle, and the CeO_2 conversion (CeO_2 to $CeO_{2-\delta}$ conversion in the thermal reduction step). The CeO_2 conversion was estimated from the amount of hydrogen produced in the subsequent W-D step [28] – it was assumed for the CeO_2/MPSZ foam device that the reduced phase ($CeO_{2-\delta}$) formed in thermal reduction step was completely re-oxidized back to original CeO_2 phase via water decomposition in the subsequent W-D step. The largest conversion of the CeO_2 among the repeated cycles was only 8% on the foam device.

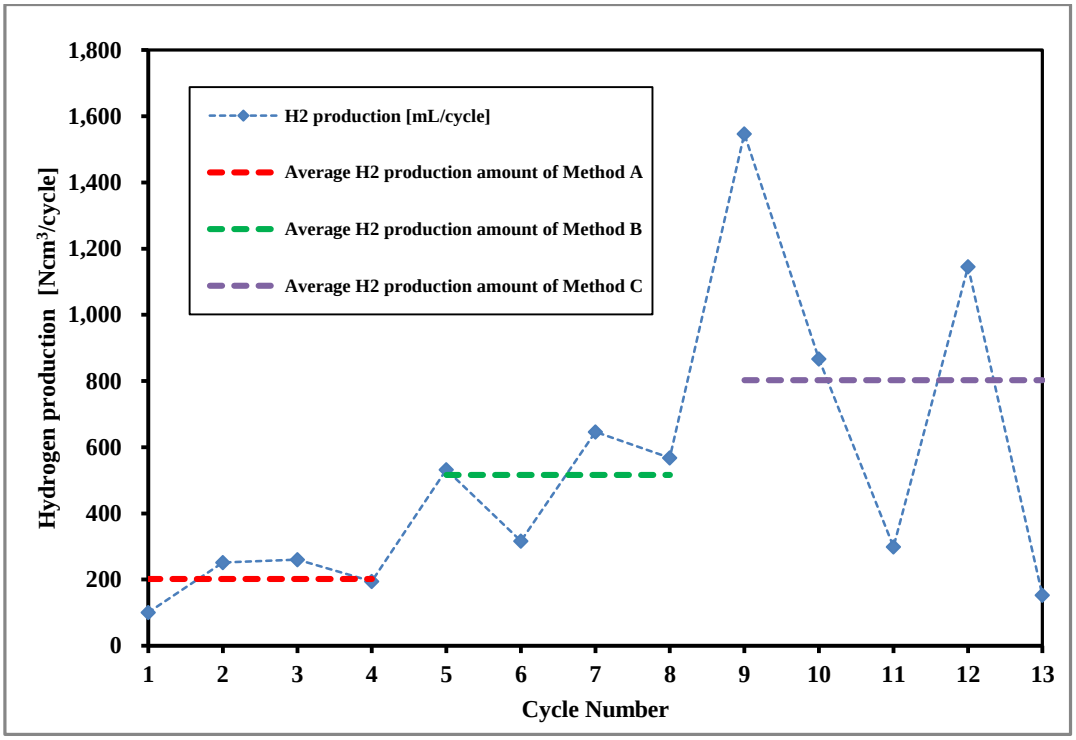

Figure III-5. Production amount of hydrogen with 1~13 cycles.

Table III-2. Test condition and hydrogen production amount

Operation	Operation method A				Operation method B				Operation method C				
Cycle Number	1	2	3	4	5	6	7	8	9	10	11	12	13
Date	2013. 06.07.	2013. 06.10.			2013. 08.20.		2013. 09.04.		2013. 09.26.		2013. 09.27.	2013. 11.07.	2013. 12.03.
Input Power (kW) / T-R	10.19	8.87	10.68	10.01	10.50	10.20	12.27	12.30	12.66	12.20	12.40	16.68	15.03
T-R step Time (min)	32	36	45	40	40	40	45	35	33	42	45	46	45
T-R step Input energy(kWh)	5.44	5.33	8.01	6.67	7.00	6.81	9.21	7.18	6.96	8.54	9.30	12.79	11.28
Input Power (kW)/ W-D	3.24	2.57	2.66	2.96	3.40	4.02	4.23	3.81	3.55	3.16	3.29	3.45	5.59
W-D step Time (min)	45	62	60	31	56	59	59	59	59	59	59	59	62
W-D step Input energy(kWh)	2.43	2.66	2.67	1.53	3.18	3.96	4.17	3.75	3.50	3.11	3.24	3.40	5.78
H_2 amount (Ncm^3)	100.7	251.6	260.7	194.6	532.3	316.4	646.6	568.0	1546.6	866.5	298.8	1145.8	153.5
Average H_2 amount (Ncm^3)	201.9				515.8				802.2				
CeO_2 Conversion (%)	0.53	1.32	1.37	1.02	2.80	1.66	3.40	2.98	8.13	4.55	1.57	6.02	0.81

III - 3 - 3. Comparison of operation methods

Operation method A:

Operation A is the reverse flow method in which nitrogen and steam were fed from the device backside by a diffuser nozzle for enhancement of gas stream distribution. The diffuser nozzle has an angle and 8 holes for expanding the interior stream direction (Fig. III-2a the operation A). As shown in Fig.III-6a, the peaks of the hydrogen evolution appeared relatively quickly (within 10 min) after steam injection and the hydrogen evolution was also completed in short time of 20 min. The response of the hydrogen evolution peaks was quick in comparison to the cases in operation methods B and C (Fig. III-6b & c) - where the largest hydrogen peaks appeared after 10 min from the steam injection. The hydrogen evolution level under operation A (the 1st to 4th cycles) was relatively stable (See the red dotted line in Fig. III-5), but the average hydrogen amount was less than those under other operation methods of B and C.

Operation method B:

The reference case was used in the operation method B, in which gas was fed from an annular inlet to the front side of the foam device (Fig.

III-2b). By changing the gas flow direction of the feeding gases for the thermal reduction and water decomposition steps as mentioned above, the average hydrogen production amount per cycle (the green dotted line in Fig. III-5) increased by more than 2 times in comparison to that in operation method A.

However, the hydrogen peaks were shifted to later time in comparison to the cases of operation A - as mentioned above, the hydrogen peaks appeared in 10-15 min after the steam injection in water decomposition step (Fig. III-6b). The hydrogen evolution continued for a longer time and ended 50 ~ 60 min after steam injection. The produced hydrogen amount was relatively lower in the 6th cycle compared to the 5th, 7th and 8th cycles. This was due to the heating condition of the foam device during the thermal reduction step as discussed below. Fig. III-7 shows the hydrogen production profile and the device center temperature of the 5th to 6th cycles.

Due to DNI fluctuation, the device center temperature in the thermal reduction step of 6th cycle was unstable compared to the 5th cycle's device temperature variation and was lower than that of 5th cycle. This would negatively affect the extent of the thermal reduction in the step, consequently the extent of water decomposition on the subsequent step.

Operation method C:

Operation C was performed using the same gas feeding method as operation B. However, the solar-heating spot on the foam device in the reactor was moved during the thermal reduction step by moving reactor position, in order to increase the thermal reduction area of the foam device. As mentioned above, the temperature gaps between the center and edge of the front side of the foam device were very large in 200 ~ 300 ^{o}C. For example, the edge temperature of the front side of the foam was around 1100 ^{o}C in the thermal reduction step (Fig. III-3). This suggests that the CeO_2 coated on the edge parts of the foam could not be thermally reduced. Only in the narrow area near the center of the foam device, the temperature reached above 1500 ^{o}C and the coated CeO_2 was thermally reduced to form $CeO_{2-\delta}$. In order to improve this point, the reactor position was slightly moved to the hot spot on the foam device during the thermal reduction step as follows:

The front surface area of the foam device was divided into 4 zones as shown in Fig. III-2c. The center of the solar spot was moved to the zone. In order to do this operation, the solar reactor was moved toward clockwise (Y-axis and Z-axis) to 4 zoned sections by using 3-axis transferable table (Fig. III-8).

Solar reactor position for each zone was efficiently decided by visibly monitoring the discoloration of the solar-irradiated foam surface via the real-time CCD camera (involved the neutral density filter) – the color changes from white to dark happens on ceria as the thermal

reduction of CeO_2 to $CeO_{2-\delta}$ proceeds.

Depending on the fluctuating weather condition, the time of solar irradiation to one zone of the foam device was properly adjusted by monitoring variation of device surface discoloration.

In the 9th cycle, the evolved hydrogen amount showed the largest value among the various cycles (1546.6 Ncm^3). In comparison with operation methods A and B, the average hydrogen production amount greatly increased being 4 times larger than that of method A, and 1.56 times larger than that of method B (Fig. III-5).

However, the total solar energy inputs to the thermal reduction step and the water decomposition step were not significantly higher in operation C in comparison to the cases of operation methods A and B (Fig. III-4).

The produced hydrogen amount varied greatly in the operation method C. Especially in the cases of the 11th and 13th cycles, the evolved hydrogen amount was relatively low. In the 11th, and 13th cycles, the device temperatures during the thermal reduction and water decomposition steps were relatively lower and more unstable than other cases under the operation C (Fig. III-9 shows the temperature variations of the foam device in the solar reactor together with DNI variation under operation C from 9th to 13th cycle).

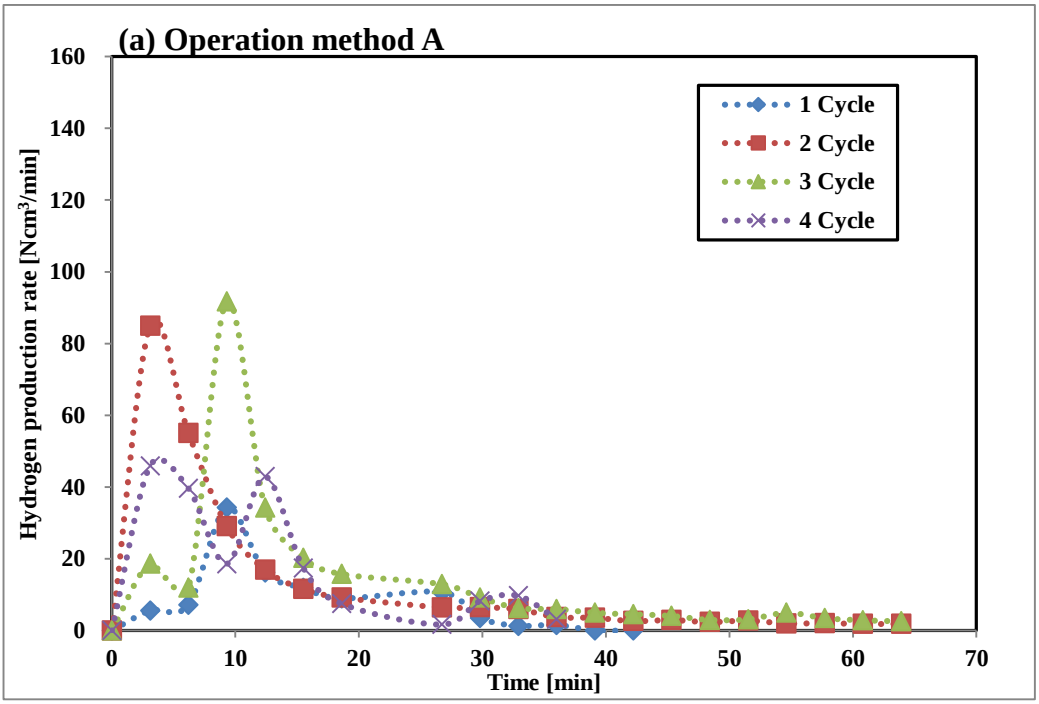

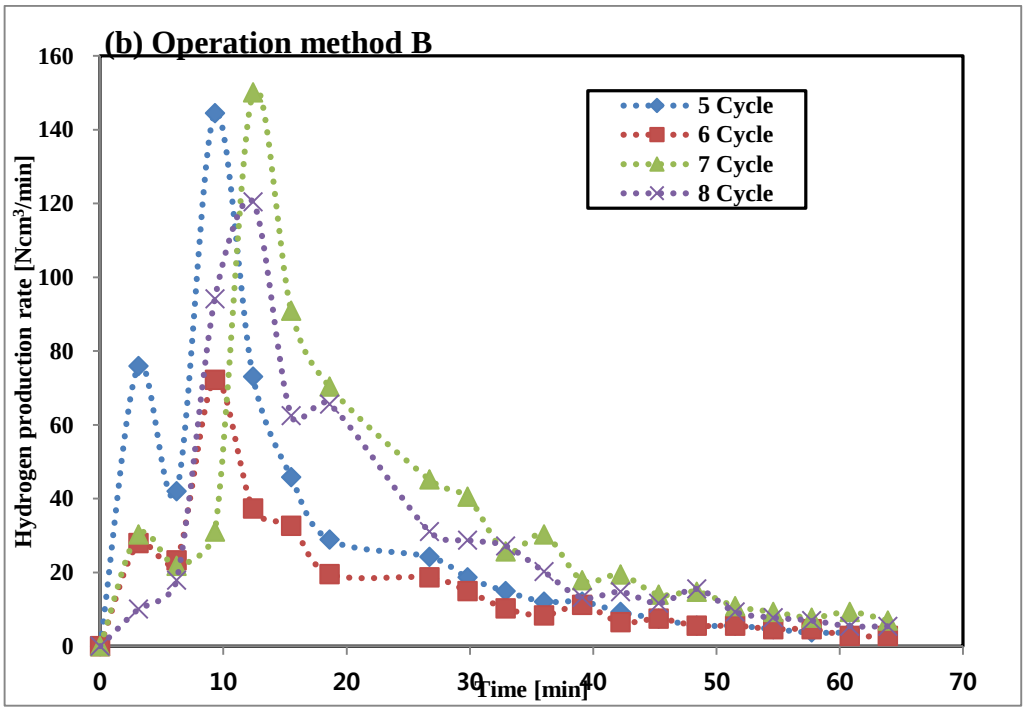

Figure III-6. Hydrogen production profiles (a) Operation method A, (b) Operation method B.

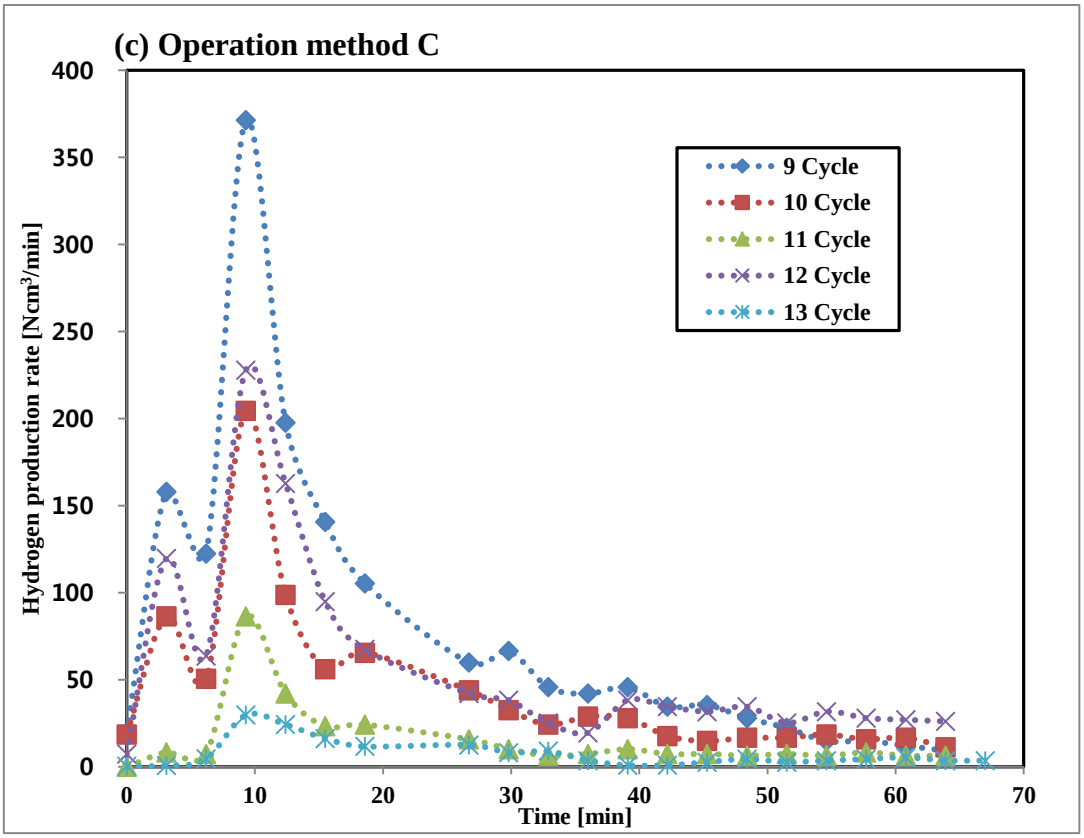

Figure III-6 (c) Operation method C.

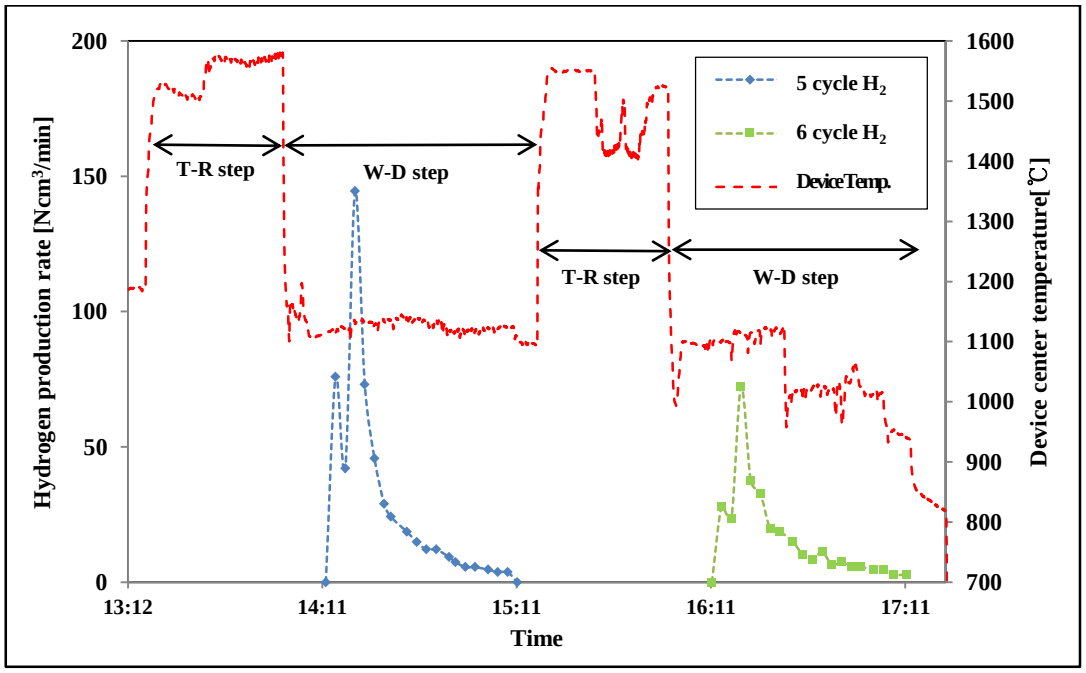

Figure III-7. Hydrogen production profiles in 5th and 6th cycles with device center temperature variations.

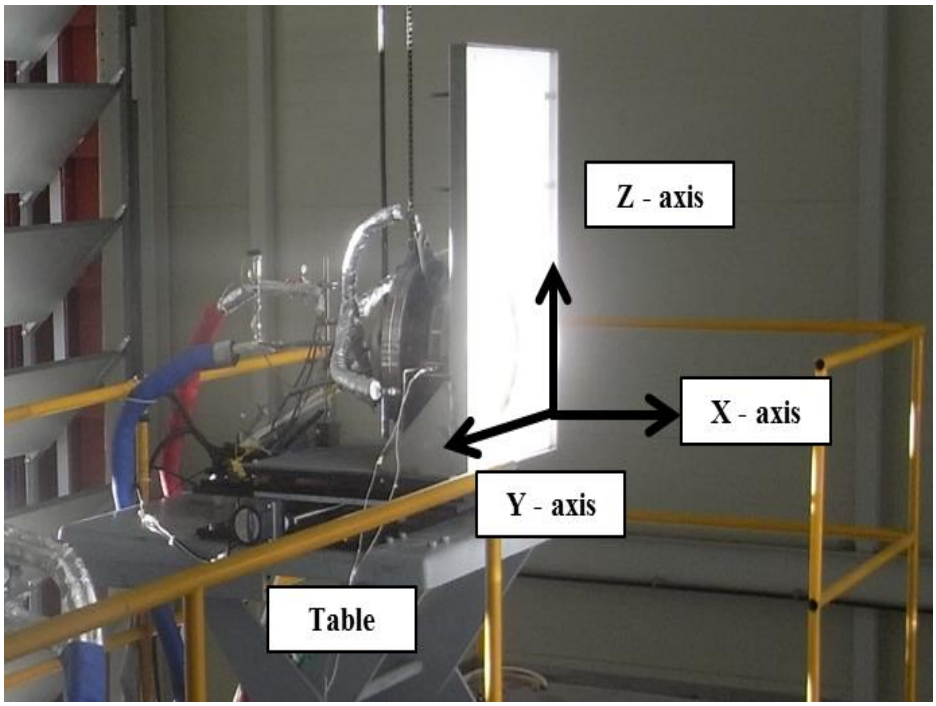

Figure III-8. Photograph of transferable table (3 – axis) and solar reactor.

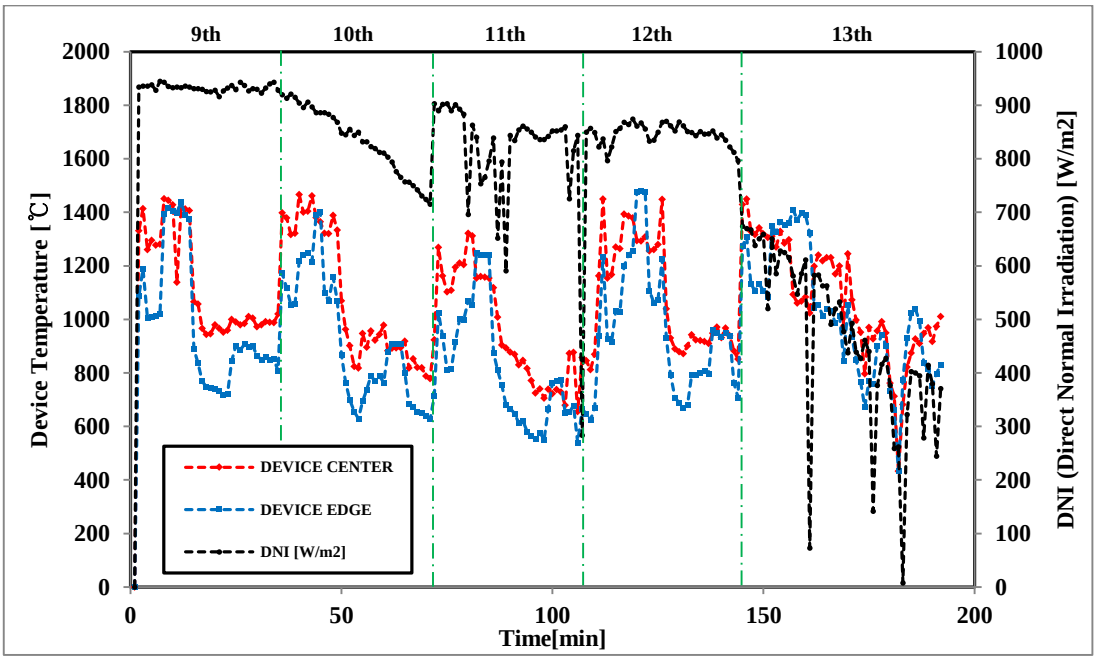

Figure III-9. Device temperature (center and edge of foam device front side) and DNI from 9th to 13th cycle.

III - 3 - 4. Extent of CeO_2/MPSZ foam device activation

Due to the characteristic of solar flux distribution by the solar furnace system [44], a large temperature gap was created between the center and edge parts of foam device. For the thermal reduction step of the 1st cycle through the 8th cycle, the peak temperature of edge area of the foam device only reached around 1200 ^oC, while the center of the foam device was heated up to 1550 ^oC. For the thermal reduction steps of the 9th through 13th cycles under operation method C, the temperature gaps between the device center and edge were reduced by moving the solar-heating spot on the surface of the foam device.

As mentioned above, the color of ceria particles changes from white to dark if the nonstoichiometric phase formation or reduction of CeO_2 proceeds to larger extent. For the 1st through the 8th cycles, only the center region of the foam device changed to dark color, while the edge area did not show color change remaining white. Fig. III-10a and b shows the photos of the front surface of the CeO_2/MPSZ foam device. The discoloration of CeO_2/MPSZ foam device to dark was observed only near the center area for the 1st through the 8th cycles (Fig. III-10a). In contrast, as shown by Fig. III-10b, dark area of the front surface area of the foam device was expended in the thermal reduction step from the 9th cycle. This indicates that the extent of the thermal

reduction of CeO_2/MPSZ foam device was improved by the operation method C [43-46].

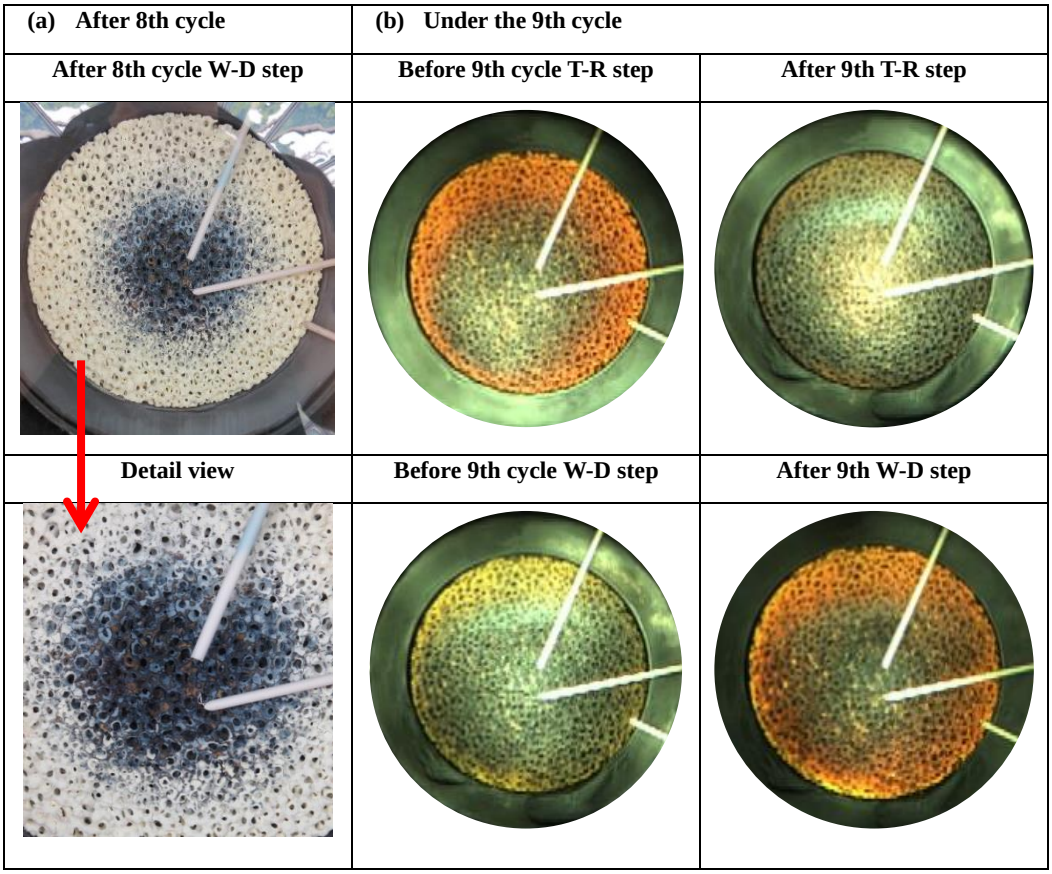

Figure III-10. Photographs of CeO_2/MPSZ foam device surface and discoloration area.

III - 4. Conclusion

The thermochemical two-step water-splitting cycle reaction by CeO_2/MPSZ foam device was demonstrated with KIER solar furnace system to improve the operation method for increasing the hydrogen production. Solar-driven thermochemical two-step water-splitting cycle experiments were conducted during Jun.2013 to Dec.2013. Experimental conditions such as input solar energy to the foam device, thermal reduction step temperature and water decomposition step temperature, and the time of each step were controlled using a blind in the solar furnace with consideration of weather condition.

The thermal reduction process and water decomposition process were evaluated by the use of one solar reactor and 3 different operation methods A, B and C. The total number of cycle tested was 13 cycles; 1st-4th cycles with operation method A, 5th-8th cycles with operation method B, 9th~13th cycles with operation method C. The operation method differed simply by the flow direction and solar irradiation focusing method. According to the operation methods, the produced hydrogen amount and hydrogen evolution rate shows significant variations.

Operation method A shows the most rapid hydrogen evolution rate among the operation methods. However, the concept of operation

method A (reverse flow direction from the diffusing nozzle) shows the lowest hydrogen production compared to other operation methods B and C. The average produced hydrogen amount of method A was produced to 201.9 Ncm^3/cycle, compared to 515.8 Ncm^3/cycle for method B and 802.2 Ncm^3/cycle for method C. The results under the operation method B shows increased hydrogen production compared to operation method A due to the feed direction change of the flow. However, the reduction process was not completed entirely on the device due to temperature deviations between center and edge of the foam device.

This was evident in visual observations of the foam device elevation. In methods A and B, only the center area shows the discoloration phenomenon in which color changes from white to dark (between CeO_2 and $CeO_{2-\delta}$ phase). In order to solve the localized thermal reduction process on the foam device, operation method C was suggested. By moving the solar-heating spot on the surface of the foam device the extent of the thermal reduction of CeO_2/MPSZ foam device was improved. The greatest hydrogen production was achieved by the operation method C. This is due to an expansion of the area where the thermal reduction process takes place. It also means that delivery of sufficient solar flux intensity over a wide area for thermal reduction process is essential for high productivity of thermochemical two-step water-splitting cycle by CeO_2/MPSZ foam device. Meanwhile

operation method C has a weakness of operating simplicity due to moving of solar reactor position with real-time visible foam device surface monitoring in comparison to operation methods A and B. The next chapter is the transformed designs of foam device and solar reactor to acquire homogenous heat flux intensity for maximize the performance of CeO_2/MPSZ foam device.

In conclusion, the thermochemical two-step water-splitting hydrogen production cycle by CeO_2/MPSZ foam device studied with 3 different operation methods. In the case of flow direction, the natural flow direction under operation method B shows better hydrogen production than reverse flow by the diffusing nozzle under operation method A. On the other hands, the focusing method also compared and operation method C shows highest hydrogen production. By the case study of each method, the thermochemical two-step water splitting cycle reaction could be enhanced by operation methods.

Chapter IV

Optical modeling of flux distributions on the foam device surfaces in solar reactor

IV - 1. Introduction

In this chapter, the flux distributions on the surface of foam device in the solar reactor with the solar furnace were studied. This chapter aims for understanding characters of concentrated sun rays through KIER solar furnace and for designing of new device shape to create more uniform temperature distribution on the device surface. At first, the KIER 45 kW_{th} solar furnace and the flat disk type device shape was simulated for understanding the experimental results (Chapter II, III). Then cylinder shape and conical shape device models were also calculated. Comparing the flat type foam device, the conical or cylindrical foam device is expected to create more uniform temperature distribution on the foam device. In addition, the conical or cylindrical foam device can improve the heat transfer between gases and foam surface.

Optical modeling of KIER solar furnace

IV - 2 - 1. SolTrace code

The SolTrace code is based on Monte Carlo ray tracing methodology for accurate representation of these varied and complex systems. SolTrace is one of several options available for modeling CSP (Concentrating Solar Power) systems. Since its inception, similar tools have been developed by others in the CSP community, such as Tonatiuh. In addition, commercial ray-tracing packages also exist, such as ASAP by Breault Research, but these are intended for more general optical system design and, as such, are not "solar friendly." While they can be used, they require significant effort to learn and model the complex solar designs using the sun as the source [47, 48].

The SolTrace code utilizes a ray-tracing methodology of Monte-carlo method. A specified number of rays are traced from the sun through the system, and each traces through the defined system while encountering various optical interactions. Such a code has the advantage over codes based on convolution of moments in that it replicates real photon interactions and can therefore provide accurate results for complex systems that cannot be modeled otherwise. Accuracy increases with the number of rays traced, and

larger ray numbers means more processing time. Complex geometries also translate into longer run times. However, the required number of rays is also a function of the desired result [47].

IV - 2 - 2. Optical modeling of KIER solar furnace with solar reactor

Fig. IV-1 shows the geometry of simulated KIER 45kW$_{th}$ solar furnace system with solar reactor involving the flat disk type foam device (represented to “foam absorber” from followings). The solar reactor equipped transparent quartz window to pass concentrated solar radiation for directly heating a redox material coated foam absorber. Fig. IV-2, Fig. IV-3 shows the schematic and photograph of the solar reactor and simulated region of solar reactor. The insulation board at the front of solar reactor, flange parts of solar reactor at the aperture, and the quartz window (267 mm) were included in the simulation. The inner wall surface of solar reactor main body, covered by Inconel steel sheet, was also considered.

The simulated sun position was assumed to place to top of heliostat, and the sun shape was used to CSR5 model – offered from the SolTrace in which parameter defining a Gaussian distribution for the suns’ disk. In terms of slope error from the heliostat and parabolic reflector (dish) were set to 2 mrad by initial value of SolTrace.

The flat disk type foam device or absorber shape was simulated to understand implemented data from experiments in 2012 and 2013.

The diameter of the flat type foam absorber is 15 cm, and thickness is 3 cm. During the experiment (from 2012 to 2013), the flat type foam absorber placed to – 8cm back side from the focal point of solar furnace. It was aim to expand the uniform heat flux on the foam device.

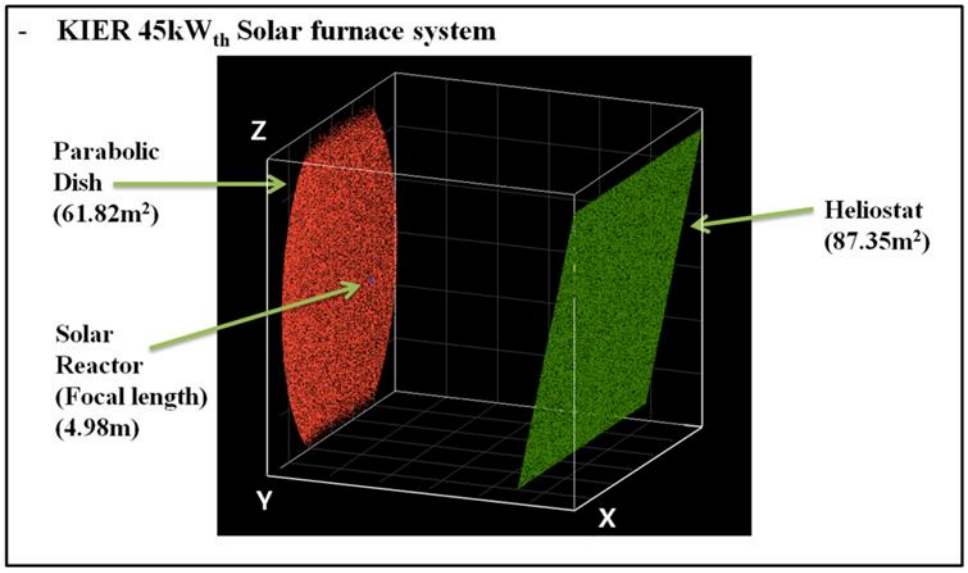

Figure IV-1. Schematic of simulated KIER 45kW$_{th}$ Solar furnace system by the SolTrace code

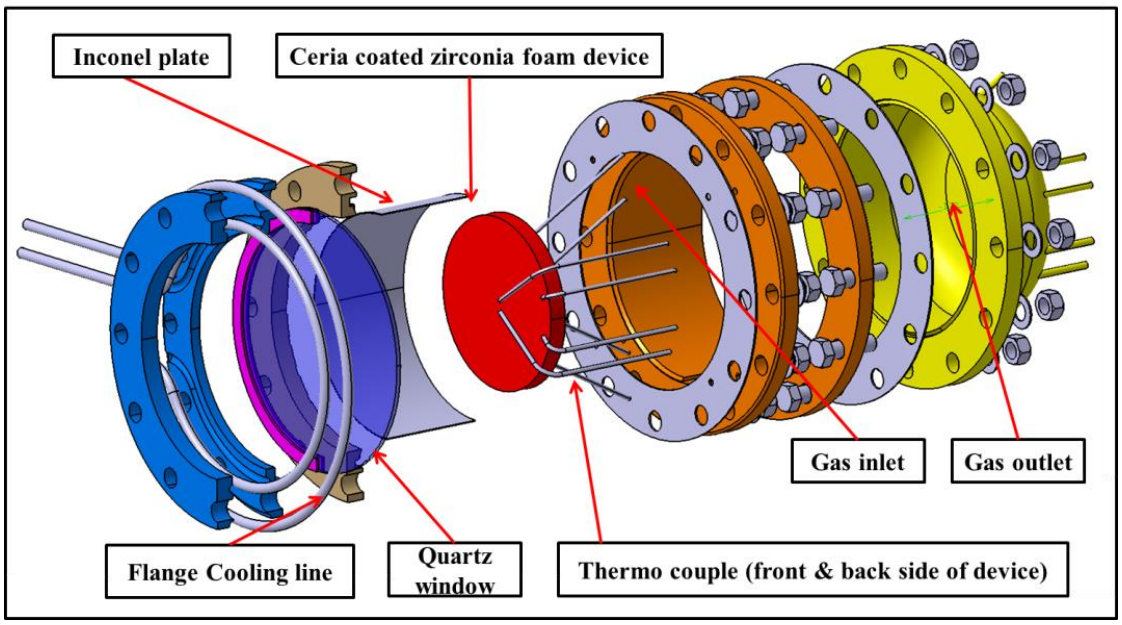

Figure IV-2. Schematic of solar reactor and flat type foam device

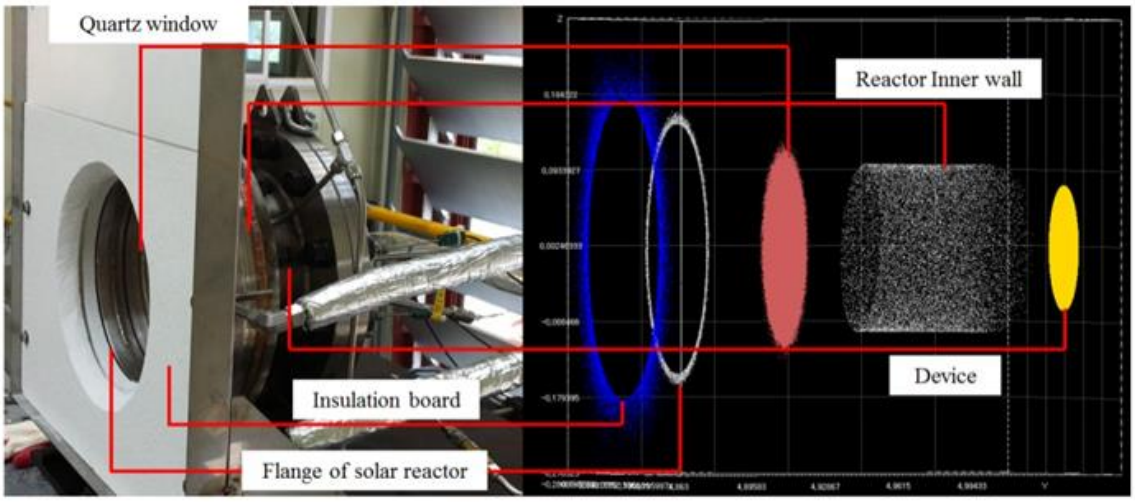

Figure IV-3. A photograph of solar reactor and the simulated part of solar reactor for the consideration of rays blocking

IV - 2. Design of foam device shape

IV - 3 - 1. Design of 5 different shape foam device shape

The design of the foam absorber shape aims to acquire uniform flux distribution over the foam absorber surface and an increase in the surface area by which is direct incident lights arrives. The first idea of the device shape was based on cavity shape, as for instance, cylinder structures and conical shapes. The simulation on flux distribution was studied using 5 models – the flat type, 4 cylinder shapes, and 1 conical shape. Each model has a different aperture size, diameters, thickness, and volume.

Fig. IV-4 and Table IV-1 shows comparisons and properties of the 5 models. In the Table IV-1, the direct exposure area (as shown Fig.IV-4 by yellow lines) ratio and volume ratio was compared with that of the flat disk device.

The outer diameter of models limited to 15cm – the same as flat disk type; the 4 cylinder model has an aperture size from 8cm to 10cm whereas the conical shape has an 11 cm. In the case of model 4, it has a stepwise structure exactly; however, it was named and assumed as a conical shape, having an aperture angle of 24 ^{o}.

The compared ratios show an increased exposure area and volume.

The increased expose area (surface area) was expected to be a benefit, by absorbing the concentrated rays more than the flat disk type device could. And the increased volume has an advantage of larger volume for more coating of reactive materials. Model 3 shows the largest exposure area and volume due to having more depth than other models.

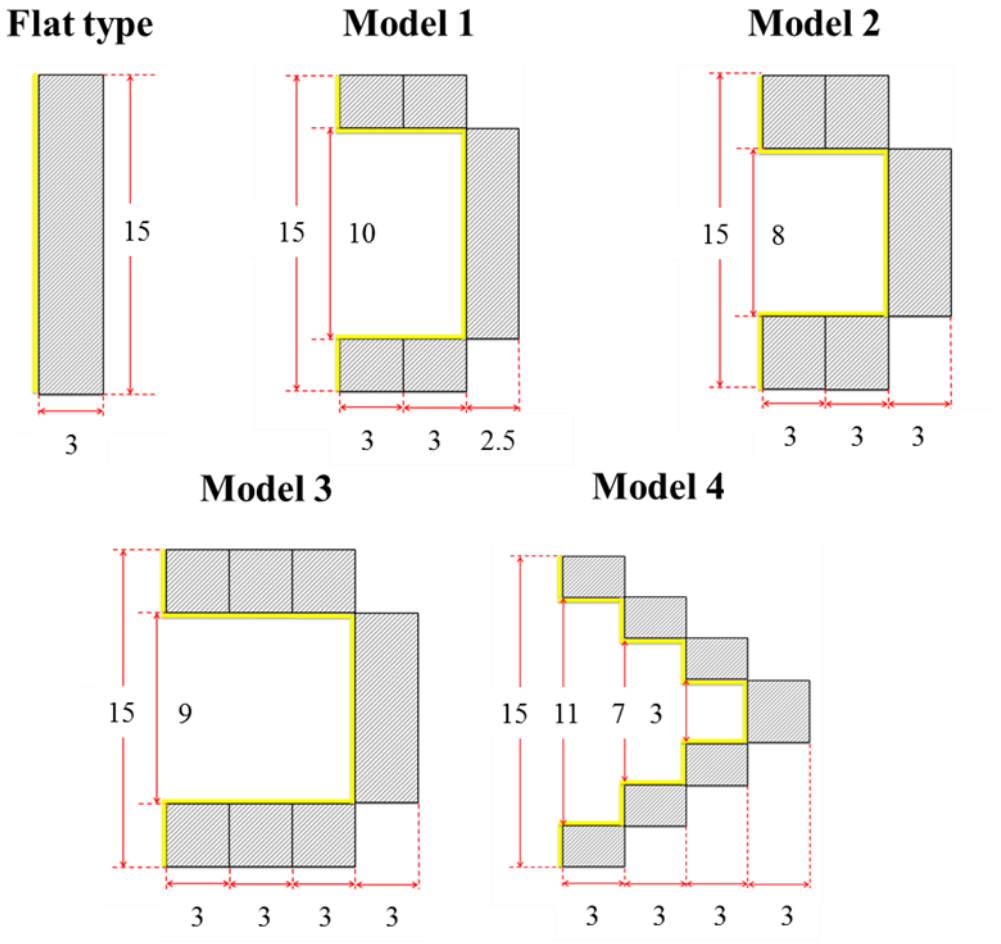

Figure IV-4. Design of foam absorbers – flat type, 4 cylinders shape, 1 conical shape (model 4 assumed to conical shapes) and the yellow lines show the area which direct exposure area (The numbers in the figure is the cm unit)

Table IV-1. Comparison of the 5 models properties – direct exposure area, volume, ratios with flat type disk device

	Flat	Model 1	Model 2	Model 3	Model 4	Unit
Exposure Area	176.625	365.025	327.345	430.965	374.445	Cm^2
	0.0176625	0.0365025	0.0327345	0.0430965	0.0374445	m^2
Volume	529.875	785	909.03	1208.115	529.875	Cm^3
	0.000529875	0.000785	0.00090903	0.001208115	0.050889195	m^3
Area Ratio	1	2.07	1.85	2.44	2.12	None
Vol. Ratio	1	1.48	1.72	2.28	1	None

IV - 3 - 2. Basic comparison of 5 models and boundary condition

A basic calculation of average heat flux intensity by the input power divide exposure area was studied. Based on the experimental data, the input power was decided with a range of 12 kW to 26 kW. Table IV-2 shows ideal heat flux intensity on the surface area of devices.

The basic calculations allow a comparison among 5 models. It can be utilized to decide the simulation condition for input power. The boundary condition reflectivity of heliostat and dish are suggested from experimented data, approximating 0.89. And the absorptivity of foam device model was excluded due to following reason. The color of foam device changed during the solar demonstration. Consequently, deciding the absorptivity was difficult, since the absorptivity relates to the color of the foam device.

Table IV-2. Basic calculation of flux intensity – An ideal heat flux intensity on the exposure area divided from input power					
Input power	Flat	Model 1	Model 2	Model 3	Model 4
	Input power / Direct Exposure Surface Area (D.I.S.A)				
kW	kW/m^2	kW/m^2	kW/m^2	kW/m^2	kW/m^2
12	679.41	328.74	366.59	278.44	320.47
14	792.64	383.54	427.68	324.85	373.89
16	905.87	438.33	488.78	371.26	427.30
18	1019.11	493.12	549.88	417.67	480.71
20	1132.34	547.91	610.98	464.07	534.12
22	1245.58	602.70	672.07	510.48	587.54
24	1358.81	657.49	733.17	556.89	640.95
26	1472.05	712.28	794.27	603.30	694.36

IV - 3. Results and discussion

IV - 4 - 1. Geometry of the 5 models from simulation

The 5 suggested models were calculated and compared. Initially, the flat disk type was set on an -8cm position to form the focal points for the KIER solar furnace, in keeping with prior experimental conditions. However, in the other case, the device position was set on focal point of the KIER solar furnace. The focal point is 4.98 m from the center of dish. The number of sun rays for calculation was 1,000,000 for obtaining higher accuracy calculation.

Fig. IV-5 shows the geometry of simulated models that are represented by several dots. The dots signify the arrival of sun rays that are in turn reflected and concentrated from dish to surface of the device.

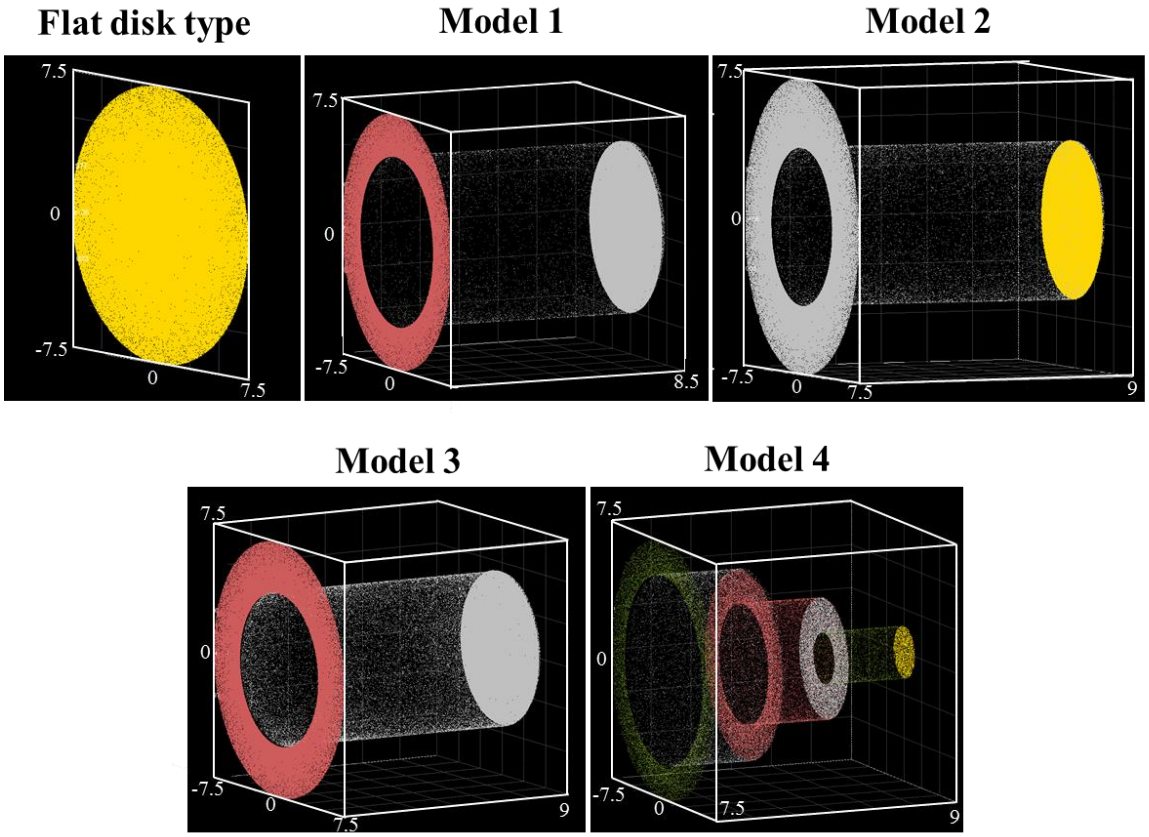

Figure IV-5. Simulated geometries – Flat disk type, 4 cylinders shape, 1 conical shape

IV - 4 - 2. Flux distributions of the 5 models

Fig. IV-6a ~ e shows the arrived heat flux contours and flux gradients of the 5 simulated models. Fig. IV-6a shows the reflected sun rays and the result of the flat disk type. The heat flux contour and flux gradient was described with separated surfaces: the ring zone, the cylinder wall zone, and the flat disk zone.

Fig. IV-6b ~ e were explained with an insisted arrow line. The cylinder wall zone was unrolled to draw a flux intensity contour.

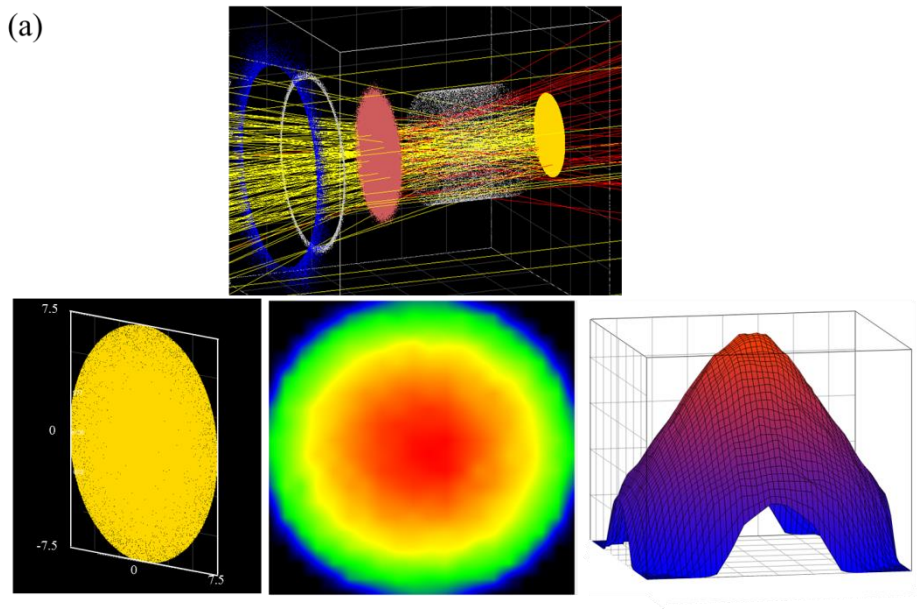

Figure IV-6 a. concentrated rays arriving to flat disk type device and the contour of flux intensity

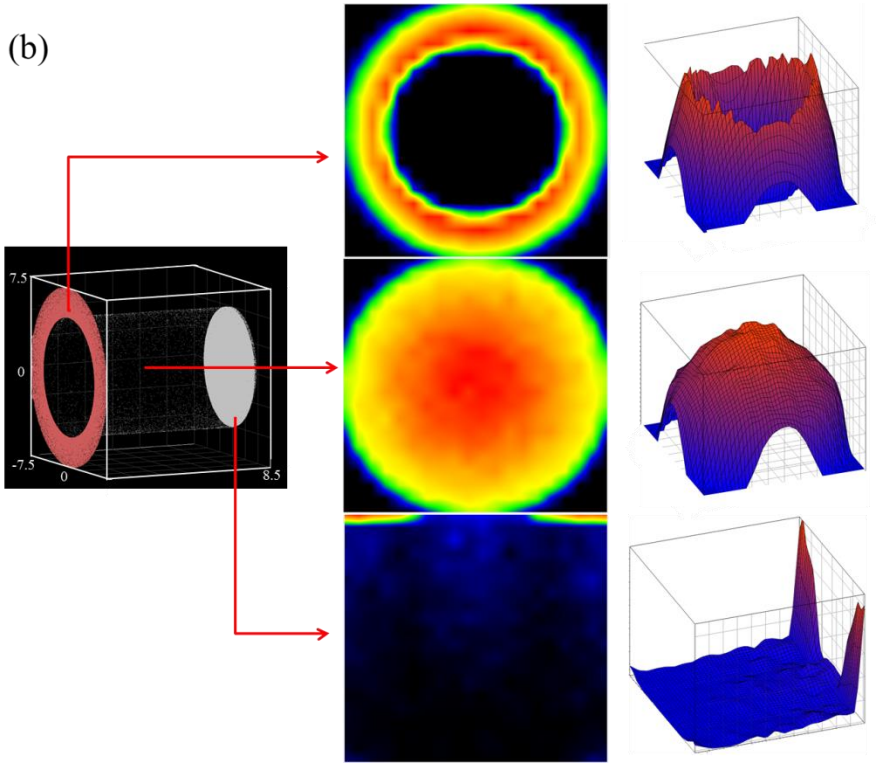

Figure IV-6 b.The contour of flux intensity – Model 1

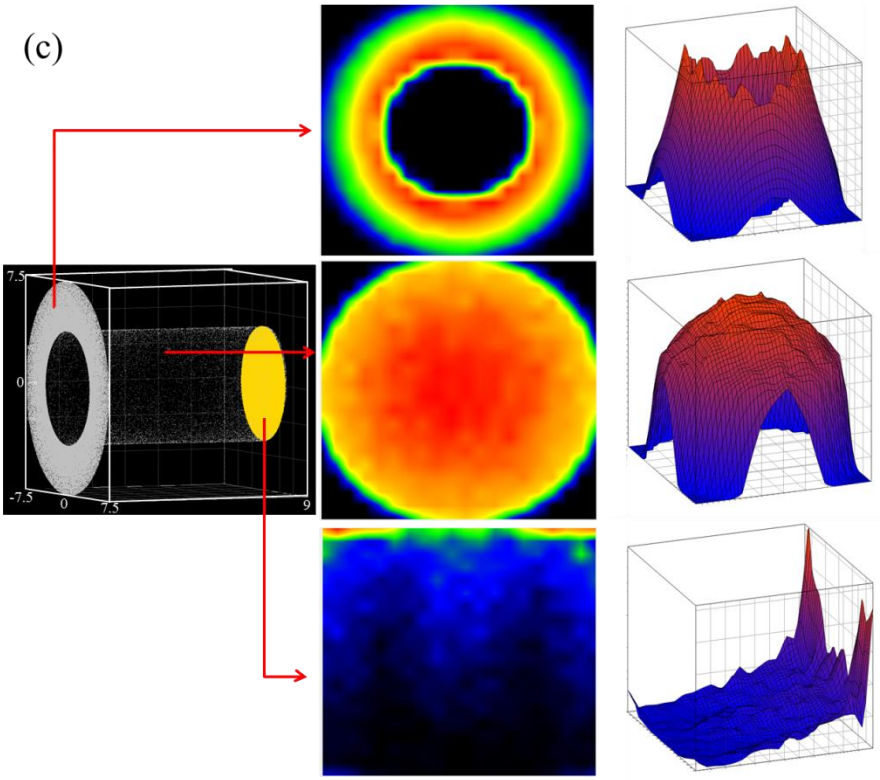

Figure IV-6 c.The contour of flux intensity – Model 2

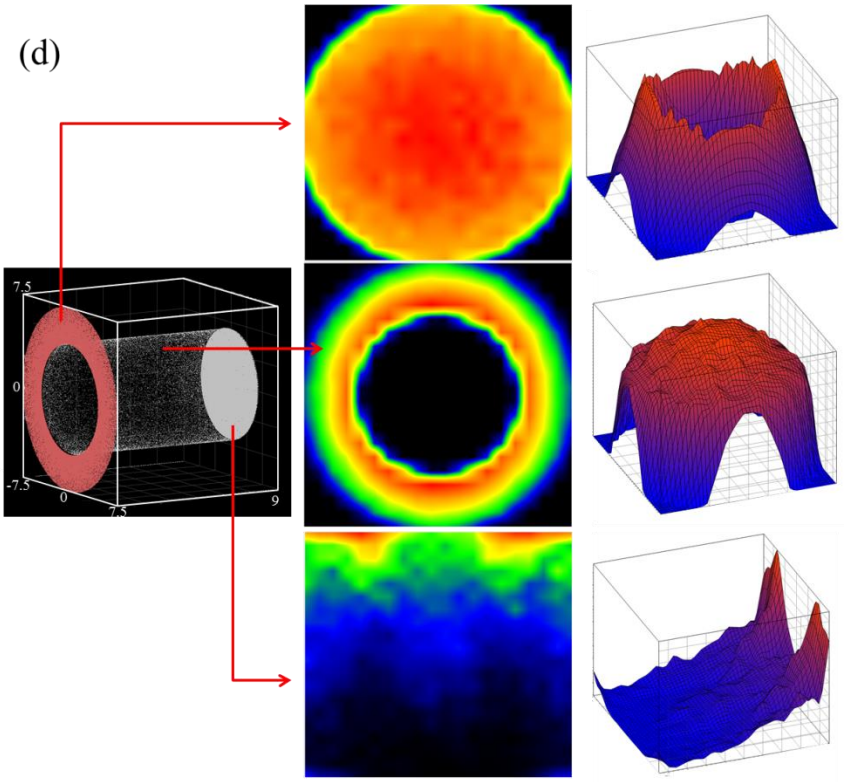

Figure IV-6 d.The contour of flux intensity – Model 3

(e)

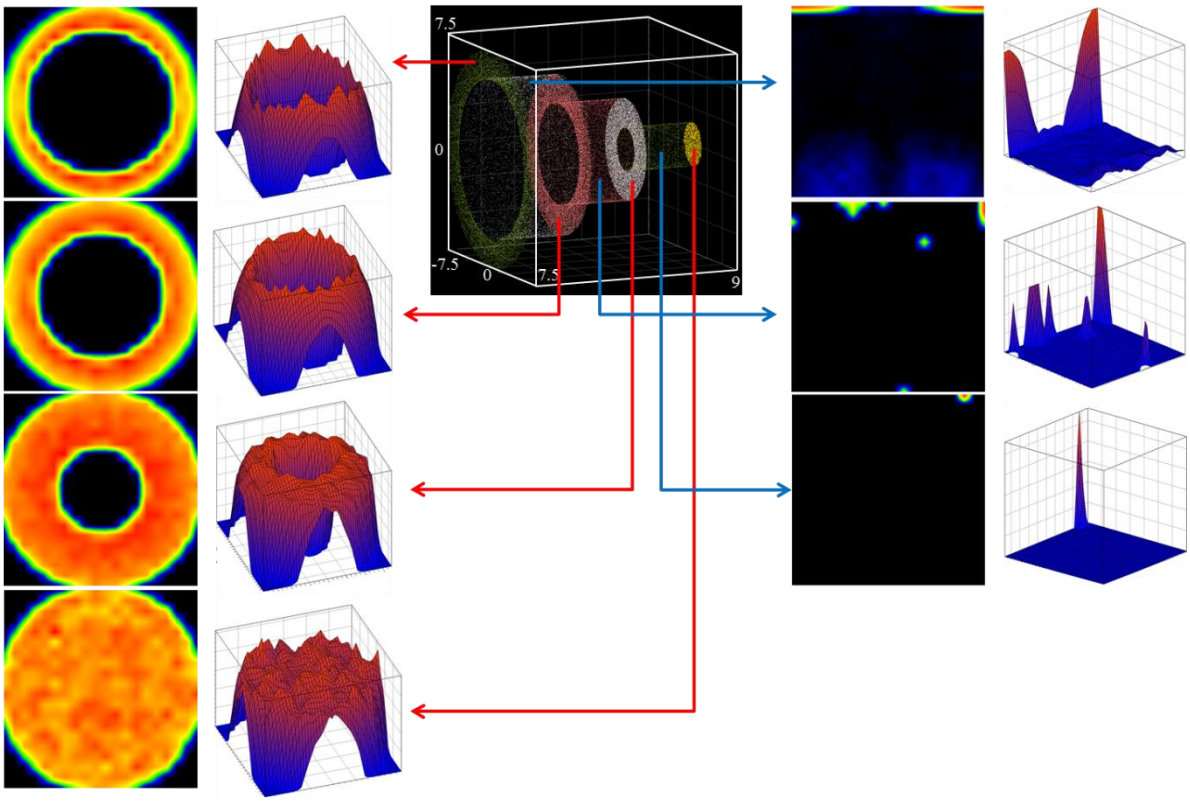

Figure IV-6 e.The contour of flux intensity – Model 4

IV - 4 - 3. Discussion

The simulation of flux distribution on the 5 suggested models was calculated by the optical simulation code Soltrace. Each model has a different shape, exposure area, and volume. The calculated results describe the heat flux intensity on separated surfaces. Table IV-3 shows the peak heat flux intensity and average heat flux at each separated zone in the 5 device models.

The input power was calculated for each device model. The range of input power was 23.2 kW to 27.4 kW for the simulation. The separated direct irradiated zone (D. A.) is different among all 5 models. In the case of the flat disk type, there is only one zone. On the other hand, the models 1, 2 and 3 have a tripartite zone detailing the results: the ring zone at the aperture region of the device; the cylinder wall zone through the device depth; and the disk zone at the end point of the device. The D.A 1 is the results of ring zone, D.A 2 is the cylinder wall zone, and the D.A. 3 is the disk zone. In the case of model 4, named conical shape, 7 separate zones describe its heat flux intensity.

As shown in Table IV-3, the heat flux intensity of the cylinder wall from models 1, 2, and 3 are considerably weaker than those pertaining to the ring zone. The results of the cylinder wall zone of

model 4 are therefore excluded from the table. Thus the values of D. A. 1 to D.A. 4 in the model 4 column show only the results of the ring zone D. A. 1 to D. A. 3 and the disk zone D. A. 4.

In models 1, 2 and 3, the heat flux intensity of separated zone reveal an increasing tendency form D.A. 1 to D. A. 3 excepting D. A. 2 (the cylinder wall zone). This means that some of the concentrated sun rays hits the aperture of devices, while most of the sun rays are delivered to the disk zone D. A. 3 through the device depth direction.

The largest peak heat flux was obtained from the case of model 1 D. A. 3 (disk zone) and the peak value was 3310.9 kW/m^2 whereas the largest average heat flux intensity was calculated to 1971.9 kW/m^2 from the case of model 2 D. A. 3 (disk zone).

The interesting points of the results obtained by the five model calculation is that the heat flux intensity of the cylinder wall zone (D. A. 2) shows very weak values compared to the ring zone and disk zone (D. A. 1 and D. A. 2). These findings reveal that concentrated sun rays have a directional characteristic, namely, predominant heat flux intensity on the normal direction on dish and perpendicular direction heat flux intensity at very low value. It means that to obtain uniform heat flux distributions on the device, normal directional surfaces have to be considered more carefully

than perpendicularly directed surfaces.

Table IV-3. Input power, peak heat flux, and average heat flux on the separated zones of the 5 device models.

Input Power (kW)		Flat disk	Model 1	Model 2	Model 3	Model 4
		23.2	26.1	27.4	23.3	26.3
D. A. 1	Peak flux	2,424.5	1,358.5	2,109.2	1,857.0	1,116.2
	Average flux	1,031.8	375.2	622.0	493.4	271.2
D. A. 2	Peak flux		252.1	270.6	218.4	2,561.9
	Average flux		15.8	28.5	37.7	874.6
D. A. 3	Peak flux		3,310.9	3,326.5	2,096.6	3,137.8
	Average flux		1,739.3	1,971.9	1,291.6	1,632.5
D. A. 4	Peak flux					2,868.2
	Average flux					1,548.2

IV - 4. Conclusion

By calculating the heat flux intensity of the above – mentioned devices, the flux distributions from the solar furnace system were simulated. The results clearly establish that concentrated sun rays have predominant heat flux intensity at a normal direction instead of perpendicular direction. After the calculation of flux intensity for 5 models, the conical shape model shows most uniformed flux distribution. So, for the next solar demonstration step, the conical shape foam device was selected and new solar reactor design also suggested. Consequently, the optical modeling study was attributed to development and improvement of solar reactor research.

Chapter V

Solar demonstration of new solar reactor with a conical foam device without ceria coating

V - 1. Introduction

This chapter describes the design, fabrication and solar demonstration of the new solar reactor with a conical shape foam device. The conical foam device without ceria coated is tested in the demonstration and the temperature distribution of the foam device is investigated. The results are compared with that of the flat disk foam device.

V - 2. Design of new solar reactor for conical shape foam device

V - 2 - 1. Conical shape foam device matrix

According to the results of chapter IV, the distribution of flux intensity is related with foam device shape or geometry. The results shows different attainable flux intensity on the foam device surfaces, and the conical shape foam device shows most smooth flux intensity distributions on the foam device surfaces. So the model 4 as shown Fig. IV-4 and Fig. IV-6e was considered for design of conical shape foam device geometry.

However, model 4 has a stepwise geometry like as stair for the easier optical modeling and calculation; it means that the model 4 is not conical shape geometry exactly. Thus, by the use of model 4 geometry, the real conical shape foam device geometry was designed. Fig. V-1 shows application process and embodies process for suitable conical shape foam device. The red line shows a final decided conical shape geometry which based on original model 4 shape.

After decide the geometry of conical shape foam device, the mechanical drawing was implemented for design of new solar reactor. Fig. V-2a and b shows a specification of final conical foam device including aperture angle.

In fact, the fabrication method of conical shape foam device and the points for temperature measuring also considered. By the dividing of several stacks (4 layers structure), previous flat type foam device matrix was utilized to conical device preparation. Fig. V-3 shows the fabricated and conical shape foam device which consist of 4 layers, and having continuous diagonal cut lines.

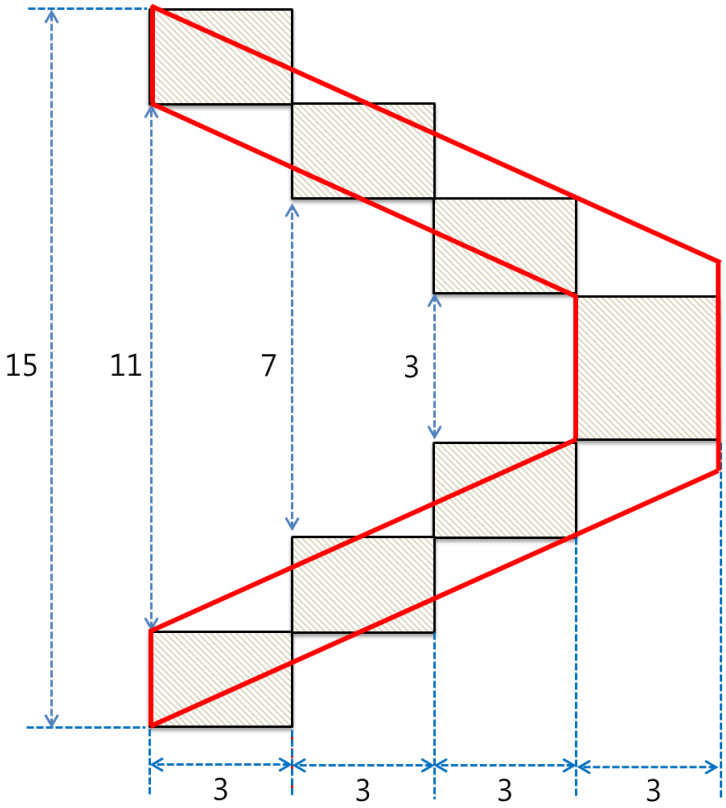

Figure V-1. The base line of conical shape foam device (The red lines show a final geometry of real conical shape)

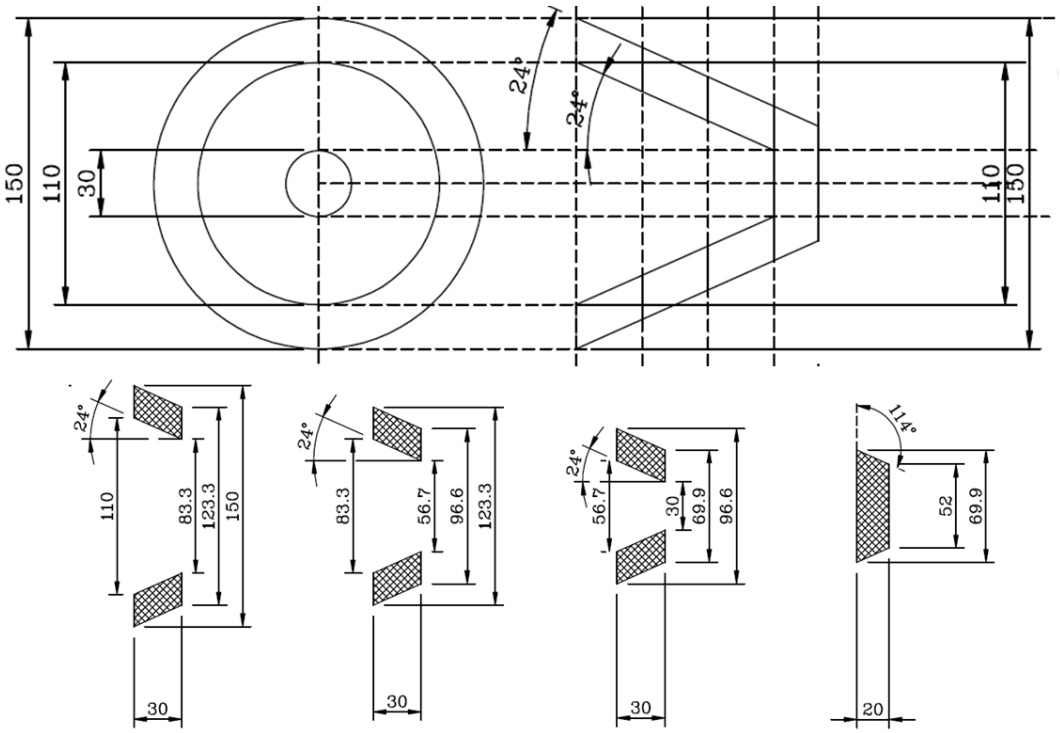

Figure V-2a. (2-D) The specification and mechanical drawing of conical shape foam device (The conical shape foam devices consist of 4 layer by the utilize of previous flat type foam matrixes)

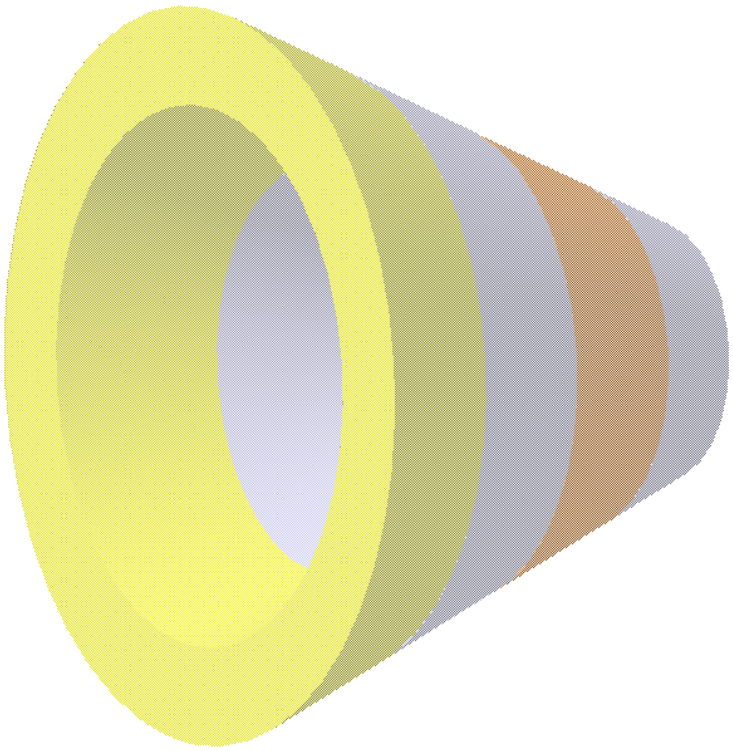

Figure V-2b. (3-D) The specification and mechanical drawing of conical shape foam device (The conical shape foam devices consist of 4 layer by the utilize of previous flat type foam matrixes)

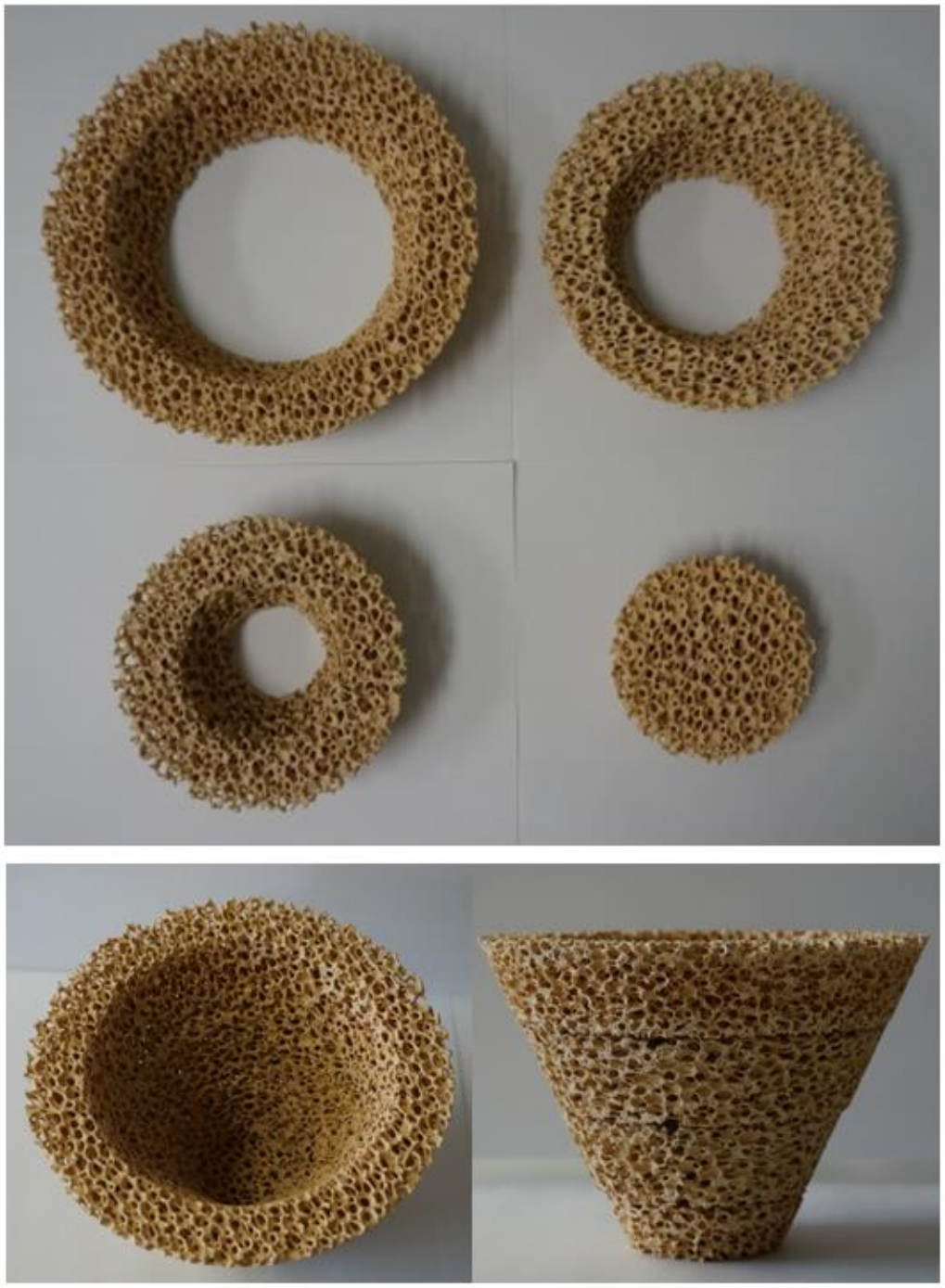

Figure V-3. The prepared conical shape foam device (The conical shape foam devices shows continuous cut lines)

V - 2 - 2. Design of new solar reactor

For the assembly of conical shape foam device and good approach of temperature measure methods, the new solar reactor was designed. The major problem was how to install the thermocouples for measure the foam device surface temperature, and fix tightly among the 4 layer pieces of foam device matrixes. Firstly, in order to avoid the increase of pressure drop by the effect of device holder, the conical shape net structure was suggested. By the applying to same aperture angle of conical foam device, the porous conical shape net structure was designed and the solar reactor body structure was considered. Fig. V-4 shows the fabricated conical shape net holder which made by Inconel 600 materials. It assists the suitable fit among the device pieces, and having the holes for easy pass of internal streams.

The number of thermocouples was decided to 3 points, and the measuring point was designed to a gap between the layers. Fig. V-5a and b shows the design of new solar reactor for the conical shape foam device, and Fig. V-6 explains the measuring point of thermocouples.

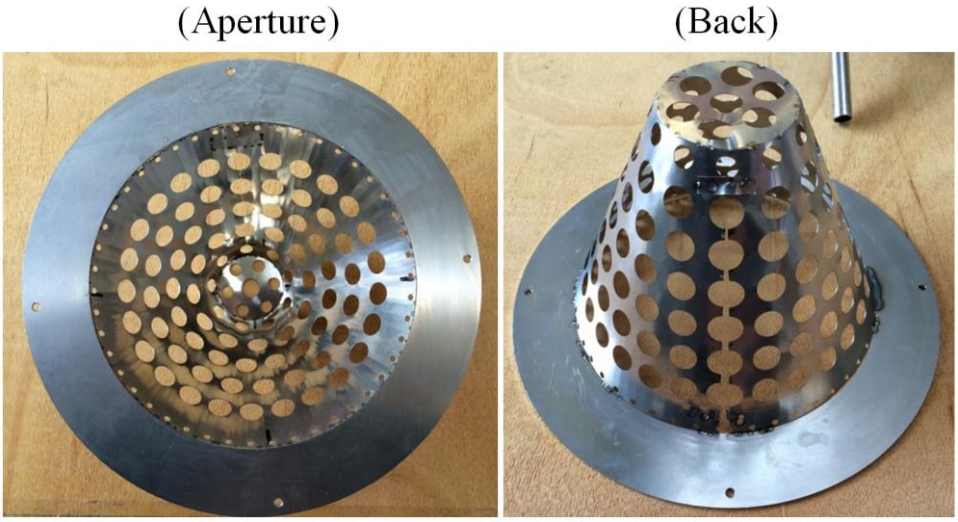

Figure V-4. The prepared conical net holder (suitable fit to foam matrixes)

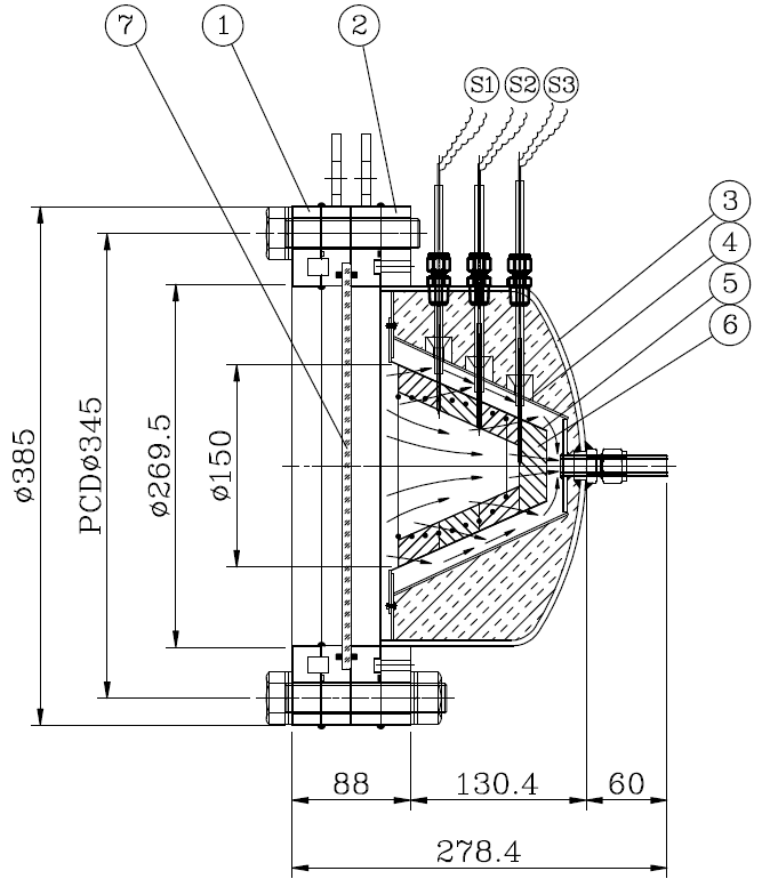

Figure V-5a. The 2-D design drawing of new solar reactor for conical shape foam device

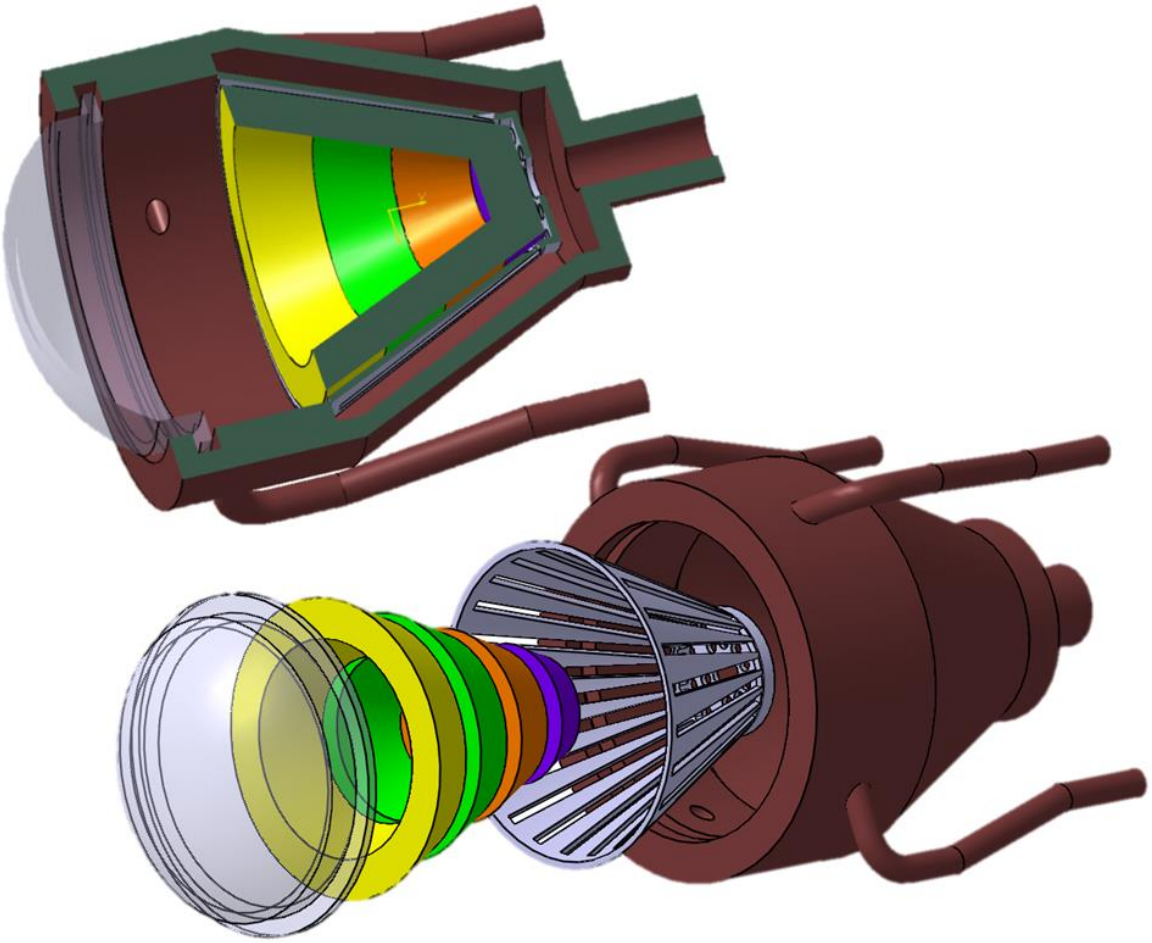

Figure V-5b. The 3-D design drawing of new solar reactor for conical shape foam device

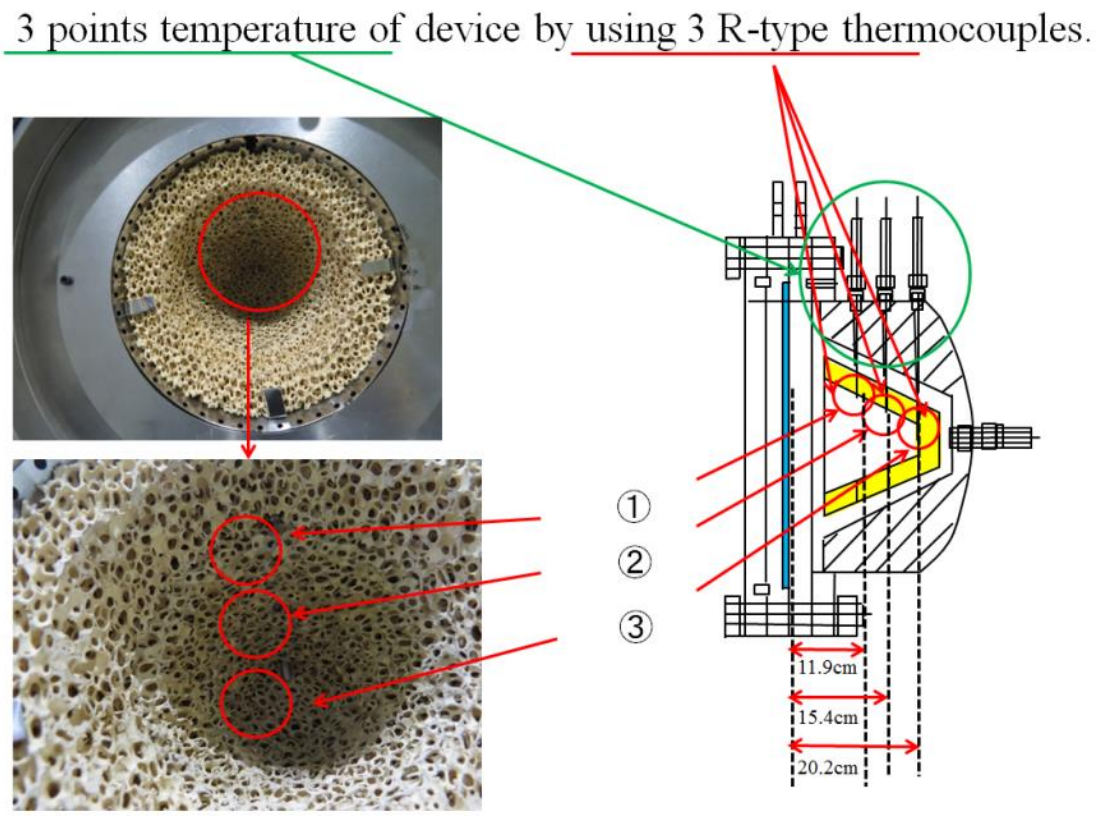

Figure V-6. The thermocouple points for temperature measure

V - 3. Experimental setup and test of new solar reactor with conical shape foam device

V - 3 - 1. Experimental setup of new solar reactor

The fabricated new solar reactor and conical shape foam device were assembled and installed to KIER solar furnace in order to test or validation of previous studied results. Fig. V-7 shows the assembly process of each part of new solar reactor and conical shape foam device.

At first solar demonstration, the quartz window was damaged due to heat up to dangerous temperature. So in order to avoid the quartz window damage, additional improvement component was considered. Fig. V-8 shows cooper lines for quartz window cooling. The cooper lines connected to air compressor it supply the ambient temperature air for cooling of quartz window surface. By the valve control, the cooling air gas flow rate was controlled. The nozzle of cooper lines placed and divided to 4 positions and it blows the quartz window surface center region as shown Fig. V-8.

Finally, the conical shape foam device and new fabricated solar reactor was installed to KIER solar furnace system. Fig. V-9 shows the experimental system where placed and installed to KIER solar furnace. The experiment and results were described to next section.

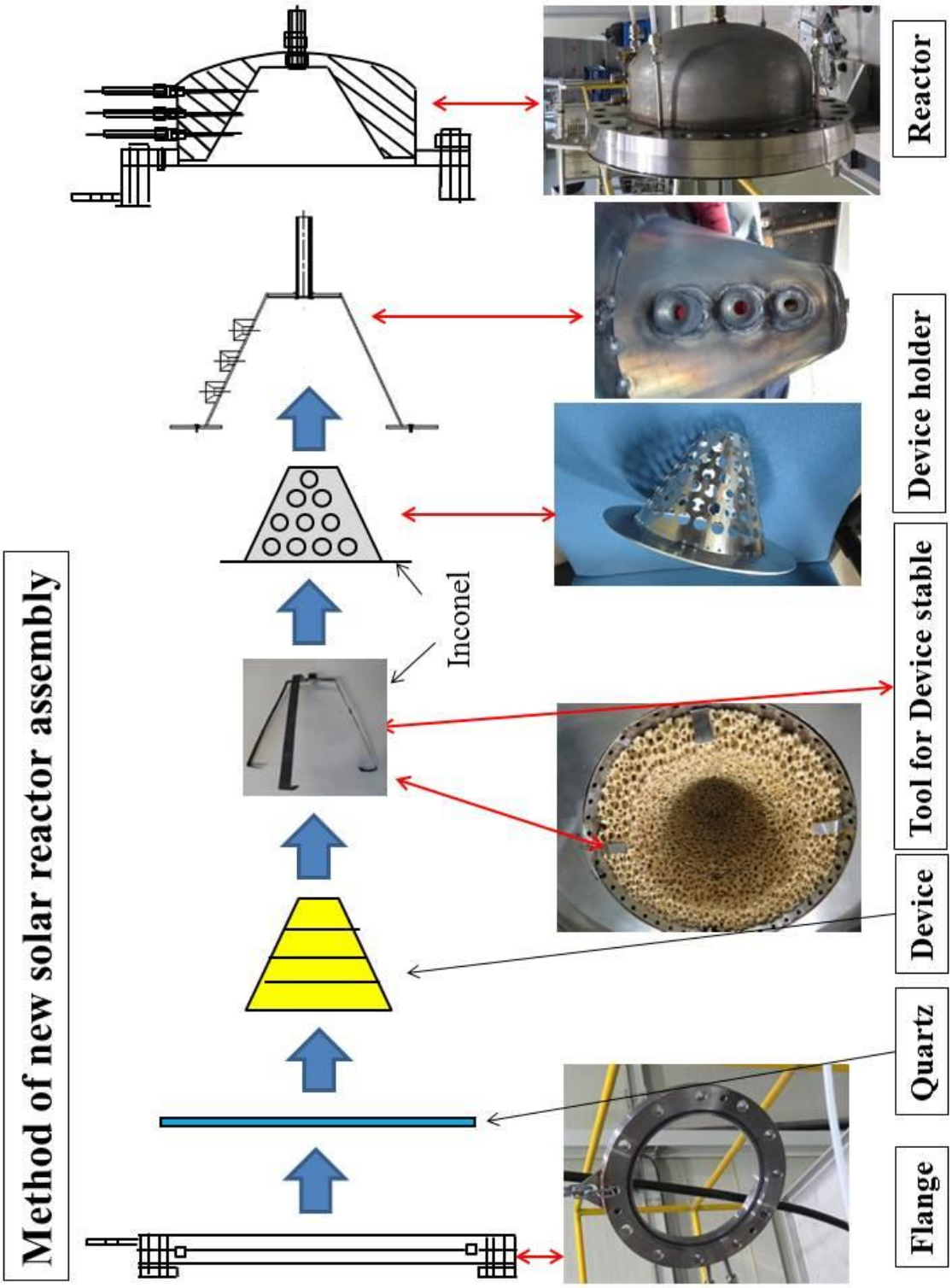

Figure V-7. The Assembly process of new solar reactor with conical shape foam device

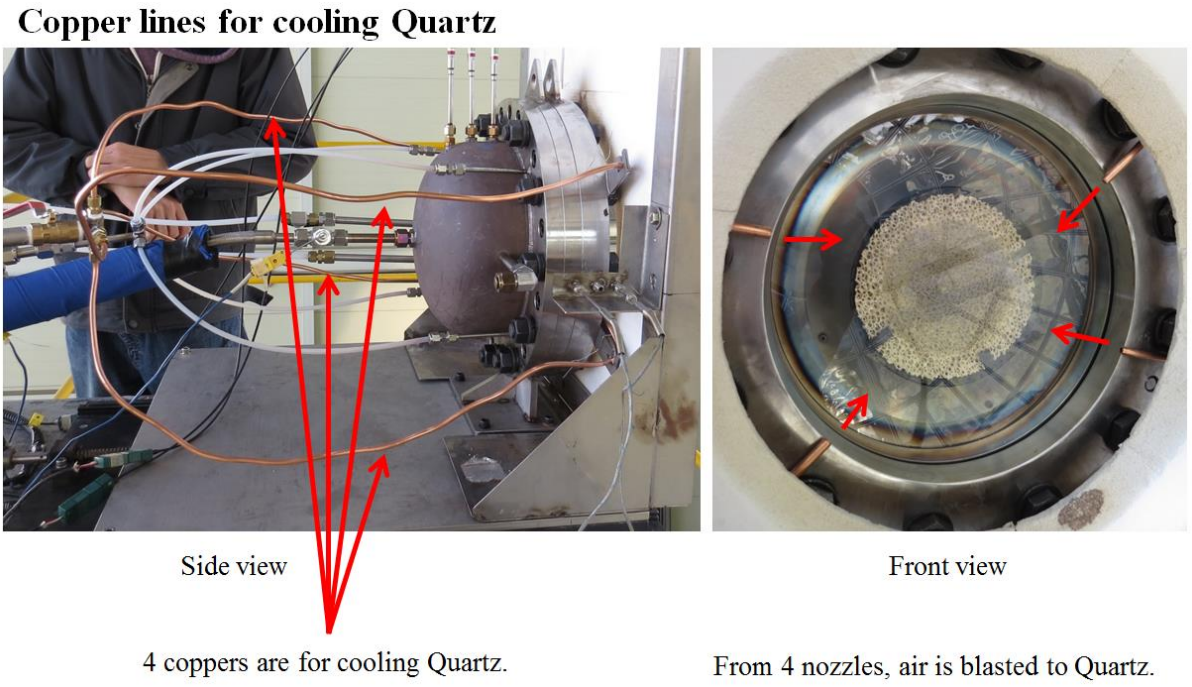

Figure V-8. The improvement component for cooling of quartz window

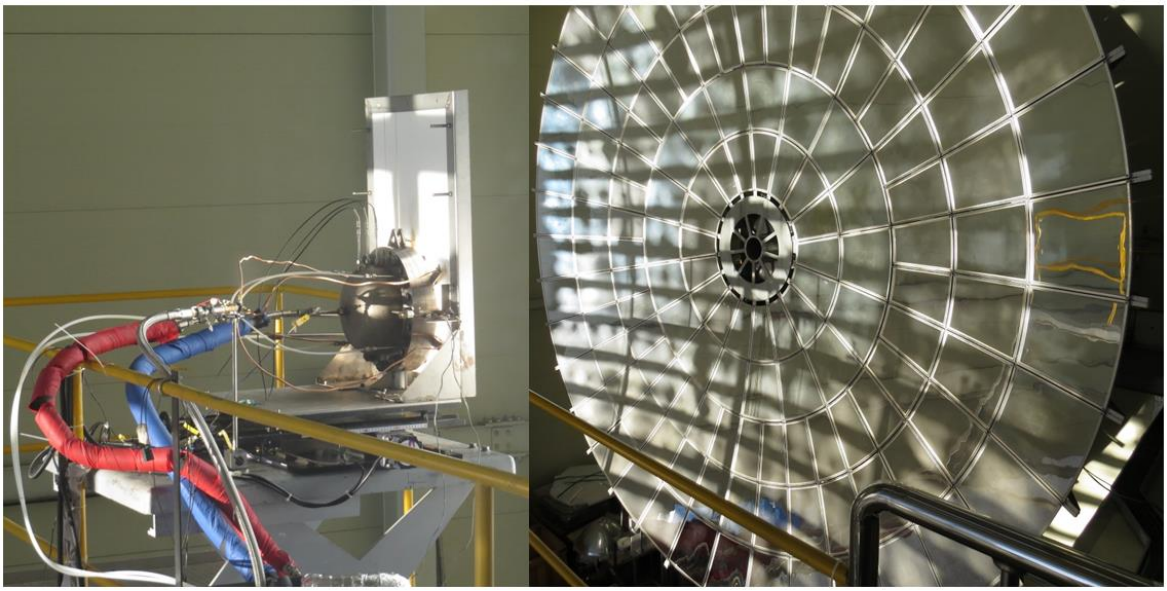

Figure V-9. The conical shape foam device and new fabricated solar reactor was installed to KIER solar furnace system

V - 3 - 2. Test of new solar reactor with conical shape foam device

The uncoated conical shape foam device was tested in KIER solar furnace system with the new solar reactor. The objective of experiment was pilot test and validation of new suggested conical foam device temperature distributions. Only the experimental condition of thermal reduction step was tested due to the conical shaped foam device wasn't coated by reactive cerium oxide. By the control the opening percent of blind in KIER solar furnace system, the temperature test and safety of new solar reactor was evaluated. The internal working fluid was supplied by N_2 gas in range of 3000 ~ 8000 Ncm^3/min with the consideration of experimental scale up. The 3 temperature points on the foam device surface were recorded to monitoring system and the temperature variations was compared and discussed with previous results. Fig. V-10 shows a photograph of new solar reactor aperture after the temperature test when captured immediately. The remained heat was observed as red color at inside of conical foam device cavity.

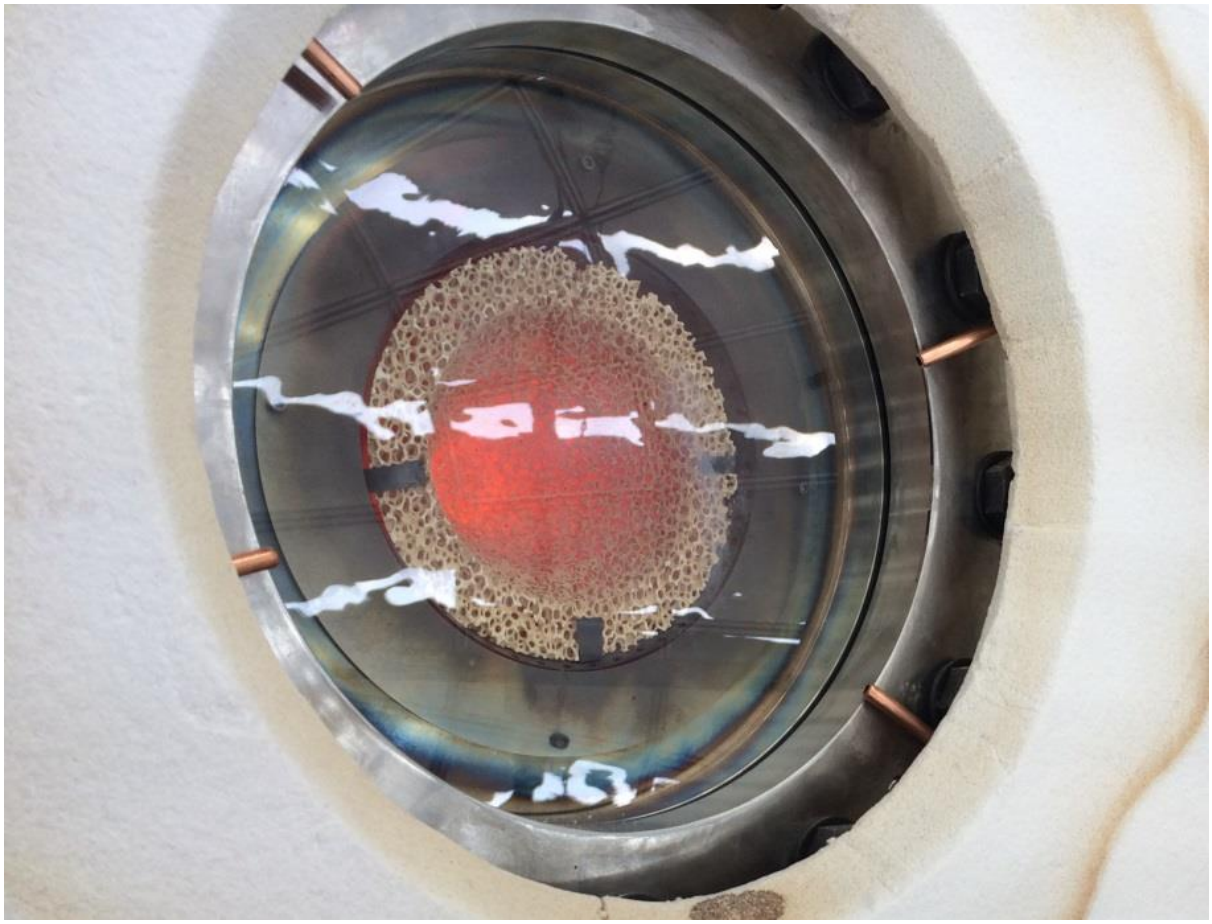

Figure V-10. The status of quartz window and the remained heat in side of conical foam device cavity

V - 4. Results and Discussions

V - 4 - 1. Temperature variations on the foam device

Fig. V-11 shows the temperature variations on the foam device during the temperature test. The temperature point was 3 points on the foam device, and named by the number T.C. 1, T.C. 2, and T.C. 3. And the DNI also recorded for the analysis of effective factor for device temperature. The preheating sections before 14:45 min was not important for test of temperature distributions, so it was skipped.

V - 4 - 2. Discussion

From 14:45 to 15:22, about 37 minutes the device temperature recorded highest value. Most high temperature point was observed to T.C. 3 (as shown green line) where placed to deepest placed on the conical shape foam device cavity.

The gap of temperature between T.C. observed to 100 ~ 200 ^{o}C roughly, it shows good improvement of the challenge which foam device shape change for acquire the uniform temperature distribution on the foam device surface.

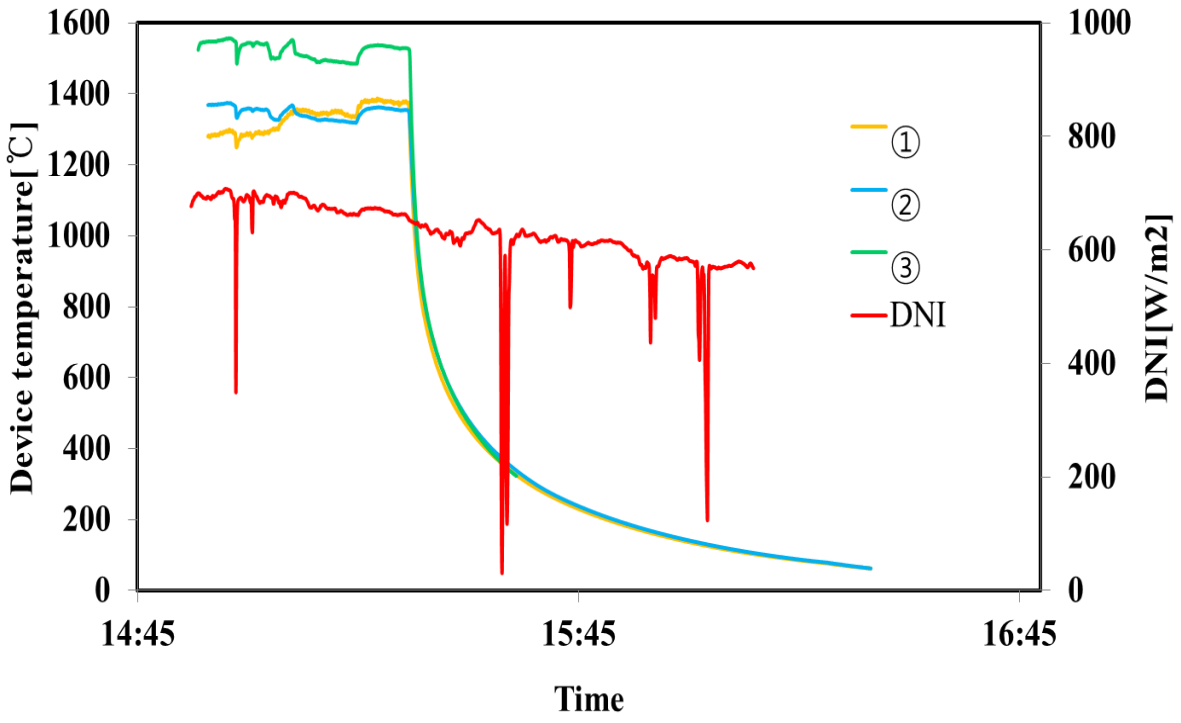

Figure V-11. Temperature variations T.C. 1 to T.C. 3 and DNI

V - 5. Conclusion

The new solar reactor design was designed, fabricated and tested with conical shape ceria uncoated foam device for validation of temperature distribution. During the process of development new solar reactor and preparation of conical shape foam device matrix, new mechanical idea, and concept were adopted to manufacturing. The temperature distribution on the conical shape foam device shows significantly improved temperature distribution. The additional component for cooling of quartz window also worked successfully, the improvement of experimental system is completed. The temperature distributions via 3 thermocouples shows good reduced temperature gap compare with previous flat type disk foam device temperature gap. By the use of tested conical shape foam device, it is expected that the increase of hydrogen productivity via cerium oxide coated conical foam device.

Chapter VI

Numerical simulation of solar reactor and case study

VI - 1. Introduction

This chapter presents a CFD (Computational Fluid Dynamics) simulation of solar reactors. ANSYS 12 CFD code was used for numerical calculation of temperature distribution on the foam device, stream, pressure drop, etc. The result was compared with experimental results. Prototype solar reactor with flat type device and second type solar reactor with conical shape device were simulated. After the numerical simulation, the results were compared and discussed.

VI - 2. CFD (Computational Fluid Dynamics) of solar reactors

The solar reactor including foam device which suggested and tested from this research has a transparent quartz window for direct input of concentrated solar radiation. The concentrated solar irradiations arrive to the surface of foam device and heat up to high temperature for derives solar fuel production reaction. So the heat transfer capability of solar reactor and foam device is very important to increase the productivity of hydrogen. To understand of major and effective factors for the heat transfer, modeling of solar reactor including foam device shape was conducted.

First, previous solar reactor which is including flat type foam device was simulated. For the modeling and simulation of solar reactor, the CFD code, ANSYS 12 was used.

Simulated region was defined only the interior region for effective calculation. Fig. VI-1a shows the simulated region on the prototype solar reactor. The red lined volume where inside of reactor includes the flat type foam device volume and the annular inlets and outlet ports. Fig. VI-1b is the generated simulation volume.

The pressure properties for the simulation, empirical equation – Forchheimer equation was adapted to calculations, and permeability, drag coefficient, and porous medium length also given by measure of

foam device property.

In order to simulation of heat transfer, the P-1 radiation model was studied. The P-1 model includes the effect of scattering and assumes that all surfaces are diffuse. And the initial temperature condition was given by experiment data, and the foam device surface zoned for give a different initial temperature. Inlet flow rate was given by experiment data, and fluid was considered to nitrogen gas.

Subsequent solar reactor also simulated with same methodology. For the calculation, the modeling process was used triangular mesh with 620 thousand grids. Fig. VI-2 shows a generated volume for solar reactor for conical foam device.

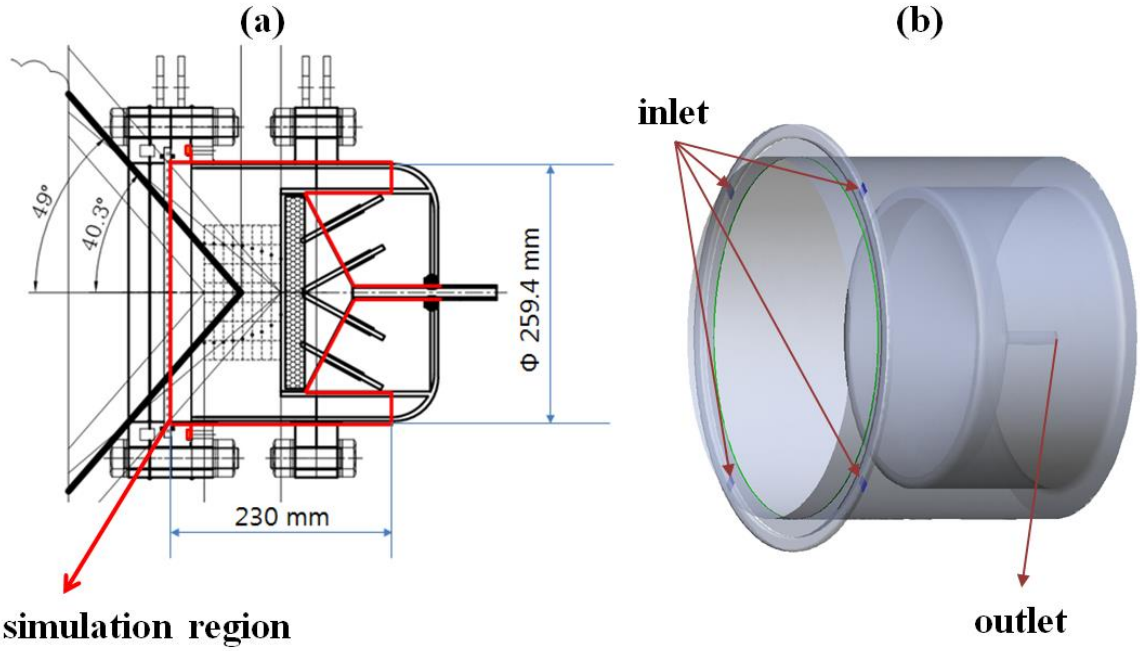

Figure VI-1a. Simulated region of the proto type solar reactor

Figure VI-1b. Generated volume for simulation

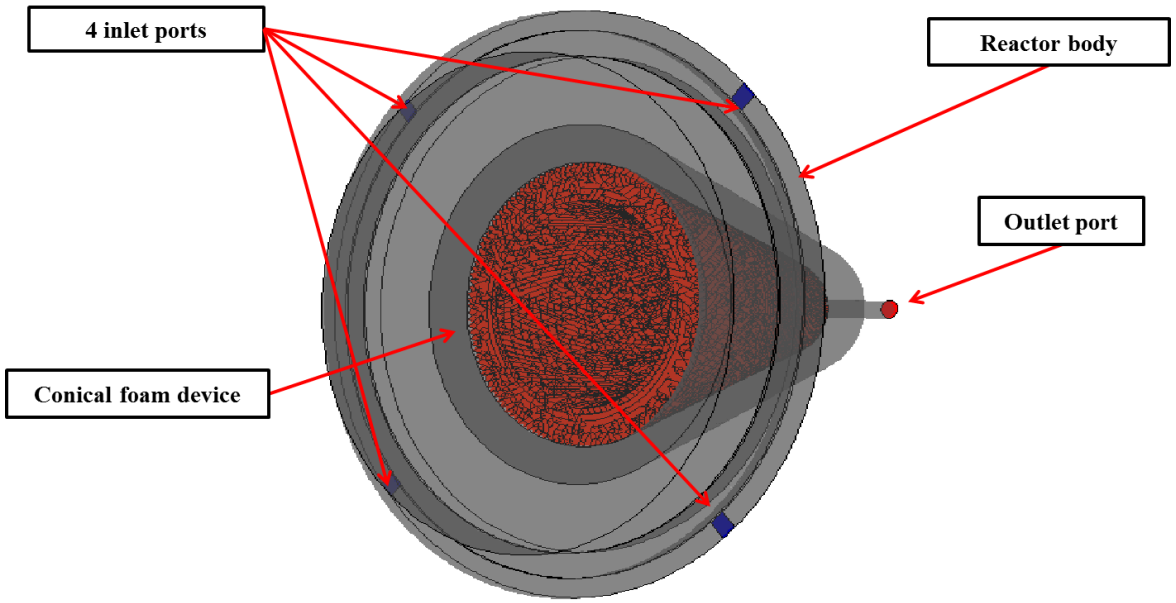

Figure VI-2. Simulated region of the conical shape foam device solar reactor

VI - 3. Results and case study

VI - 3 - 1. Result of simulation pressure drop gradient, temperature, and path line

Fig. VI-3, Fig VI-4, and Fig. VI-5 shows the simulation results of prototype solar reactor. Fig. VI-3 is the pressure drop gradient through the solar reactor inlet to outlet. Fig. VI-4 is the temperature gradient of solar reactor. Temperature profile was described by Kelvin scale. Fig. VI-5 shows the path lines of the flows where solar reactor interior volume.

Continuously, Fig. VI-6 , Fig. VI-7, and Fig. VI-8 is the results of conical shape foam device solar reactor. Fig. VI-6 is the pressure drop gradient, Fig. VI-7 is the temperature gradient, and Fig. VI-8 is the path line of the flows.

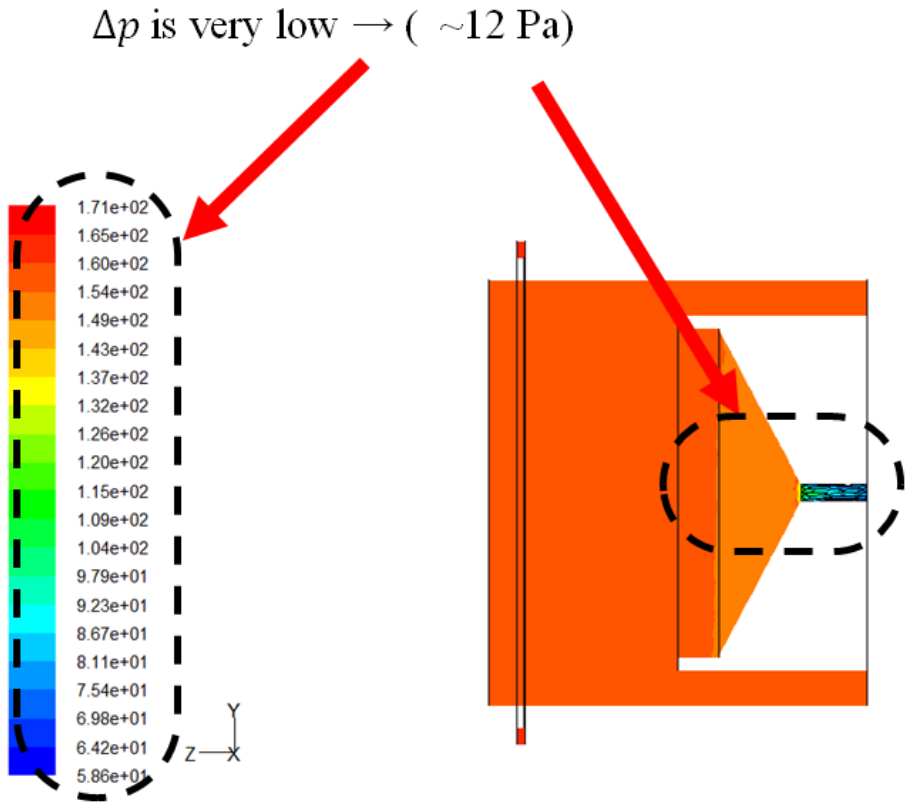

Figure VI-3. Pressure drop gradient of proto type solar reactor

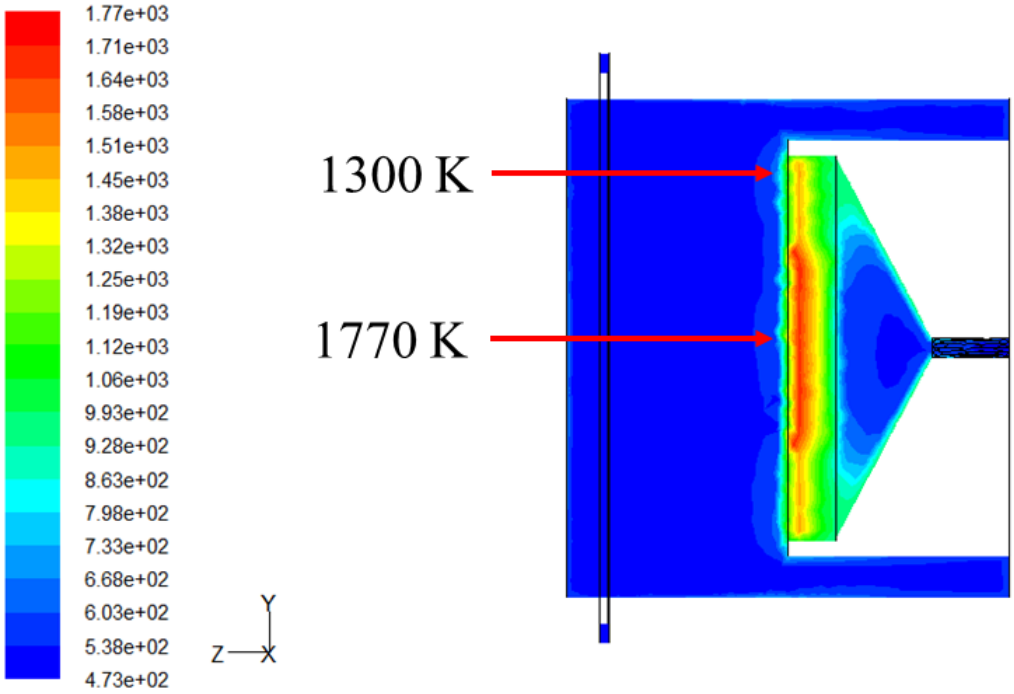

Figure VI-4. Temperature gradient of proto type solar reactor

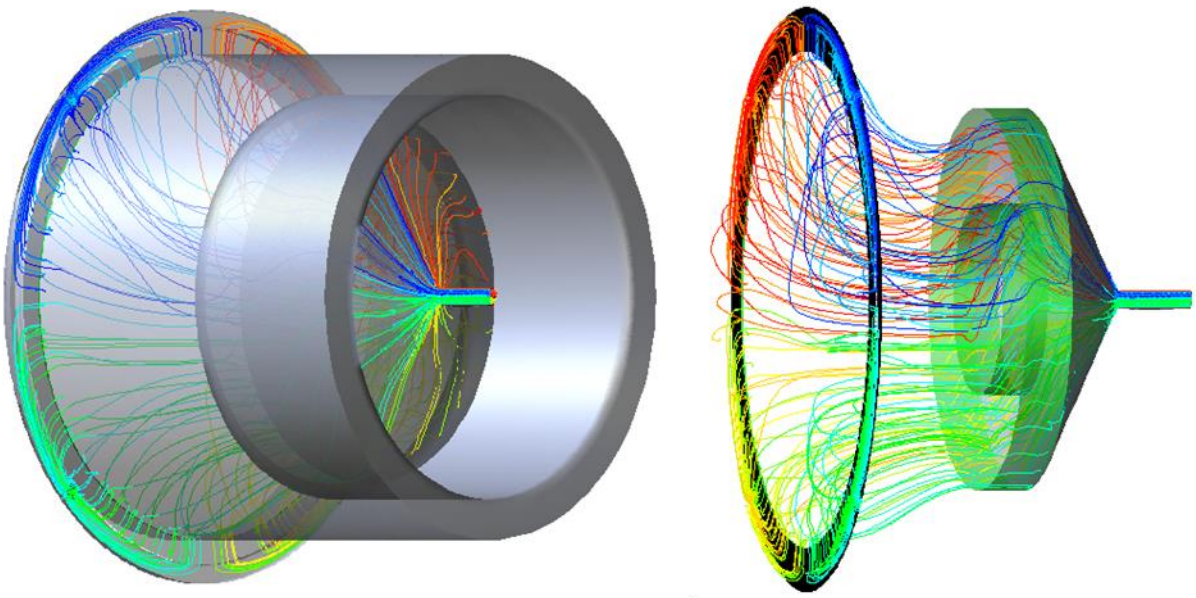

Figure VI-5. Path line of inter gas flows (Proto type solar reactor)

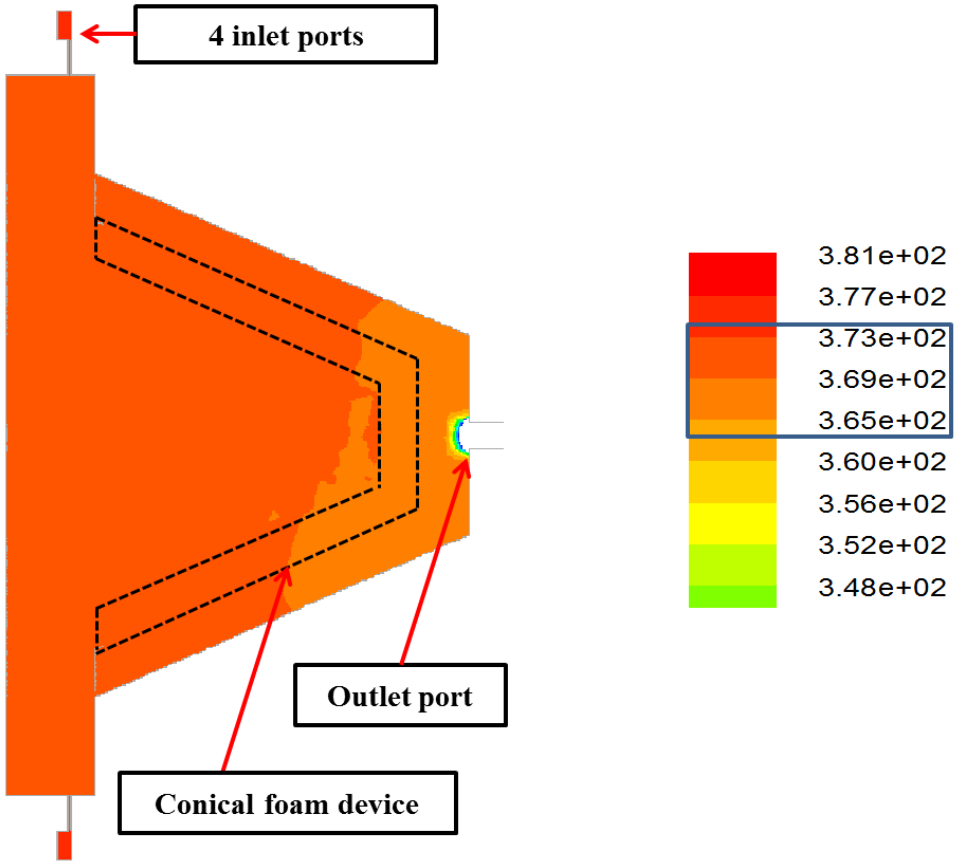

Figure VI-6. Pressure drop gradient of conical shape foam device solar reactor

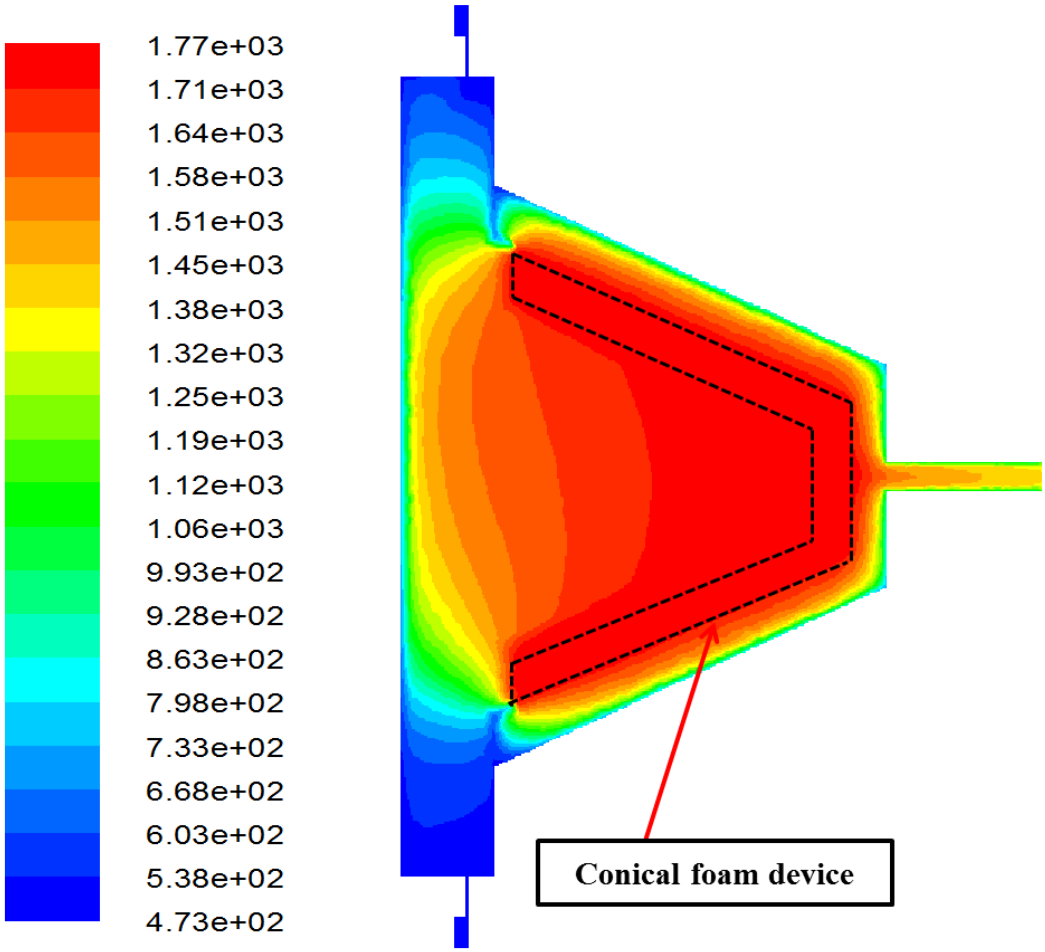

Figure VI-7. Temperature gradient of conical shape foam device solar reactor

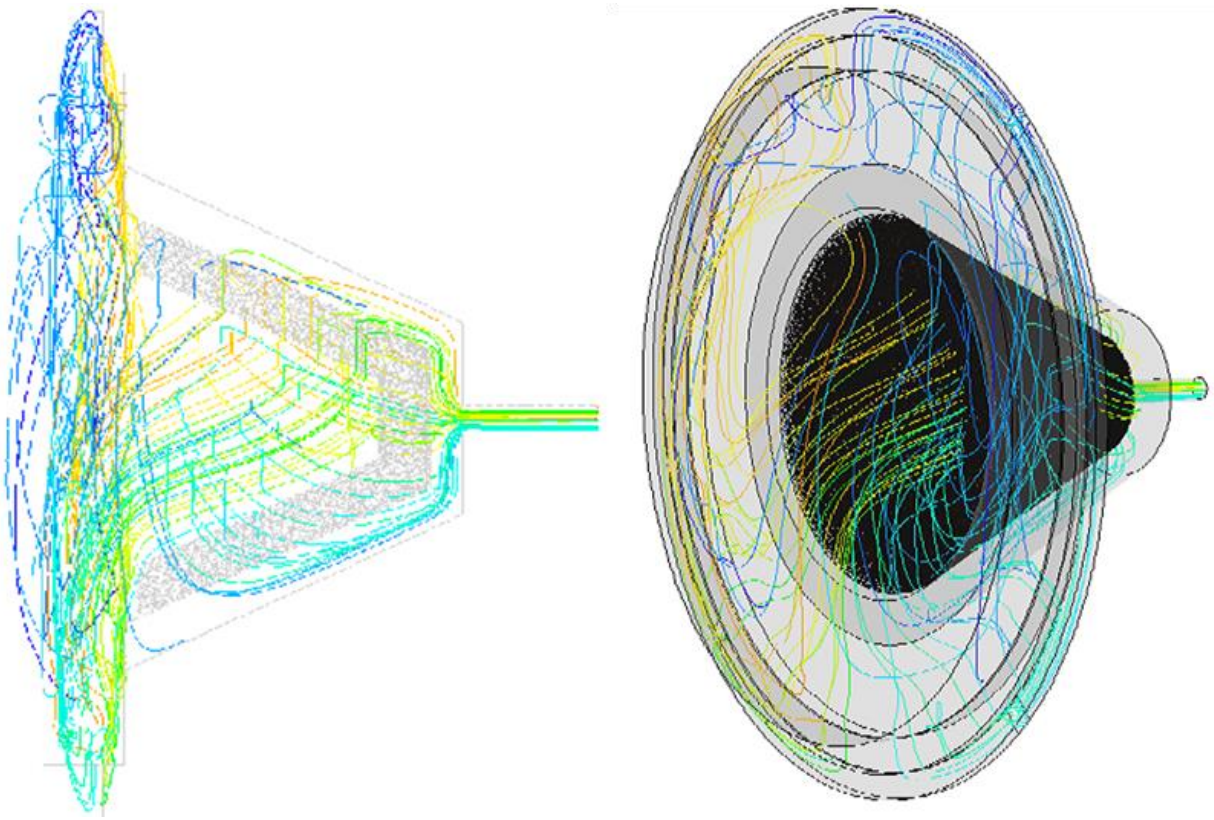

Figure VI-8. Path line of conical shape foam device solar reactor

VI - 3 - 2. Case study of simulation results

The simulation result was compared with previous experiment results in order to validate the agreements between simulation and experiment results. A good established simulation model has a benefit for expect the experiment result within reasonable basis.

First, the comparison of temperature distribution between flat type foam device solar reactor experiment results and its simulation results. Fig. VI-9 shows the comparison of temperature gradient. The result shows a good agreement for temperature value and distribution. At the center temperature of flat type foam device was reached to 1400 ~ 1500 ^{o}C from the experiment, and the simulation results indicate 1497 ^{o}C and then at the edge point, the experiment result recorded 1000 ^{o}C around and simulation results reached to 1107 ^{o}C.

It means that the simulation result of the temperature distribution on the foam device shows a good agreement with experiment results.

And the comparison of temperature distribution between two solar reactors was studied. Fig. VI-10 shows the comparison of temperature distributions between two solar reactor models. When experiment the proto type solar reactor, the maximum input energy was limited due to solar reactor safety and foam matrix damage from over the melting point. However, the conical shape foam device reactor has a larger

possibility of input energy range because of enhanced skills and approaches were adapted. So, as shown Fig. VI-10, the input energy was given differently.

The temperature distributions on the foam device areas show significantly enhanced and uniformed distribution from conical shaped foam device solar reactor.

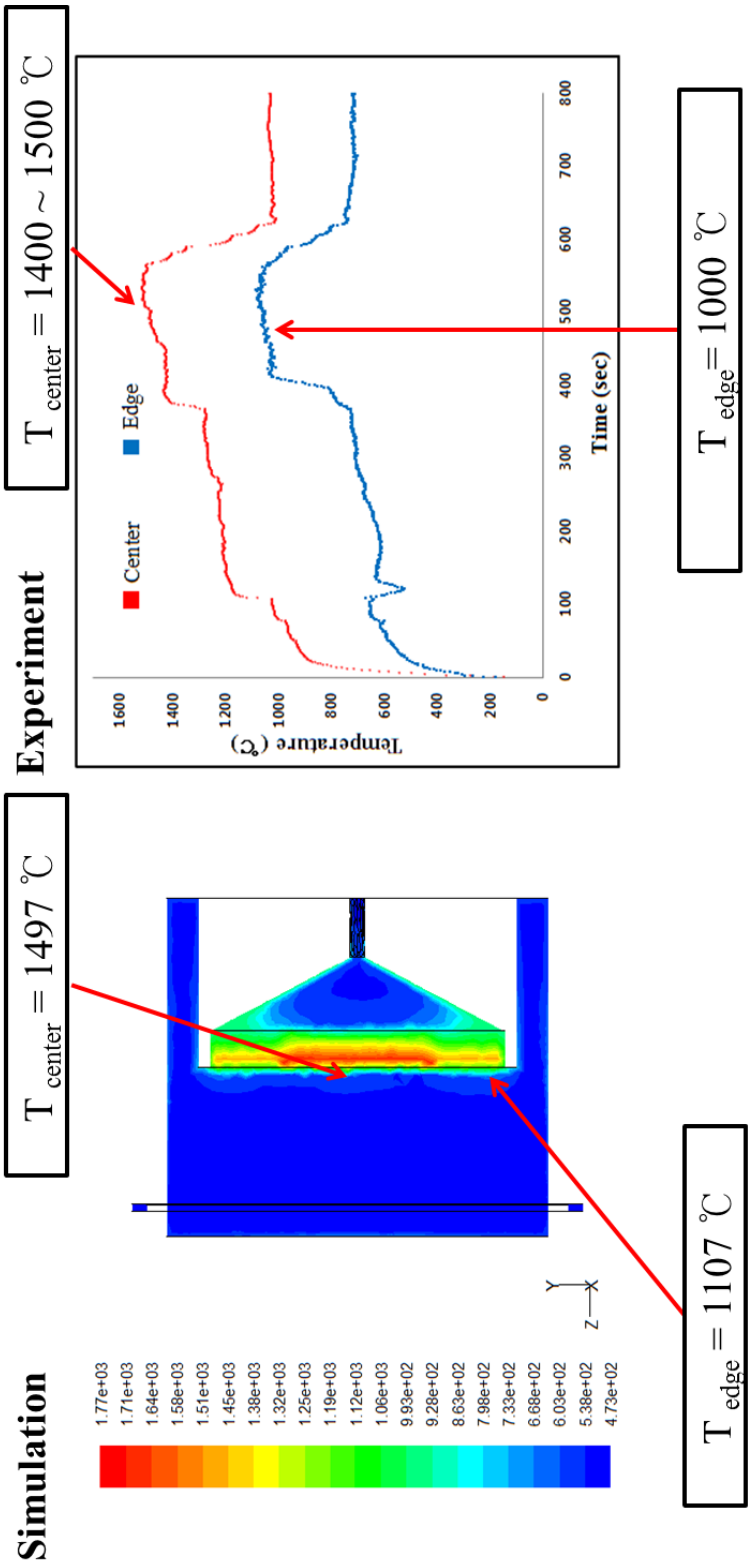

Figure VI-9. Temperature comparison of proto type solar reactor

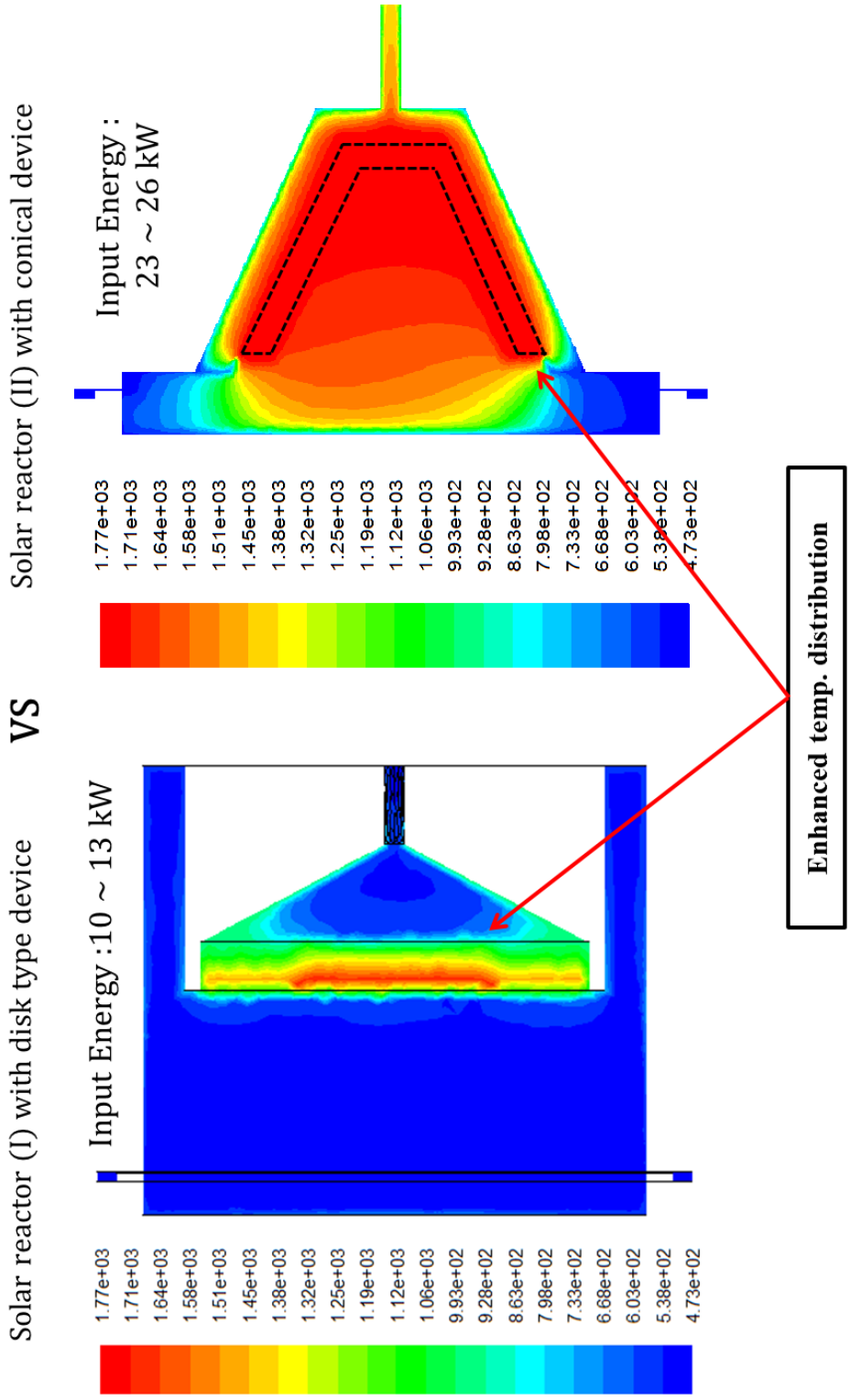

Figure VI-10. Temperature comparison between two solar reactor

VI - 4. Conclusion

By the use of ANSYS 12 as a simulation tool, the modeling of two solar reactors was studied and compared. Prototype solar reactor with flat type foam device and conical shape foam device solar reactor were simulated. The boundary conditions for simulation were suggested from the experiment data, and the heat transfer model was adopted with P-1 radiation model. The result shows a good agreement with experiment results. And the temperature distributions on the foam device areas show significantly enhanced and uniformed distribution from conical shaped foam device solar reactor.

Chapter VII

Conclusion

Two-step thermochemical water splitting cycle is one of the promising processes for converting concentrated solar high-temperature heat into clean hydrogen. The two-step water splitting cycle requires higher temperature above 1400˚C minimum. Niigata University has been studied the small scale two-step waster splitting cycle with ceria coated foam device. In the basis of previous work, the two-step water splitting cycle with ceria coated foam device was scaled up from sun-simulator scale to solar demonstration scale by this research.

For the validation of scaled up two-step water splitting cycle, proto type solar reactor were designed, fabricated, and demonstrated with large size flat type ceria coated foam devices. Proto type solar reactor was tested with three different ceria coated foam devices at the KIER solar furnace, and during the solar demonstration cycles the three different operation methods also investigated in order to increase the hydrogen productivity. 30 cycles of the two-step water splitting were demonstrated in total, and solar operation method of this foam device reactor was improved. Hydrogen could be

successfully produced in the repeated cycles by input of 10-18 kW_{th} of concentrated solar irradiation.

On the basis of the experimental data of the solar demonstration, a new design of the solar reactor with a conical or cylindrical foam device was proposed in order to improve hydrogen production performance. Comparing the previous flat foam device, the conical or cylindrical foam device can create a more uniform heat flux distribution on the foam device surface, which expands the solar-heated high-temperature region of the foam device. In addition, the conical or cylindrical foam device can improve the heat transfer between gases and foam surface.

Four different-shaped foam devices of conical or cylindrical types were designed, and numerical simulation was done for them by optical modeling. Then the second-type of the solar reactor with a conical shape foam device without ceria coating was fabricated. And the new solar reactor was tested on temperature distribution of conical foam device at the KIER solar furnace. 23 ~ 24 kW_{th} of solar concentrated radiation was irradiated to the conical foam device. More uniform temperature distribution was created on the surface of the conical device comparing with that of the flat device. The high temperature region ($T > 1400\ ^oC$) could be expanded as expected.

Additionally, the numerical simulation in terms of pressure drop, temperature distribution, and path lines of the two tested solar reactors was studied and the results show good agreement with experimental data.

Overall investigation and results are expected to applicate to development of high productivity solar reactor.

Reference

1. KODAMA, Tatsuya; GOKON, Nobuyuki. Thermochemical cycles for high-temperature solar hydrogen production. Chemical Reviews, 2007, 107.10: 4048-4077.
2. SolarGIS © 2015 GeoModel Solar
3. Lakshmanan S, Manasse F, Mathur V. Production of fuels from high temperature solar thermal synthesis—economic analysis. In: Farag I, Melsheimer S, editors. Fundamentals and applications of solar energy. AICHE symposium series no. 198, vol. 76; 1998. p. 156.
4. Fletcher E. On the thermodynamics of solar energy use. J Minn Acad Sci 1984;49(2):30–4.
5. Sizmann R. Solar driven chemistry. CHIMIA 1989;43: 202–6.
6. Grasse W, Tyner C, Steinfeld A. International R&D collaboration in developing solar thermal technologies for electric power and solar chemistry: the solarPACES program of the International Energy Agency (IEA). J Phys IV Fr 1999; 9:Pr3-9–Pr3-15.
7. Tamaura Y. Solar hybrid methanol production from coal and natural gas by solar thermochemical process: CO2 reduction and cost evaluation. In: Kreetz H, Lovegrove K, Meike W, editors. Solar thermal. Proceedings of the 10th SolarPACES International Symposium on Solar Thermal Concentrating Technologies, Sydney, Australia; 2000. p. 189–92.
8. Steinfeld A, Schubnell M. Optimum aperture size and operating temperature of a solar cavity-receiver. Solar Energy 1993;50(1):19–25.
9. Fletcher E, Moen R. Hydrogen and oxygen from water. The use of solar energy in a one-step effusional process is considered. Science 1977;197:1050–6.
10. Nakamura T. Hydrogen production from water utilizing solar heat at high temperatures. Solar Energy 1977;19:467–75.

11. Ihara S. Feasibility of hydrogen production by direct water splitting at high temperature. Int J Hydrogen Energy 1978;3: 287–96.

12. SCHEFFE, Jonathan R.; STEINFELD, Aldo. Oxygen exchange materials for solar thermochemical splitting of H 2 O and CO 2: a review. Materials Today, 2014, 17.7: 341-348.

13. CHUEH, William C.; HAILE, Sossina M. A thermochemical study of ceria: exploiting an old material for new modes of energy conversion and CO_2 mitigation. Philosophical Transactions of the Royal Society A: Mathematical, Physical and Engineering Sciences, 2010, 368.1923: 3269-3294.

14. KUHN, M., et al. Structural characterization and oxygen nonstoichiometry of ceria-zirconia ($Ce_{1-x}Zr_xO_{2-\delta}$) solid solutions. Acta Materialia, 2013, 61.11: 4277-4288.

15. STEINFELD, A., et al. Solar-processed metals as clean energy carriers and water-splitters. International Journal of Hydrogen Energy, 1998, 23.9: 767-774.

16. STEINFELD, A. Solar hydrogen production via a two-step water-splitting thermochemical cycle based on Zn/ZnO redox reactions. International Journal of Hydrogen Energy, 2002, 27.6: 611-619.

17. ROEB, Martin, et al. Materials-related aspects of thermochemical water and carbon dioxide splitting: A review. Materials, 2012, 5.11: 2015-2054.

18. ABANADES, Stéphane; FLAMANT, Gilles. Thermochemical hydrogen production from a two-step solar-driven water-splitting cycle based on cerium oxides. Solar Energy, 2006, 80.12: 1611-1623.

19. Diver R, Fletcher E. Hydrogen and oxygen from water. II. Some considerations in the reduction of the idea to practice. Energy 1979;4:1139–50.

20. Kogan A. Direct solar thermal splitting of water and on-site separation of the products. II. Experimental feasibility study. Int J Hydrogen Energy 1998;23(2):89–98.

21. KODAMA, T.; GOKON, N.; YAMAMOTO, R. Thermochemical two-step water splitting by ZrO 2-supported Ni x Fe 3− x O 4 for solar hydrogen production. Solar Energy, 2008, 82.1: 73-79..

22. NAKAMURA, T1. Hydrogen production from water utilizing solar heat at high temperatures. Solar Energy, 1977, 19.5: 467-475.

23. STEINFELD, Aldo. Solar thermochemical production of hydrogen—a review. Solar energy, 2005, 78.5: 603-615.

24. KODAMA, Tatsuya; GOKON, Nobuyuki. Two-step thermochemical cycles for high-temperature solar hydrogen production. Advances in Science and Technology, 2011, 72: 119-128.

25. FURLER, Philipp, et al. Solar thermochemical CO_2 splitting utilizing a reticulated porous ceria redox system. Energy & Fuels, 2012, 26.11: 7051-7059.

26. LE GAL, Alex; ABANADES, Stéphane. Dopant incorporation in ceria for enhanced water-splitting activity during solar thermochemical hydrogen generation. The Journal of Physical Chemistry C, 2012, 116.25: 13516-13523.

27. CHUEH, William C., et al. High-flux solar-driven thermochemical dissociation of CO2 and H2O using nonstoichiometric ceria. Science, 2010, 330.6012: 1797-1801.

28. LEE, Chong-il, et al. Solar hydrogen productivity of ceria–scandia solid solution using two-step water-splitting cycle. Journal of Solar Energy Engineering, 2013, 135.1: 011002.

29. KANEKO, H., et al. Cerium ion redox system in CeO_2–xFe_2O_3 solid solution at high temperatures (1,273–1,673 K) in the two-step water-splitting reaction for solar H2 generation. Journal of Materials Science, 2008, 43.9: 3153-3161.

30. BADER, Roman, et al. Thermodynamic analysis of isothermal redox cycling of ceria for solar fuel production. Energy & Fuels, 2013, 27.9:

5533-5544.

31. KAWAKAMI, S., et al. Thermochemical Two-step Water Splitting Cycle using Ni-ferrite and CeO_2 Coated Ceramic foam Devices by Concentrated Xe-light Radiation. Energy Procedia, 2014, 49: 1980-1989.

32. NEISES-VON PUTTKAMER, Martina, et al. Material Analysis of Coated Siliconized Silicon Carbide (SiSiC) Honeycomb Structures for Thermochemical Hydrogen Production. Materials, 2013, 6.2: 421-436.

33. KODAMA, Tatsuya, et al. Thermochemical two-step water splitting by zirconia-supported ferrites and its foam device for solar demonstration. In: 15th Solar PACES International Symposium. 2009.

34. GOKON, Nobuyuki, et al. Ferrite/zirconia-coated foam device prepared by spin coating for solar demonstration of thermochemical water-splitting. International journal of hydrogen energy, 2011, 36.3: 2014-2028.

35. WAGAR, W. R.; ZAMFIRESCU, C.; DINCER, I. Thermodynamic analysis of solar energy use for reforming fuels to hydrogen. International Journal of Hydrogen Energy, 2011, 36.12: 7002-7011.

36. AL-SHANKITI, I., et al. Solar Thermal Hydrogen Production from Water over Modified CeO_2 Materials. Topics in Catalysis, 2013, 56.12: 1129-1138.

37. DASARI, Hari Prasad, et al. Hydrogen production from water-splitting reaction based on RE-doped ceria–zirconia solid-solutions. International Journal of Hydrogen Energy, 2013, 38.14: 6097-6103.

38. MEHDIZADEH, Ayyoub M., et al. Investigation of hydrogen production reaction kinetics for an iron-silica magnetically stabilized porous structure. International Journal of Hydrogen Energy, 2012, 37.18: 13263-13271.

39. SINGH, A., et al. Production of hydrogen via an Iron/Iron oxide looping cycle: Thermodynamic modeling and experimental validation. International journal of hydrogen energy, 2012, 37.9: 7442-7450.

40. MALLAPRAGADA, Dharik S.; AGRAWAL, Rakesh. Limiting and

achievable efficiencies for solar thermal hydrogen production. International Journal of Hydrogen Energy, 2014, 39.1: 62-75.

41. LE GAL, Alex; ABANADES, Stéphane. Catalytic investigation of ceria-zirconia solid solutions for solar hydrogen production. International Journal of Hydrogen Energy, 2011, 36.8: 4739-4748.

42. GOKON, Nobuyuki; SAGAWA, Sachi; KODAMA, Tatsuya. Comparative study of activity of cerium oxide at thermal reduction temperatures of 1300–1550℃ for solar thermochemical two-step water-splitting cycle. International Journal of Hydrogen Energy, 2013, 38.34: 14402-14414.

43. KODAMA, T.; GOKON, N.; YAMAMOTO, R. Thermochemical two-step water splitting by ZrO_2-supported $NixFe_{3-x}O_4$ for solar hydrogen production. Solar Energy, 2008, 82.1: 73-79.

44. LEE, Hyunjin, et al. Optical performance evaluation of a solar furnace by measuring the highly concentrated solar flux. Energy, 2014, 66: 63-69.

45. CHO, H. S., et al. Solar Demonstration of Thermochemical Two-step Water Splitting Cycle Using Ce_{O2}/MPSZ Ceramic foam Device by $45k_{Wth}$ KIER Solar Furnace. Energy Procedia, 2014, 49: 1922-1931.

46. GOLDSTEIN, Joseph I., et al. Scanning electron microscopy and X-ray microanalysis. A text for biologists, materials scientists, and geologists. Plenum Publishing Corporation, 1981.

47. GARCIA, Pierre; FERRIERE, Alain; BEZIAN, Jean-Jacques. Codes for solar flux calculation dedicated to central receiver system applications: a comparative review. Solar Energy, 2008, 82.3: 189-197.

48. CHANG, Chong-Min, et al. Design of illumination and projection optics for projectors with single digital micro mirror devices. Applied optics, 2000, 39.19: 3202-3208.